UNIVERSITÀ DI PISA

Facoltà di Ingegneria

Laurea Specialistica in Ingegneria dell'Automazione

Tesi di laurea

HAPTIC SUPPORT SYSTEMS FOR CURVE NEGOTIATION IN A DRIVING SIMULATOR

Candidato:

Luca Profumo _____

Relatori:

Prof. Lorenzo Pollini - Università di Pisa _____

Prof. David Abbink - Delft University of Technology _____

Sessione di Laurea del 14/12/2012
Archivio tesi Laurea Specialistica in Ingegneria dell'Automazione
Anno accademico 2011/2012
Consultazione consentita

Abstract

A human operator performing a manual control task can be assisted by haptic shared control, a novel approach in literature which makes use of a continuous-time force feedback to guide the operator in a specific control direction.
In a previous research, a haptic controller has been designed and tested in a for curve negotiation support in a driving simulator. This support system provides a force feedback the operator has to give way to in order to correct the vehicle lateral deviations from a reference trajectory. It was proved in an experiment to yield benefits in terms of increased performance and reduced effort from the operator with respect to manual driving.
As a variation from the haptic shared control philosophy, a novel approach has been introduced in literature for supporting a human operator piloting RPVs in a simulated environment. This haptic controller is called Indirect since the force feedback it provides has the only effect of changing the neutral point of the control interface. The operator can exploit this aiding by contrasting the force feedback and keeping the control device close to the central position. The Indirect haptic controller was proved in an experiment to increase performance and was found helpful by the pilots, as well as the Direct controller, which is the classic approach, and compared to manual piloting.
This novel approach in haptic shared control has only been investigated as a support for piloting RPVs. In this project the Indirect controller is being designed in a modeling study and tested for a curve negotiation task in a driving simulator.
The Indirect controller for curve negotiation is designed in a model-based study, where a scheme is employed simulating the behaviour of a human operator and the haptic controller. The outcome of this study are some previsions on different driving conditions, where an operator can drive manually or be assisted by the classic Direct haptic controller or by the novel Indirect controller.
An experimental campaign with a driving simulator is performed, based on the previsions figured in the modeling study. The results of the experiment tells us that both the Direct and Indirect controllers can be helpful for performance and effort of the operator in low visibility conditions, while in normal visibility a contrast in goal can arise between operator and shared controller, due to a different way of the operator to cut curves. In a situation of evasive maneuver with a faulty controller, where the operator has to reject the force feedback, the Indirect controller is proved to be more damaging than the Direct support. Finally, some negative after-effects on performance and effort are encountered after the Indirect controller is switched-off, due to an intense adaptation of the operator to the different dynamics to control.
The Indirect haptic support can be a valid alternative to the typical Direct control scheme for curve negotiation support, although there is room for improving its functioning. Future developments should be focused on making the Indirect controller easier to understand, to cope with more effectively in case of failures and possibly to switch to manual driving without confusion.

Abbreviations

HSC	**H**aptic **S**hared **C**ontrol
DHA	**D**irect **H**aptic **A**iding
IHA	**I**ndirect **H**aptic **A**iding
NMS	**N**euro-**M**uscular **S**ystem
FT	**F**orce **T**ask
PT	**P**osition **T**ask
SW	**S**teering **W**heel
FFW	**F**eed **F**or**w**ard
FB	**F**eed**b**ack

Parts of the experiment:

NVB	**N**ormal **V**isi**b**ility
LVB	**L**ow **V**isi**b**ility
OAE	**O**bstacle **A**voidance with controller **E**rror
ADP	**Ad**a**p**tation
AEF	**A**fter **Ef**fects

Contents

List of Figures

List of Tables

Chapter 1

Introduction

1.1 Haptic Shared Control

The original principle of Haptic technology is to reproduce the sense of touch in a virtual environment in order to assist a remote operator to perform some task. The artificial tactile sensation reproduces the real sense of touch, which is not available in a remote environment. This information is complementary to visual feedback and it is used to enhance the manual control task of a certain device.
Apart from merely being a sensory information, the artificial feeling can be actually used to guide the operator in a certain control direction, if it is designed as a time-continuous feedback signal. Following this line of thought, a general scheme can be drawn where two entities are cooperating in the control task: human operator and a so-called *haptic shared controller*. Both the actors have their own control goals and strategies, which can be different from each other, and their control inputs are shared on the control interface which actually becomes a man-machine interface. This idea of Haptic Shared Control (HSC) was presented in [1].
Supporting an operator to perform a task with a haptic shared controller can lead to many advantages, awareness and safeness amongst all. However, several issues arise from the design process of a haptic controller. First of all, the haptic controller is named *shared* for a specific reason: the controller should only help the operator to perform the task and not replace him. The concept of *shared* stands actually in between manual control and full automation and the desired power of the controller must be chosen from a a scale of different levels of authority [2]. A sufficient power from the shared controller guarantees that the information is helpful to the operator. If a perfect and faults-free shared controller was designed, it could be easily employed as an automatic controller entirely replacing the human control. This perfect automatic controller would lead to the highest performance in the task accomplishment. The idea of limiting the controller power comes therefore from a safety issue: in case of errors the operator should be able to override the faulty controller and make his own decision. A shared control strategy can be hence a valid stage in between full automation, where the operator has the role of supervisor, and manual control, in all the applications where safety is important

and the automation is prone to failures, due for example to flaws in the sensory system.

1.2 Investigation of HSC strategies for curve negotiation

A haptic shared controller has been designed and tested in a previous study [3] for assisted curve negotiation in simulated car driving. The haptic controller, given a desired vehicle reference trajectory and the information on the current vehicle state from a virtual sensory system, provides a force input on the steering wheel in order to correct the car deviations from the reference. The pilot is therefore assisted by this system and simply has to give way to the force feedback and amplify it, provided that he agrees with the haptic controller on the control goal. The system was tuned with a limited force feedback gain, in order to be safe and to let the driver override it if necessary.
A different shared control strategy was introduced in [4] in an application for piloting simulated RPVs (remotely piloted vehicles). This new approach was called Indirect Haptic Aiding (IHA), in order to distinguish it from the usual haptic control strategies called Direct Haptic Aiding (DHA) such as the one for curve negotiation support described above. The IHA controller is based on a mechanical decoupling of the control interface from the vehicle. The force feedback provided by the system is only an aiding signal to suggest the operator the right maneuver and it does this by changing the neutral point of the control interface. The operator can control the vehicle by using the control column as a force interface, that is simply by contrasting the force feedback from the controller. Moreover, the IHA controller does not modify the amount of control input required from the operator, which is the same as in manual control. However, it changes the dynamics of the system to control since the usage of the control column is different from the conventional one.
Notice the different implementations of the haptic controllers. In [3] the force feedback was calculated in order to correct the vehicle lateral deviation from a reference trajectory. In [4] the aiding signal from the controller was calculated in order to correct a vertical wind gust disturbance, while in the obstacle avoidance task of [5] it came from a force field around the obstacles.
In the experiment performed in [3] for curve negotiation, the potentiality of the DHA support was assessed with respect to manual driving. Performance, mental and physical effort were measured in this experiment with specific statistical metrics. With respect to manual driving, the DHA shared control produced a slight increase in performance and lower mental effort of the operator. However, a controversial result was found in physical effort, since it increased with the DHA controller on. Notice that in this experiment drivers were instructed and trained on how to use the support system.
In [4] the IHA support is argued to exploit the natural rejection response of the operator to a force feedback, which in the first place is perceived as a disturbance

and not a direct help. For this reason the IHA controller is claimed to be a more natural and intuitive approach than DHA, while DHA requires some learning. However, a shared controller can be more or less natural depending on the application where it has been designed.
The DHA and IHA controllers were compared to manual control in [5] in an obstacle avoidance experiment with simulated RPVs. In this experiment, performance was measured with a statistical metrics, while a questionnaire was employed to assess the pilots effort and their feeling of the haptic support. Notice that no specific instructions were given to the pilots. IHA was proved to be a valid alternative to DHA: it produced the best performance in the first repetitions, while pilots the the DHA support performed better in the last repetitions. DHA and IHA were both considered helpful by the pilots. However, a higher effort was felt by the pilots with both the systems.
Let us now make conclusions on this investigation on haptic control strategies. In the application of interest for this project, which is curve negotiation support, the DHA controller has already been implemented and found helpful in the previous experiment [3]. On the other side, the IHA controller was only tested for piloting simulated RPVs in [5] and proved a valid alternative to DHA. In this case, the control interface was a control column and the task was to follow an artificial horizon. However, curve negotiation is a different task since it involves a more complex decision process of the driver from the visual feedback to the control action. In the task with RPVs the error from the reference is directly presented to the pilot and this makes the pilot easily agree with the controller on the control goal. Whereas, in curve negotiation the driver has to identify the reference trajectory to follow and a contrast is more likely to arise between the control goals of operator and driver, for example in case an operator decides to cut curves differently. Therefore, the results found with IHA for piloting RPVs can only be indicative for what can be expected for a curve negotiation implementation.

1.3 Goal and approach

The goal of this project is to design and test the IHA controller as a novel support for curve negotiation in a driving simulator.
In the light of what found in literature, it seems important to begin with a modeling study, in order to understand how the IHA mechanism can be redesigned for this application, as well as for making previsions on the behaviour and results with this system compared to the DHA support and manual control.
Schemes of haptic shared control for curve negotiation are presented in chapter 2, where particular attention is given to the modeling of the human operator behaviour in this task and the two adopted shared control strategies, DHA and IHA. In chapter 3, a computer model to simulate the two shared control strategies is employed, in order to acquire a broad understanding of their functioning in relation with the human operator control goal. As an outcome of this modeling study, some experimental hypothesis on different driving situations are formulated.

Once the shared control systems have been studied in computer simulation, an experiment is set-up and carried out based on the previsions made. The implementation and tuning of the DHA controller and the IHA controller in a driving simulator is presented in chapter 4, along with the experiment structure. In chapter 5, the experimental campaign on shared control strategies is performed and its results are used to verify the hypotheses figured from the modeling study.
In the final chapter 6 the conclusions on the project are drawn along with some guidelines for future developments.

Chapter 2

Modeling HSC for curve negotiation

2.1 Human control and Haptic shared control

In the modeling study, schemes of shared control for a curve negotiation task are used to investigate these systems in relation to the human operator behaviour in different driving situations.
Here the different models designed and employed in this project are introduced. The schemes illustrated in this section are inspired from those in [6]. The description begins from a top view of the general system and is followed by detailed explanations of the various subsystems.

2.1.1 Generic model of haptic shared control

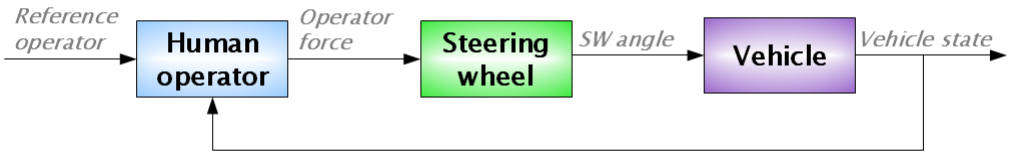

FIGURE 2.1: Model of manual control

A generic scheme of manual control for a curve negotiation task is presented in figure 2.1. In this scenario, the human operator has a reference trajectory to follow and the current vehicle state as inputs. From the vehicle error to the reference

trajectory, a force to apply on the steering wheel is computed.
The manual control scheme can be enhanced with an external control device which helps the human operator to perform the curve negotiation task. The main principle at the basis of shared control is the sharing of a human operator force input and a controller input on an interaction interface, a steering wheel in the case of curve negotiation support, from which the output is given to the vehicle to be guided. Forces are generated in order to make the vehicle follow a certain reference trajectory.
Operator and controller contribute together to the vehicle dynamics, each one with a certain control energy: the fundamental idea is that the controller energy should be limited within certain boundaries in order to give the operator full authority in every possible situation.
The most generic model of haptic shared control (figure 2.2) consists of four main

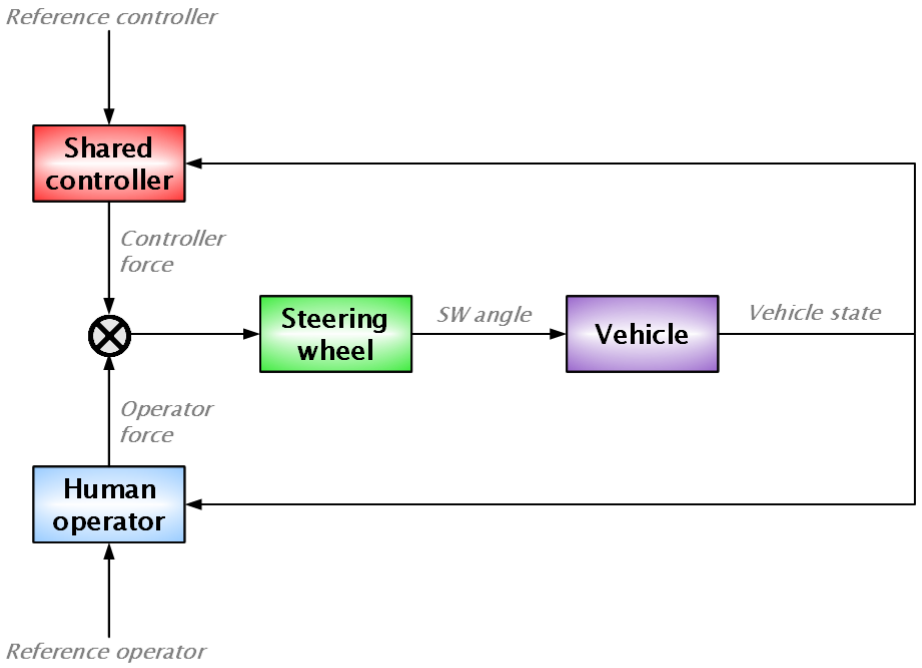

FIGURE 2.2: Generic model of haptic shared control

subsystems:

- Human operator
- Haptic shared controller
- Steering wheel
- Vehicle

In this scheme the operator and the controller have two different reference trajectories. If those trajectories are equal we can simulate a situation where operator and controller cooperate for the same control aim. In case there is a mismatch between those trajectories, operator and controller will fight for different control goals.
Both operator and controller can be modelled in a similar fashion by distinguishing the *Visual control* from *Haptic control*. Inside the human control process for curve negotiation, Visual control can be defined as the mental process that, given the current state of the vehicle and the operator goal, e.g. keeping the vehicle in the right lane, produces the optimal trajectory that must be realized on the control interface, that is the steering action to follow the desired goal. Notice that in this scheme both the sensor system of the haptic controller and the sensory organs of the operator that detect the vehicle state are supposed to be exact and with no delay, that is a unitary gain. Haptic control is instead the force control, that is the mental-physical process from this optimal trajectory to the force that must be exerted on the control interface. Notice that this distinction is just a trick that allows us to simplify the human control process by dividing it into two blocks. Moreover, a shared controller can be built with the same internal structure and the main advantage is that Visual block and Haptic block can be designed and tuned separately. The haptic shared guidance scheme with this internal structure both for human operator and shared controller is shown in figure 2.3.

The Visual block takes in input the reference trajectory (control goal) and the

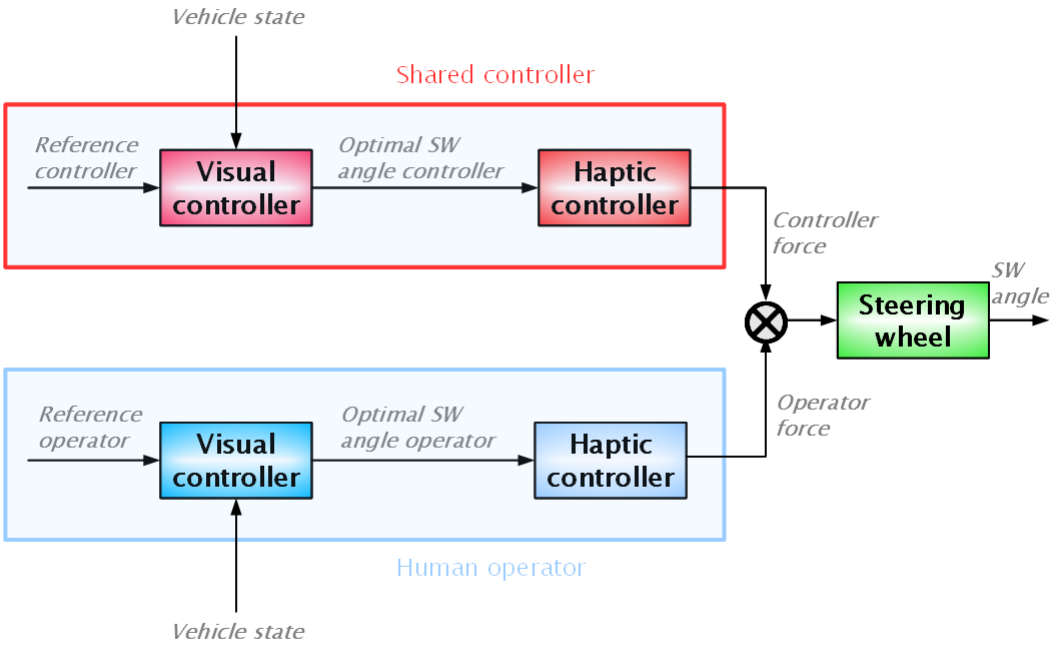

FIGURE 2.3: Internal structure of operator model and controller

current state of the vehicle in order to compute an optimal trajectory that must

be imposed on the control interface, in this case an optimal steering wheel angle. The optimal trajectory is fed to the Haptic block which has to compute a force to apply on the control interface to realize the optimal steering wheel angle.
Visual block and Haptic block of human operator and controller can be internally designed in different ways. On one side, the human operator model should be as realistic as possible, in order to obtain valid results from the model. Whereas there are many different choices for the controller model with variable complexity. In this project two different haptic support strategies are compared and in order to make the comparison as clear as possible, the employed controller structure has been designed in a simple way as described in section 2.2.

2.1.2 Human operator model

The Human operator model that will be introduced has been developed in previous studies [8]. Some changes were made on the original model in order to fit it into this study on two strategies of haptic shared control and in the different driving situations that will be investigated.
As already mentioned, the Human operator subsystem (figure 2.4) takes in input the reference trajectory to follow and gives in output a torque to be applied on the Steering wheel. It is modelled with a Visual block and a Haptic block in series.
The current reference trajectory is used along with the current vehicle state to

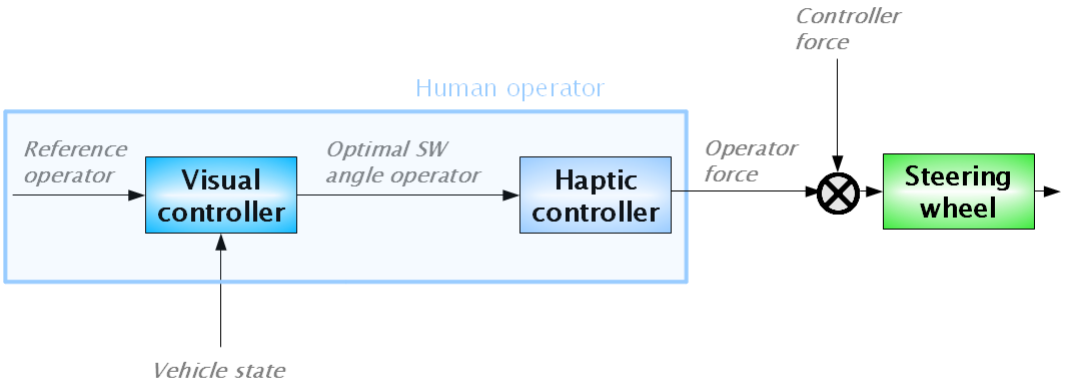

FIGURE 2.4: Human operator model

compute an optimal steering wheel angle to be realized on the steering wheel. This is done in the subsystem called Visual controller.

In figure 2.5a it is shown in detail the structure of this Visual block. First an algorithm is employed to predict the vehicle global state after an interval of time called look-ahead time TLH (Predictor block). In practice, the current tyre angle is frozen at each time step and used to compute the future global position and orientation.

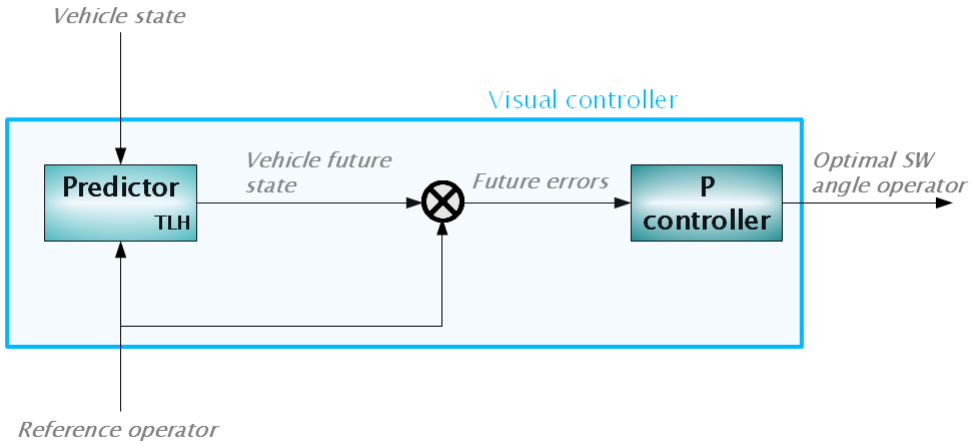

(a) Operator Visual block

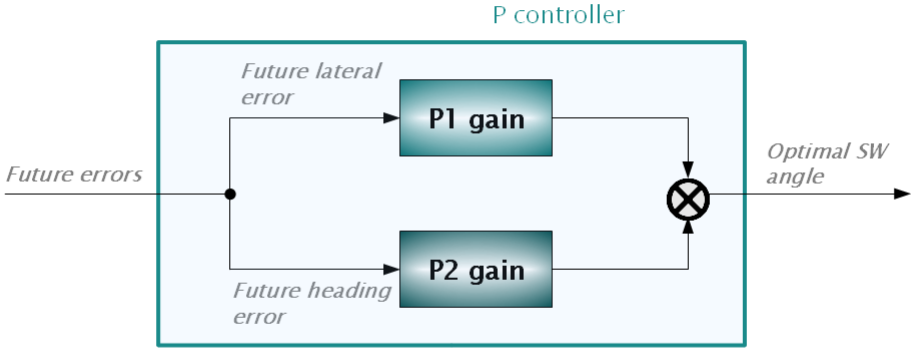

(b) Future error to optimal SW angle

FIGURE 2.5: Operator Visual block

Secondly, from the vehicle current and future global states two variables are determined:

- Future lateral error
- Future heading error

Finally, two different proportional gains are applied to the future errors and then they are added up to provide the optimal steering wheel angle. This is done in the block P controller of figure 2.5b.
Equation 2.1 is the mathematical formula for the operator optimal steering wheel

angle computation $\theta_{SW,opt(hum)}$ from the future lateral $(e_{lat}|_{TLH})_{hum}$ and heading $(e_{head}|_{TLH})_{hum}$ errors where the subscript TLH indicates the look-ahead time at which the future errors are computed.

$$\theta_{SW,opt(hum)} = P_1 \, (e_{lat}|_{TLH})_{hum} + P_2 \, (e_{head}|_{TLH})_{hum} \tag{2.1}$$

The optimal trajectory generated by the Visual controller must be then converted

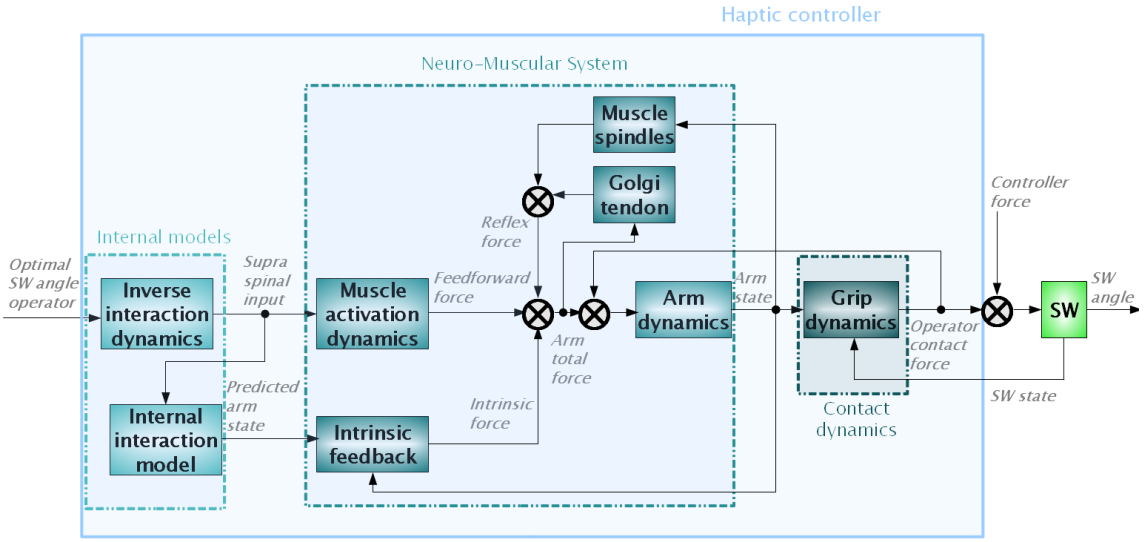

FIGURE 2.6: Operator Haptic block

into a force signal to be applied on the control interface. This is done into the Haptic block, that for the human operator is modelled with three subsystems as shown in figure 2.6:

- Internal models
- Neuro-Muscular System
- Contact dynamics

The human arm force signal can be represented by three different components as shown in the NMS subsystem of figure 2.6:

- Feedforward force
- Intrinsic feedback force
- Reflex force

These three contributes can be employed for a realistic description of the human arm response. The feedforward signal is the one used in nominal and ideal condition for the curve negotiation task. Practically, if the operator had full knowledge of the closed loop guidance model without any kind of uncertainties and if there were no additional external disturbances in the system, the human operator would be able to realize the optimal steering wheel angle on the actual steering wheel and make the vehicle perfectly follow the chosen reference trajectory. In the scheme of figure 2.6 the feedforward signal is computed by the Inverse interaction dynamics block. This function represents the human knowledge of the total interaction between arm and steering wheel: it is the mapping from the optimal steering wheel angle computed by Visual control to a torque input to be exerted in order to realize the optimal angle on the actual steering wheel. The feedforward signal is also called Supra-Spinal input and is fed to the Muscle activation dynamics to determine the actual feedforward arm force. The Muscle activation dynamics block is modelled as a butterworth filter with a 2 Hz cross-over frequency to represent normal low-pass muscular response to an activation signal from the cerebral cortex.
Still the operator may have a limited knowledge of the system to control and also many kinds of disturbance signals can have access to the system state, such as noise or also the input from a shared controller, therefore a feedback activity is required to compensate for these unpredicted signals. The feedback signal can be divided into intrinsic feedback and reflexes. The intrinsic feedback force represents the muscle co-contraction action and it is a purely haptic loop, much faster than the visual control loop. What happens is that the operator is predicting his own arm state from his knowledge of the controlled system but in presence of model uncertainties or disturbances the arm can be found in a different state. Therefore, muscle co-contraction can be modelled as a spring-damper system around the predicted arm state bringing the arm to the desired position. In the scheme of figure 2.6 the Intrinsic feedback subsystem computes the intrinsic force from the difference between current and predicted state of the arm. The predicted state comes from the Internal interaction model that will be parametrized in chapter 3. This Internal interaction model is the new block that has been added to the original model for the sake of this analysis on two haptic shared control strategies.
The second part of human arm feedback is the reflex activity. This is the fastest human response to disturbance since reflexes are not generated by the central nervous system (conscious response) but by the peripheral system that provides a faster loop. Reflex activity can be divided into spindles reflex, that is a reflex to a change in muscular length and velocity, and the Golgi tendon that is a reflex to a force generated by the muscle itself.
Inside the NMS block of figure 2.6 the total human arm force is generated by composing feedforward and feedback signals. The total arm force is in input to the Arm dynamics which produces the human arm current position and velocity.
The grip between human arm and steering wheel is modelled in the Contact dynamics subsystem of figure 2.6 as a spring-damper system with two grip parameters that can be set according to the current muscular co-contraction. Basically with this modeling choice the grip is a spring-damper system between the human arm state and the steering wheel state.
A contact torque is produced from the grip between human arm and steering wheel

and this is the actual operator input torque on the steering wheel itself. An additional external torque can also be present on the steering wheel, for instance the input from a shared controller or some kind of external noise. The torque inputs on the Steering wheel determine the steering wheel current position and velocity. The Steering wheel has been modelled as a mass-spring-damper system in order to simulate the steering wheel inertia and self alignment to the neutral central position. A linear characteristic has been chosen resembling the power steering systems in modern cars.
As already mentioned, the original Human operator model has been developed in previous studies [8], with particular attention to the muscle co-contraction activity parameters identification. In the identification experiments performed, a steering wheel with an external identification torque signal was provided to a human operator in absence of visual feedback and the subject was asked to follow two different approaches, called *Force task* (FT) and *Position task* (PT). In the FT the subject was instructed to give way to the torque signal provided by the control system, while in the PT the operator had to contrast the torque input by using co-contraction in order to keep the steering wheel to the central neutral position. As identification signals for the experiment, both a noise torque signal and the torque feedback coming from a shared controller were used. The spring-damper intrinsic feedback parameters were therefore identified in the two different settings and are the ones employed in this model. They are shown in table 2.1

Table 2.1: Intrinsic feedback and Grip parameters

	FT	PT
$B_{int}(Nm/rad)$	1.047	0.85
$K_{int}(Nms/rad)$	1.87	151
$B_c(Nm/rad)$	7.00	19.5
$K_c(Nms/rad)$	10.8	1039

and it can be noticed that they are higher in a PT where muscle co-contraction is stronger. It should be noticed that in the current model the intrinsic feedback parameters are adapted to a different situation from the experimental conditions where they were identified: now the co-contraction is not around a steering wheel angle equal to zero, since a visual feedback is present, but between current arm state and predicted arm state. This is the novelty introduced with this model.
Grip parameters have also been identified together with intrinsic feedback parameters in the same experiment for FT and PT settings table 2.1. It can be noticed that grip parameters are higher for a PT where the grip is reasonably tighter than in a FT.

2.2 Schemes of HSC strategies

In this section two different strategies for haptic shared control in a curve negotiation task are introduced. The first approach, named Direct controller, has already

been implemented and tested in previous studies. Whereas, for the first time a scheme of Indirect controller is presented as a curve negotiation support in this section.

2.2.1 Direct Haptic Aiding

In the classic direct haptic controller scheme [3], the shared controller provides a force feedback on the steering wheel that directly commands the vehicle to follow a certain reference trajectory. Both the operator force and the force feedback affect the vehicle dynamics. The operator is required to give way to the force feedback and amplify it in order to follow the aiding from the shared controller.

$$\theta_{SW} = SW(s)(T_{hum} + T_{DHA}) \tag{2.2}$$

In equation (2.2) the steering wheel angle θ_{SW} is the output of the steering wheel dynamic model transfer function $SW(s)$ to which both the human operator torque T_{hum} and the controller torque T_{DHA} are in input. θ_{SW} is therefore the SW angle to directly guide the vehicle.

The Direct controller, also *DHA* (Direct Haptic Aiding) controller, illustrated in

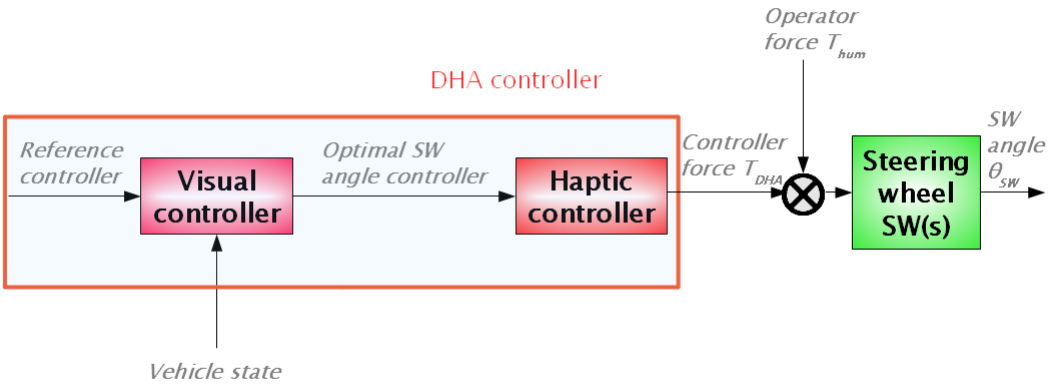

FIGURE 2.7: DHA controller

2.7 has been implemented in a similar fashion to the human operator model. It is composed of Visual and Haptic subsystems.

The current reference trajectory along with the vehicle global state are used to compute the controller optimal steering wheel angle in the Visual controller block. In the model employed, the controller Visual block has the same internal structure of that of the human operator 2.5. The Visual subsystem for the DHA controller is shown in figure 2.8.

The Visual block equation is 2.3 where $\theta_{SW,opt(DHA)}$ is the optimal steering wheel

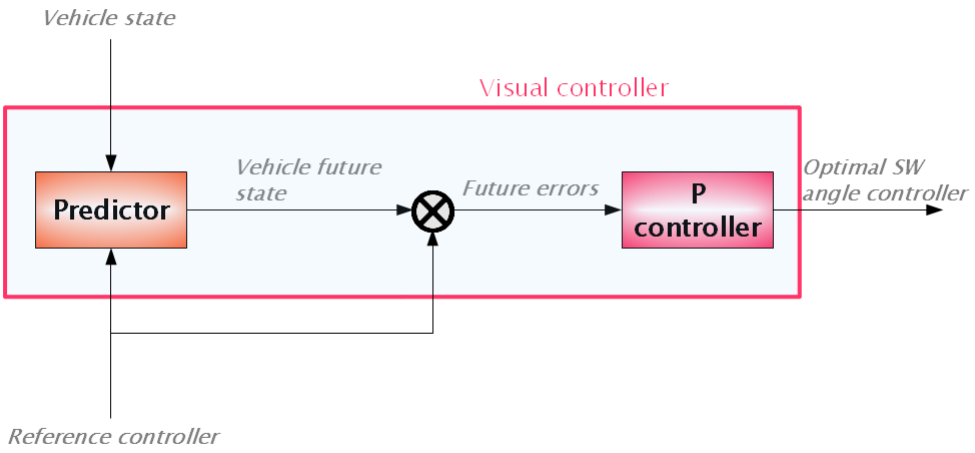

FIGURE 2.8: DHA Visual block

angle for the DHA controller. This equation is equivalent to 2.1.

$$\theta_{SW,opt(DHA)} = P_1 \left(e_{lat}|_{TLH}\right)_{DHA} + P_2 \left(e_{head}|_{TLH}\right)_{DHA} \tag{2.3}$$

Therefore, if the reference trajectories of controller and operator are chosen identical, the optimal steering wheel angles of controller and operator will also be equal. What changes between shared controller model and human model is the haptic subsystem. On one side, the operator is linked to the steering wheel through the whole neuromuscular system and the grip on the steering wheel. Whereas the controller can directly provide a torque input on the steering wheel and this is the main difference with the human control. The shared controller Haptic block can be realized in different ways to make it more or less close to the human control logic. However, in order to make the comparison between the two different haptic systems simple, it has been chosen a simple proportional control. Therefore, the controller torque is proportional to the optimal steering wheel angle through a gain that must be tuned in order to choose the controller energy appropriately. In fact, in the shared control philosophy the controller must have a precise level of authority, which means a limited amount of energy in order to give the operator the power to potentially override the control input on the shared interface [3].

$$T_{DHA} = G_{DHA}\, \theta_{SW,opt(DHA)} \tag{2.4}$$

The Haptic subsystem of the DHA controller is shown in figure 2.9 and represented by (2.4), where T_{DHA} is the DHA controller torque and G_{DHA} the proportional gain.

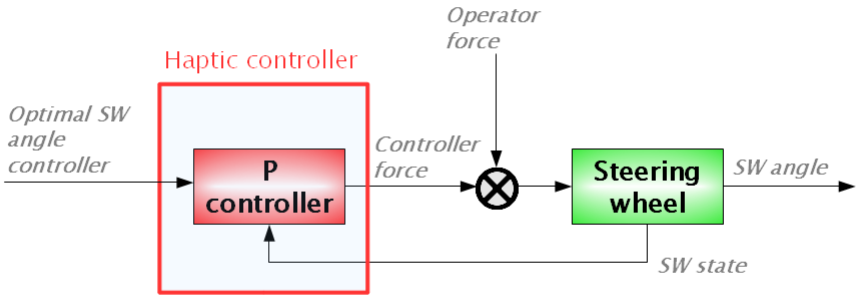

FIGURE 2.9: DHA Haptic block

2.2.2 Indirect Haptic Aiding

In this paragraph the Indirect shared controller is introduced for the first time as a support system for curve negotiation. It has been designed so to resemble its original version developed for a flight simulator [4]. The Indirect controller will also be called *IHA* (Indirect Haptic Aiding) controller.
The main principle is that the shared controller must not directly affect the vehicle dynamics, but only the control interface, on which a force feedback signal is fed that must be interpreted by the human operator as a disturbance. The action of the IHA controller is only a shift in the steering wheel neutral point. The operator can follow the haptic aiding by simply contrasting the disturbance force and with lower steering actions like small deviations from the center.
The IHA controller in its internal structure can be designed in the same way as the DHA, except for the force gain of the Haptic block which must be inverted. This way the force feedback commanding the steering wheel is perceived as a disturbance by the operator. In order to make the IHA affect only the neutral point of the steering wheel, a model of the steering wheel is also to be implemented inside the IHA controller. The force feedback from the IHA controller must be fed also to this SW model, and the output SW model angle subtracted from the current steering wheel angle, to produce the input angle that goes to the vehicle. This correction block, implemented inside the IHA controller, basically changes the steering wheel dynamics by decoupling it from the vehicle.
In figure 2.10 it is shown the IHA model. It is composed of the following subsystems:

- Visual controller
- Haptic controller
- Correction block

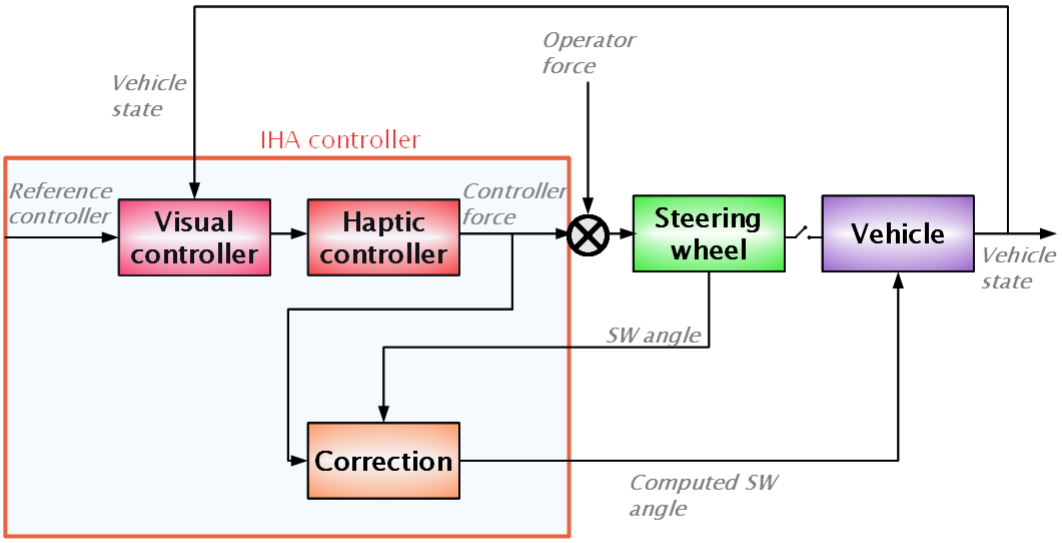

FIGURE 2.10: IHA controller

The IHA Visual block is chosen with the same structure of that of human operator 2.5 and DHA 2.8. Therefore the optimal steering wheel angle is computed with the usual formula 2.5.

$$\theta_{SW,opt(IHA)} = P_1 \left(e_{lat}|_{TLH}\right)_{IHA} + P_2 \left(e_{head}|_{TLH}\right)_{IHA} \tag{2.5}$$

The Haptic block is also realized in the same fashion, but the proportional gain to obtain the controller force is chosen with the opposite sign of the DHA as in 2.6.

$$T_{IHA} = -G_{IHA}\, \theta_{SW,opt(IHA)} \tag{2.6}$$

This means that the controller force will make the steering wheel turn in the opposite direction of the optimal one but with the same absolute angle. This is the actual disturbance signal provided by the controller on the steering wheel.

The Correction block is shown in detail in figure 2.11. In order to make the control input affect only the actual steering wheel dynamics and not the vehicle, a model of the steering wheel must be provided. This model has in input the controller torque and its output is subtracted from the actual steering wheel angle. This way the steering wheel torsion is determined both by operator input and control input but the net input to the vehicle, that is the computed steering wheel angle in figure 2.10, is determined by the operator torque solely.

$$\theta_{SW} = SW(s)(T_{hum} + T_{IHA}) \tag{2.7}$$

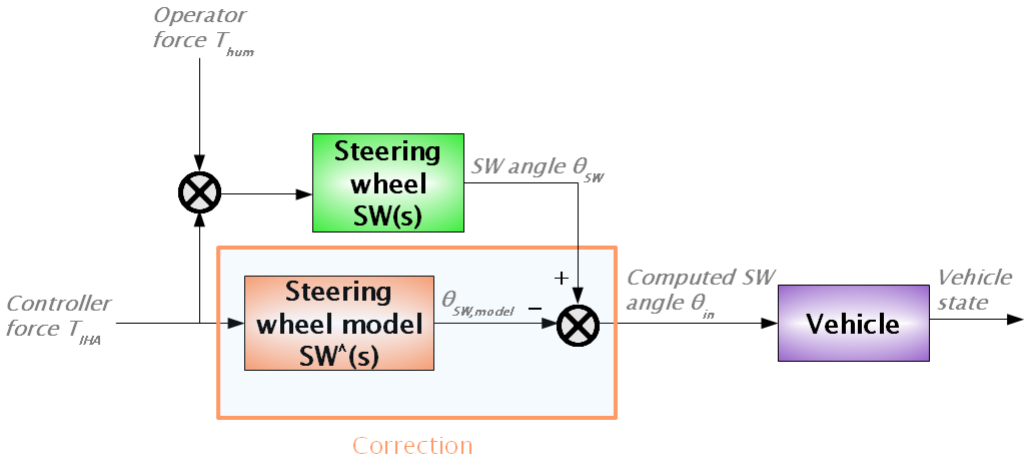

FIGURE 2.11: IHA Correction block

In equation (2.7) the steering wheel angle θ_{SW} is the output of the steering wheel dynamic model transfer function $SW(s)$ to which both the human operator torque T_{hum} and the IHA controller torque T_{IHA} are in input.

$$\theta_{in} = \theta_{SW} - \theta_{SW,model} = (T_{hum} + T_{IHA})SW(s) - T_{IHA}\hat{SW}(s) \tag{2.8}$$

However, θ_{SW} is not the SW angle to directly guide the vehicle. The angle that goes in input to the vehicle is θ_{in} which is computed by the correction block as difference between the SW angle θ_{SW} and the angle $\theta_{SW,model}$ computed from the SW model inside the IHA controller, which has $\hat{SW}(s)$ as transfer function. This is expressed in equation (2.8).
The steering wheel model inside the IHA controller matches the actual steering wheel, therefore when the human operator does not provide a torque on the steering wheel it can be observed the steering wheel turning in the opposite direction of that computed by the operator Visual block, but still the vehicle will go straight on since the net input to the vehicle is zero (2.9)-(2.10).

$$\theta_{in} = \theta_{SW} - \theta_{SW,model} = SW(s)T_{hum} + (SW(s) - \hat{SW}(s))T_{IHA} \approx SW(s)T_{hum} \tag{2.9}$$

$$T_{hum} = 0 \Rightarrow \theta_{SW} \approx SW(s)T_{IHA},\ \theta_{in} \approx 0 \tag{2.10}$$

Steering wheel and tyres have actually been mechanical decoupled as observed in figure 2.10 where the connection between Steering wheel and Vehicle is interrupted.

Chapter 3

Testing HSC for curve negotiation in computer simulation

3.1 Model parametrization and settings

In chapter 3 a generic model of haptic shared control has been introduced, with a detailed description of the designed human operator model and two different strategies for HSC.
Three shared control schemes for curve negotiation have been implemented in MATLAB Simulink:

- A. Manual control
- B. Operator-DHA shared control
- C. Operator-IHA shared control

They have been developed from the original model used in [9].
In this section the adopted model parametrization and specific settings for these schemes are presented.

3.1.1 Vehicle model

In the modeling phase, the car dynamics has been modelled with a simple linear bicycle model.
The vehicle state can be divided into body state x_{body} and global state x_{global}. The body state is composed of the vehicle current lateral velocity v_{lat} and yaw rate $\dot{\psi}$ as in 3.1.

$$x_{body} = (v_{lat}, \dot{\psi}) \tag{3.1}$$

The body state describes the state of the car in its body reference frame, while the global state is used to spot the car in a global fixed reference frame. The vehicle position $P_{vehicle}$ and yaw angle ψ constitute the global state as in 3.2.

$$x_{global} = (P_{vehicle}, \psi) \tag{3.2}$$

In figure 3.1 it is shown the Vehicle subsystem. The steering wheel angle coming

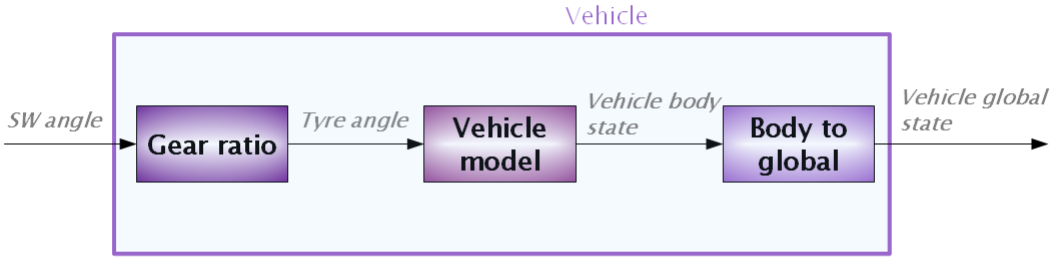

FIGURE 3.1: Vehicle model

from the control interface is converted into a tyre angle by the transmission gear (gear ratio).

$$\dot{x}_{body} = A\, x_{body} + B\, u \tag{3.3}$$

$$y = x_{body} \tag{3.4}$$

The Vehicle model is a state-space representation of the bicycle model 3.3-3.4 employed to compute the current velocity and yaw rate from the tyre angle as input $u = \delta$. The Vehicle model takes also into account the cornering stiffness of front and rear tyre, which are used as a linear approximation of the Pacejka formula [7] for the tyre realignment force.
In the last block of the Vehicle model body variables are converted into global variables.

3.1.2 Vehicle and Steering Wheel parametrization

Here are introduced the parameters for the Vehicle model and the Steering Wheel which are adopted for the whole modeling study.
The bicycle model of the vehicle is set with the following parameters:

- mass: $m = 1600\, Kg$
- distance c.o.g.-front tyre: $d_f = 1.4\, m$

- distance c.o.g.-rear tyre: $d_r = 1.4\,m$
- moment of inertia = $I_{zz} = m\,d_f\,d_r$
- cornering stiffness front tyre: $C_f = 30\,KN/rad$
- cornering stiffness rear tyre: $C_r = C_f\,l_f/l_r$

In this study the vehicle longitudinal velocity has been set to a constant value of $v_{long} = 25m/s$ in order to get rid of undesired additional degrees of freedom and focus on the steering action as control for curve negotiation.
The gear ratio from the steering wheel to the vehicle wheels is set to $gear_{SW} = 1/15$ which is a typical value for commercial cars.
The steering wheel is modelled as a simple mass-spring-damper system. This resembles current power steering systems that are designed so to have a linear characteristic angle-torque. The parameters were set to:

- moment of inertia $I_{SW} = 0.3\,Nms^2/rad$
- viscous damping $B_{SW} = 2\,Nms/rad$
- stiffness $K_{SW} = 4.2\,Nms/rad$

3.1.3 Road profiles designed for the computer simulation

In the modeling study, several road profiles have been designed in order to test different conditions in car driving. They can be divided into two categories: agreement profiles and disagreement profiles.
In the first group, the same reference trajectory is generated for both human operator and controller and a situation of agreement can be tested where operator and shared controller cooperate for the same task, that is to follow the same reference road. This group is composed by three profiles:

- Large turn
- Lane change
- Obstacle avoidance

In figures 3.2-3.4 are shown the road curvature and the actual profile for those roads. The trajectory in red is chosen as reference road for both operator and controller. Notice that this trajectory lies in the middle of the right lane of the road.
The large turn profile has been generated with a curvature close to the maximum one allowed with respect to the car dimensions, weight and longitudinal velocity.
The lane change represents a situation where the vehicle has to deviate from a straight trajectory in order to surpass a vehicle on the right lane.

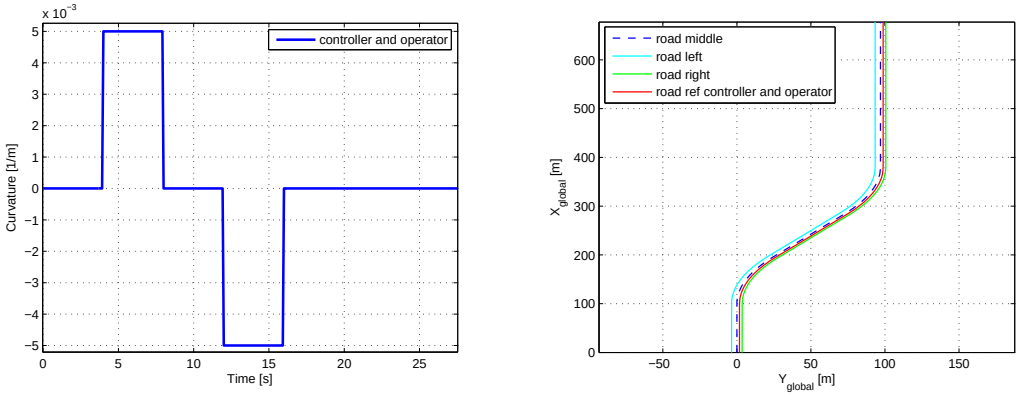

(a) Curvature profile (b) Road profile

FIGURE 3.2: Large turn road

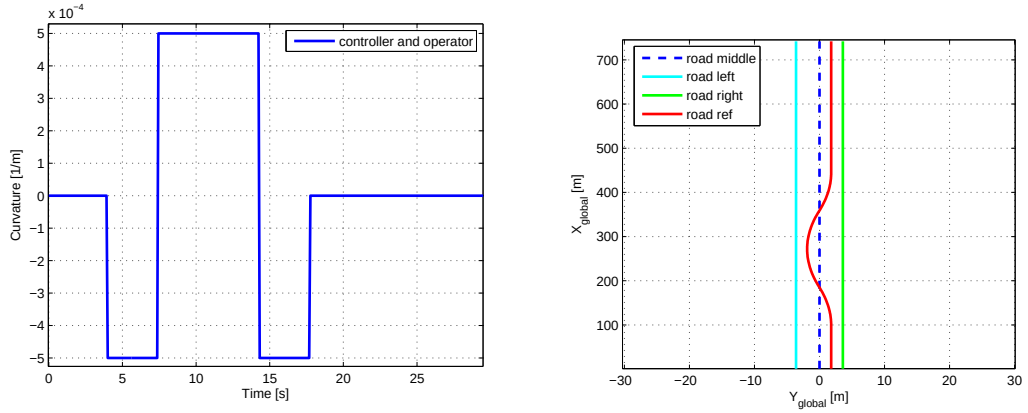

(a) Curvature profile (b) Road profile

FIGURE 3.3: Lane change road

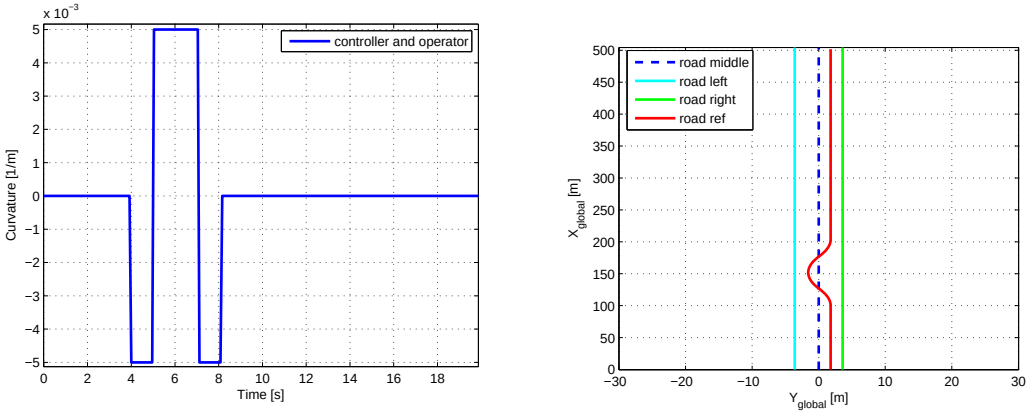

(a) Curvature profile (b) Road profile

FIGURE 3.4: Obstacle avoidance road

In the obstacle avoidance profile a virtual obstacle is present on the right lane and must be avoided by moving the car to the left lane. Notice that this profile is

different from the lane change one because here the curvature is higher as it can be observed by comparing 3.3-3.4. Obstacle avoidance is a more critical maneuver than a lane change and this is simulated with a higher curvature of the trajectory that the vehicle has to follow.
Road profiles from the second group represent a situation of mismatch between operator and controller and can be used to simulate critical conditions such as some flaws in the human control or even a controller error. Two road profiles belong to this group:

- Lane change with operator low visibility
- Lane change with controller error

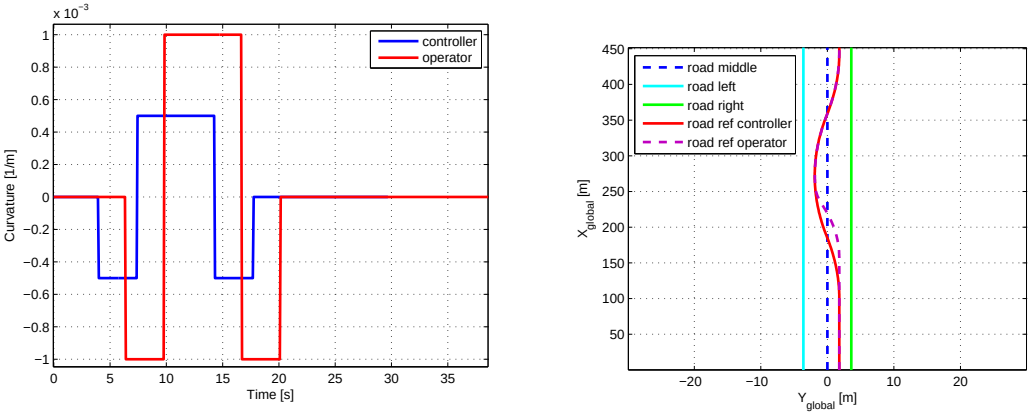

(a) Curvature profile (b) Road profile

FIGURE 3.5: Lane change road with operator low visibility

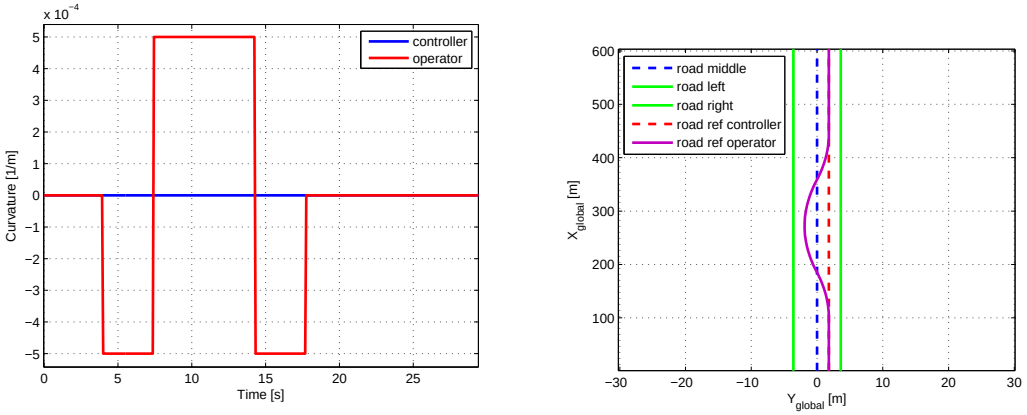

(a) Curvature profile (b) Road profile

FIGURE 3.6: Lane change road with controller error

They are shown in figures 3.5-3.6. The first profile represents a situation where there is a car to surpass on the right lane. The controller has detected the car sufficiently in advance and has a smooth lane change trajectory. On the other side,

the operator has low visibility due to fog on the street for instance and the vehicle is detected with a certain delay. Therefore, the operator trajectory is delayed with respect to the controller one and the rising profile of the curve is sharper. After the operator reference trajectory reaches the left lane center, it has been set as smooth as the controller one in the descending profile.
The other profile represent a situation where there is an error in the controller reference trajectory. The human operator has detected a car on the right lane to surpass and has a lane change profile as reference trajectory. Whereas the controller has not detected the obstacle due again to an error in the sensory system and its reference is a straight road.
The generated road profiles in input to the control scheme consist of three signals: X-reference, Y-reference and Psi-reference (heading). Those signals are displayed in figure 3.7 for a lane change profile as example.

The X-reference is ramp-shaped due to the constant longitudinal velocity that

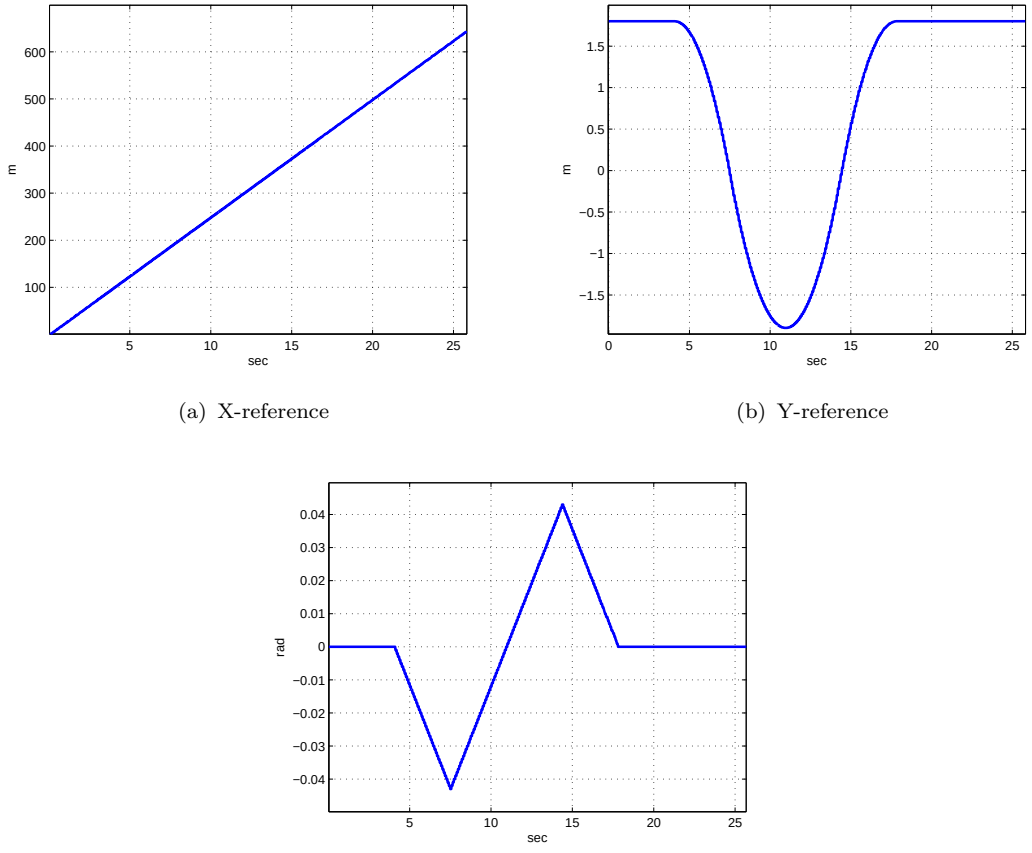

(a) X-reference

(b) Y-reference

(c) Psi-reference

FIGURE 3.7: Reference signals for a lane change road

has been chosen and this is valid for all the road profiles generated. What changes between different road profiles are the Y-reference and Psi-reference and these are the signals that can be taken into account to measure performance as well as the Y-reference error and Psi-reference error between vehicle center of gravity and current reference.

3.1.4 Operator Neuro-Muscular System parametrization

The intrinsic feedback parameters B_{int}, K_{int} from a previous identification study have already been introduced in table 2.1. In this table are also shown the grip parameters B_c, K_c which model the contact dynamics between human arm and steering wheel as a spring-damper system. The following parameters complete a realistic description of the Neuro-Muscular System:

- human arm inertia $I_{arm} = 0.247\ Nms^2/rad$
- muscle activation dynamics cross-over frequency $f_{act} = 2\ Hz$

The reflex activity parameters have been set to zero in all the tests performed in the modeling study since they have not been identified yet in any former experiment. Therefore the only feedback contribute of the NMS is the intrinsic feedback that is muscular co-contraction.

3.1.5 Inverse interaction dynamics transfer function

In the human operator model it has been showed that the human operator torque is composed of feedforward torque and feedback torque (figure 2.6). The feedforward torque is generated by the Haptic controller subsystem taking as input the optimal steering wheel angle generated by the operator Visual controller block. It has also been said that the human haptic control should consist of a transfer function of the total inverse interaction dynamics.

In the original model, this transfer function had been approximated as a 2nd-

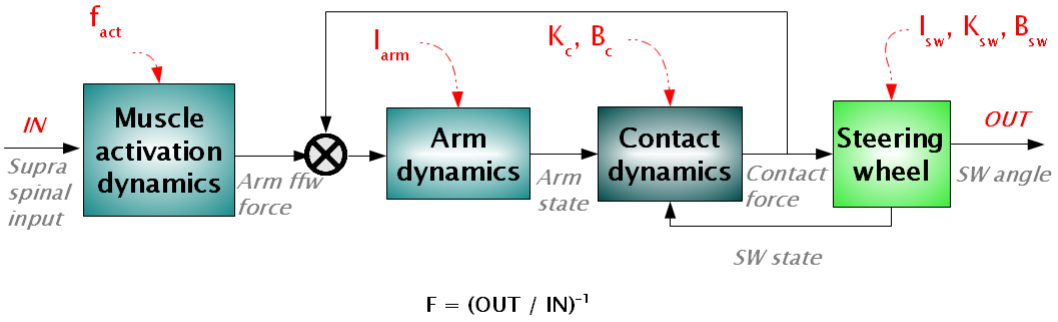

FIGURE 3.8: Model for the interaction Transfer Function

order low-pass filter which contained parameters from the operator feedforward NMS, which is the muscle activation dynamics, and from contact dynamics and steering wheel dynamics.
In this modeling study the inverse transfer function was analytically computed from the scheme in figure 3.8 that includes the following blocks:

- Operator feedforward NMS
- Contact dynamics
- Steering wheel dynamics

First the direct transfer function between operator torque and steering wheel angle has been mathematically computed from this scheme. Notice that the feedback and reflex part is not included in the scheme: the operator computes in feedforward the torque input to realize the optimal steering wheel angle and then the feedback activity is used to compensate for errors in the actual steering wheel angle. Equation (3.5) is the calculated inverse transfer function that links the optimal steering wheel angle as input to the correspondent feedforward signal as output. Notice that since the transfer function contains the grip parameters, two different transfer functions can be computed, one for a FT and the other for a PT.

$$\begin{aligned} F = \frac{1}{\pi^2(K_c + B_c s) f_{act}^2}((K_c(K_{sw} + s(B_{sw} + (I_{arm} + I_{sw})s))+ \\ s(I_{arm}s(K_{sw} + s(B_{sw} + I_{sw}s))+ \\ B_c(K_{sw} + s(B_{sw} + (I_{arm} + I_{sw})s))))(0.25s^2 + 0.7\pi s f_{act} + \pi^2 f_{act}^2)) \end{aligned} \tag{3.5}$$

Still this transfer function is not proper and it cannot be directly employed in the model. A filter must be added to its denominator to yield a strictly proper transfer function. The filter has been tuned in order to achieve a good compromise between minimization of the error between optimal and actual steering wheel angle and smoothness of the feedforward signal produced. In fact, the higher is the frequency of the filter poles, the closer the actual steering wheel angle will be to the optimal one. Still if that frequency is too high the feedforward signal will present high oscillations. Therefore a compromise must be found.
First a frequency power analysis has been performed on the optimal steering wheel angle. It has been employed the scheme *A. Manual control* in which the intrinsic feedback has been deactivated. The optimal steering wheel angles produced with the three road profiles of the first group has been analysed in their power content at different frequencies. In practice a Fast-Fourier transform has been applied in order to compute the frequency spectrum of the optimal steering wheel angle.

In figure 3.9 the spectrum for each one of the three road profiles is shown. It can be noticed that for the large turn and the lane change profiles the steering power is concentrated for frequency lower than 5 rad/sec, while for the obstacle avoidance profile there is still power up to 20 rad/sec.
In order to compare the steering wheel optimal and actual angles, an algorithm has been implemented to compute an average time-lag between those two variables. It has been observed that by employing the inverse transfer function the error

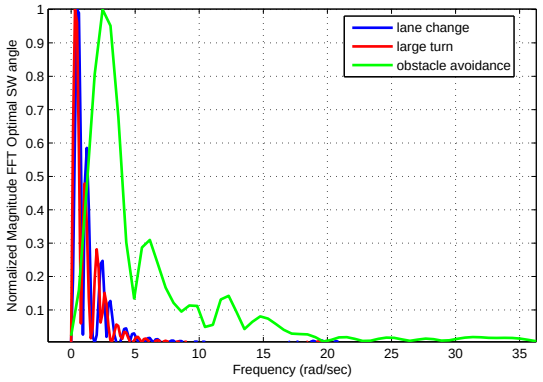

FIGURE 3.9: Steering Frequency Spectrum

between them consists mainly in a lag. There is also a small damping in the actual steering wheel angle but this is a negligible contribute to the error.
The filter on the inverse transfer function has been then tuned in order to obtain a good compromise between minimization of this average lag and smoothness of the feedforward signal. The filter has finally been chosen as in (3.6).

$$H = \frac{1}{(1 + s/5)(1 + s/30)^5} \tag{3.6}$$

It is composed of a low-frequency pole at 5 rad/sec and a high-frequency term at 30 rad/sec. This range of frequencies is in accordance with the optimal steering wheel angle spectrum power distribution of figure 3.9. This has been found to be an optimal choice for the three road profiles implemented. In figure 3.10 it is finally displayed the Bode diagram for the original inverse transfer function (not proper) and the filtered one, both for FT and PT.
An interesting observation can be made on the inverse transfer function. The

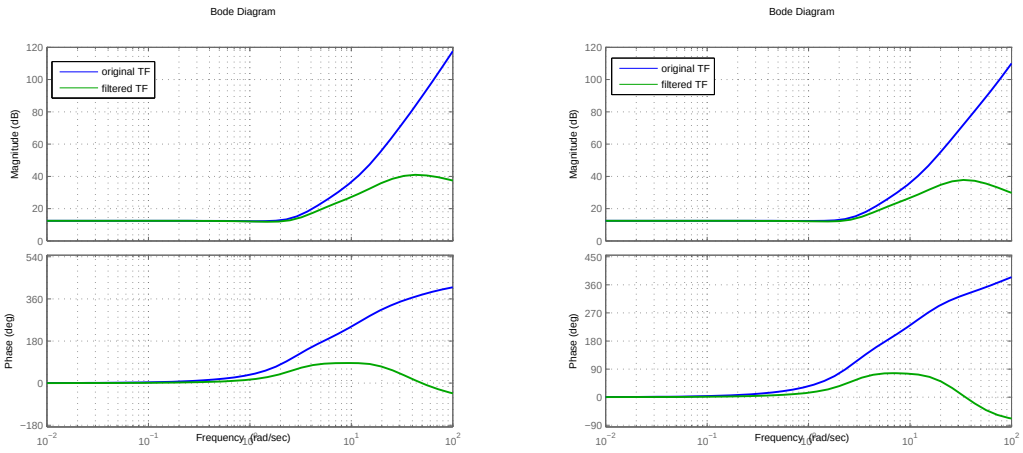

(a) Bode diagram of the inverse TF (FT)

(b) Bode diagram of the inverse TF (PT)

FIGURE 3.10: Bode diagram of the inverse TFs

continuous gain is exactly equal to the steering wheel stiffness. This means that in order to obtain a constant steering wheel angle it is sufficient to contrast the steering wheel stiffness only, neglecting the whole dynamics of the human NMS and that of the steering wheel itself.
The inverse interaction dynamics transfer function computed with this procedure is considered to be more reliable than the approximated one from the original scheme. In fact the procedure started with an analytical computation of the exact inverse transfer function, followed by a procedure of filtering to make it proper. Whereas in the original model the transfer function had been approximated in the first place without taking into account the control scheme from which it should be derived.

3.1.6 Internal models for feedback

As described in section 2.1.2, the human control signal is also composed of a feedback term. Regarding the intrinsic feedback, in the presented generic model it has been explained that the human operator reacts to uncertainties and disturbances to match the actual arm state with the predicted arm state computed by the Visual controller subsystem and this mechanism has been modelled as a spring-damper system.
In this section the Internal models of figure 3.11 that produce the input of the Intrinsic feedback are explained in detail. Basically this is the new part that has been added to the original Human operator model in order to study the behaviour of the shared control schemes in different situations.

The Internal interaction model, in detail in figure 3.12, represents the operator knowledge of the interaction between the human arm and the steering wheel. From this internal representation a predicted arm state can be computed. Notice that the steering wheel in this internal model has in input the human arm feedforward signal but may have in addition a predicted external force signal.

This additional input represents the human knowledge of an external device that is present in the actual system, for example a shared controller. When the operator is aware that an external signal is provided to the control interface, the arm position and velocity are predicted by using also the expected signal.

The torque external input comes from an internal model of the controller inside the human operator that is show in figure 3.13. This internal controller can be for instance chosen as the DHA controller but notice from figure 3.11 that its reference input is chosen equal to the operator reference. By including an internal model of the controller we can simulate a situation where the operator is aware that a shared controller is present and therefore no intrinsic feedback will arise if the actual controller has the same reference of the human operator that is if human and controller agree on the control goal. An uncertainty proportional gain can be set to the internal controller torque output in order to simulate different conditions. If this gain is set to 1, the internal controller output is equal to the actual controller output and no intrinsic feedback will be produced. This is the ideal situation when the operator exactly predicts the controller behaviour and no compensation is required. On the other side, a uncertainty gain of 0 can be

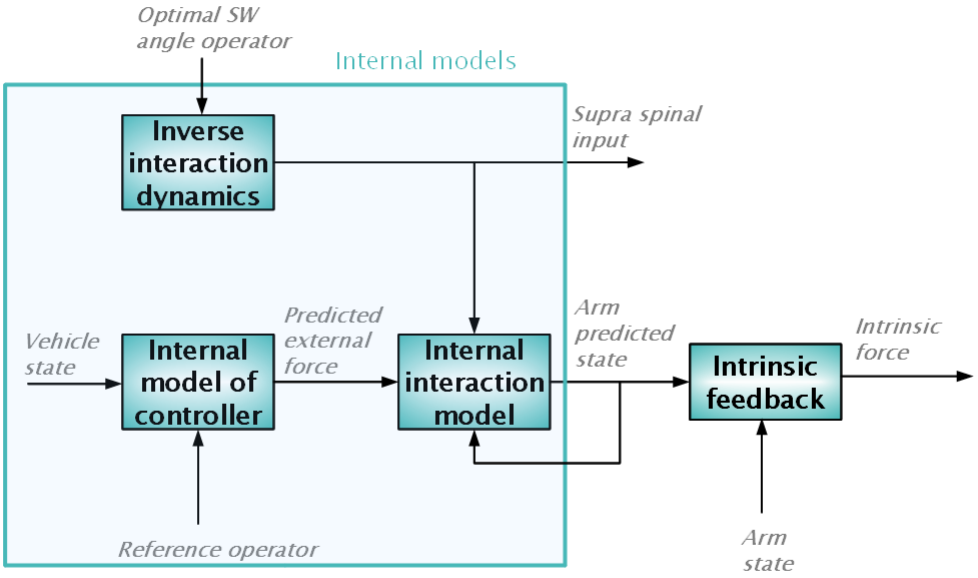

FIGURE 3.11: Internal models for feedback

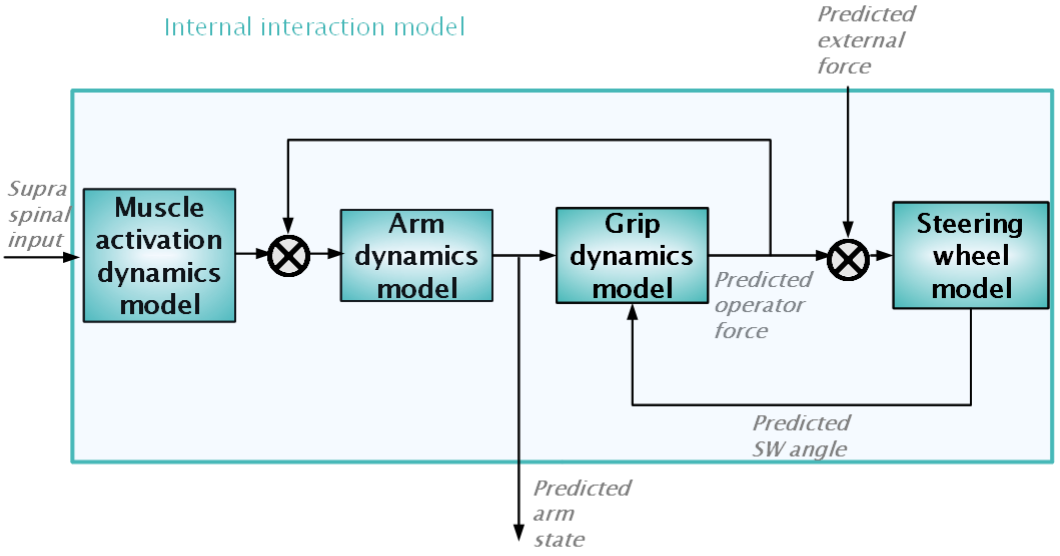

FIGURE 3.12: Internal interaction model

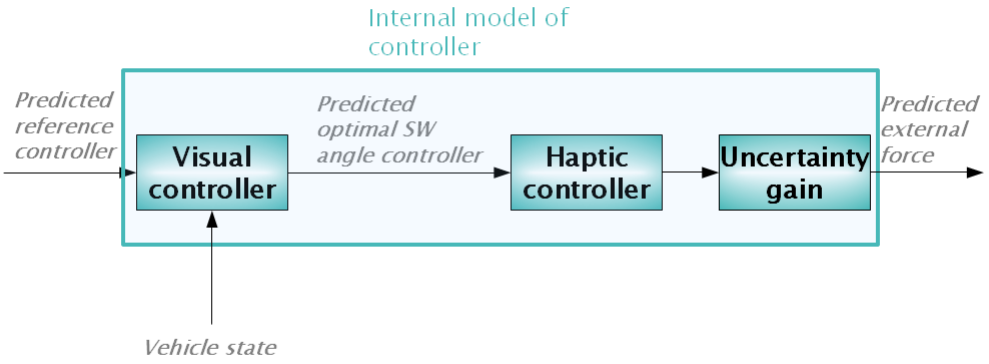

FIGURE 3.13: Internal model of controller

chosen to simulate a different condition where the driver voluntarily decides to react to the controller output and this way we can simulate a different task for the operator.
In section 2.2 two different haptic controllers have been introduced. The main difference between them lies in the kind of aiding they provide and the operator setting that must be chosen in order to follow the aiding.
Regarding the DHA controller, it has been explained that it provides an aiding signal that the human operator should give way to in order to get a benefit from it. The optimal setting for the human intrinsic feedback should therefore be a force task, namely giving way to forces during active guidance. In this FT it can be therefore assumed that the operator is aware of the controller aiding and does not want to fight with it. The uncertainty gain of the internal controller is then set to 1 for a FT. This way, if the controller reference matches the operator one there will no intrinsic feedback.
On the other side, in a position task the operator decides to contrast the controller aiding and maintain the steering wheel in an optimal position by considering only his own input, therefore the uncertainty gain of the internal controller is set to 0. This way in a PT there will be some intrinsic feedback present, also in case the reference trajectories of operator and shared controller are equal.
It has been explained that IHA controller provides a signal in a form of disturbance. Therefore, the uncertainty gain has been set to 0 both for a FT and PT. This way, the operator decides to react to the force feedback in both cases and what changes between them is the intensity of the resistance.
This is summarized in table 3.1.

TABLE 3.1: Uncertainty gains on the Internal model of controller

	FT	PT
DHA	1	0
IHA	0	0

3.1.7 Visual subsystem operator and controllers settings

The Visual blocks of operator (2.1), DHA shared controller (2.3) and IHA controller (2.5) have been chosen with the same parameters. This way, in case operator and shared controller agree on the reference trajectory of the vehicle to follow, the optimal steering wheel angles produced will also be equal. With this assumption, which removes one unnecessary degree of freedom, the systems behave in such a way that a clear analysis can be performed. The Visual block parameters were set so to ensure the stability of the systems with the employed road profiles:

- look-ahead time of the Predictor (figure 2.5): $TLH = 1\,sec$
- gain on the future lateral error: $P_{1,hum} = P_{1,DHA} = P_{1,IHA} = 1\,rad/m$
- gain on the future heading error: $P_{2,hum} = P_{2,DHA} = P_{2,IHA} = 0.01$

3.1.8 Haptic subsystem controllers settings

The Haptic block of the controller must still be tuned in a shared control fashion. This means that the controller should be given a limited control energy so to allow the operator to potentially override the controller torque on the steering wheel. Therefore, the haptic control gain has been tuned in a scheme where operator and DHA controller were present, that is scheme *B.Operator-DHA shared control*. The gain of (2.4) was chosen $G_{DHA} = 1N/rad$ and the torque signals are shown in figure 3.14 in a sample test. Notice that this gain is about equal to one forth of the continuous gain of the inverse transfer function in the operator haptic subsystem. The same gain has been chosen for the IHA (2.6) in order to make the comparison with DHA as clearest as possible, $G_{IHA} = 1\,N/rad$.

3.2 Results of the computer simulation

In this section the shared control schemes implemented in Simulink are tested with the introduced road profiles and settings. The tests performed in simulation allow to reach a higher understanding of the behaviour of the human-machine system under different driving conditions and what changes when the operator decides to give way to the force feedback or to contrast it. Some experimental hypotheses will come out from these results to be tested with an experimental campaign.

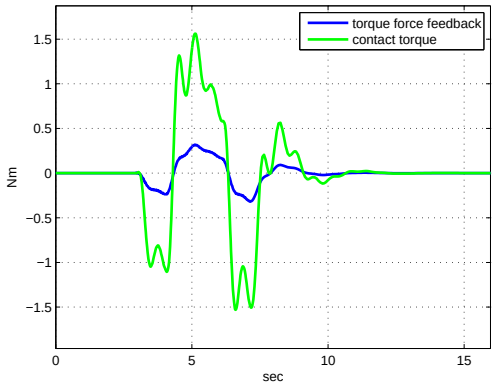

FIGURE 3.14: Comparison between operator contact torque and controller torque

3.2.1 Manual control

First of all the scheme *A. Manual control* is tested to show how the operator is able to guide a vehicle in ideal conditions where no uncertainties and disturbances are present. In a second test a torque disturbance is added on the steering wheel to investigate on how the NMS setting can influence performance in this case.
As mentioned before, when the operator has full knowledge of the system to control and there are no additional disturbances it is possible to guide the vehicle in a feedforward fashion. The operator calculates in a closed loop the torque input to provide on the steering wheel through visual feedback and prediction of the future error of the vehicle with respect to the road reference.
In a first test, the lane change profile is employed. The NMS can be set to a FT or PT. What changes between FT and PT in this case is just the inverse transfer function and the grip parameters. In figure 3.15 are shown the results for a FT setting and in figure 3.16 for a PT setting. First notice that the supra-spinal input signals of figures 3.15a-3.16a are more noisy than the correspondent torque signals from figures 3.15b-3.16b and this is because the supra spinal input passes through the muscle activation dynamics function that works as a low-pass filter. Secondly, from figures 3.15c-3.16c it can be observed that the feedback torque is zero in both cases. In figures 3.15d-3.16d are displayed the steering wheel and arm angles. The main difference between FT and PT is the arm angle with respect to the steering wheel angle, with a 0.01 rad slip between them relative to a 0.045 rad maximum steering wheel angle in a FT setting and virtually no slip in PT. However, this difference does not affect performance: the actual steering wheel angle is close to the optimal one in both FT and PT (figures 3.15e-3.16e) and also the reference following is guaranteed in both cases (figures 3.15f-3.16f). In figure 3.17 the errors between the vehicle center of gravity Y-position and the Y-reference are compared in FT and PT. Notice that there is no actual difference in performance.
If there is an external torque signal on the steering wheel the operator will react with a feedback force to bring back his arm to the desired position. This is because an external noise is an unpredictable signal not included in the operator internal model and therefore a normal reaction will be to reject it.

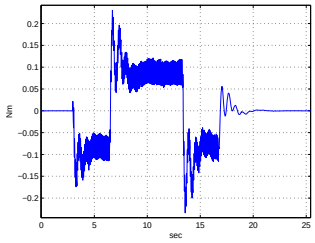

(a) Supra spinal input

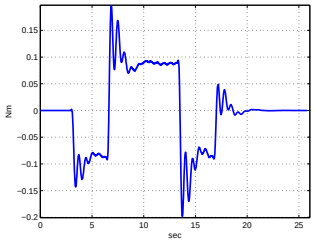

(b) Operator torque

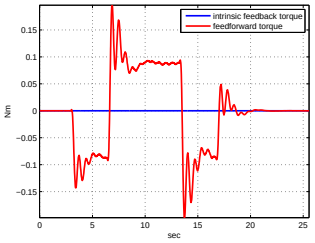

(c) Operator FFW-FB torques

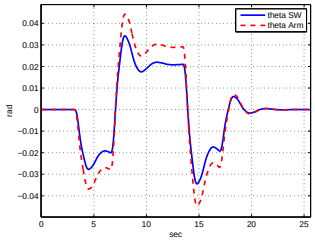

(d) Arm angle

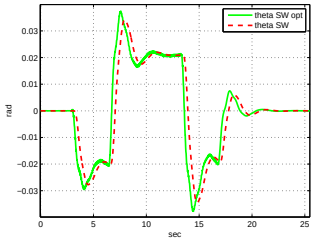

(e) SW angle

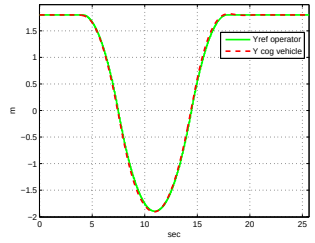

(f) Reference following

FIGURE 3.15: Manual control (FT) in lane change

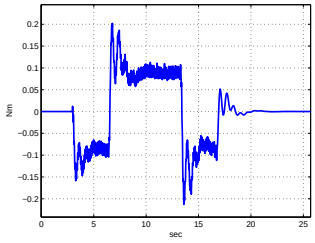

(a) Supra spinal input

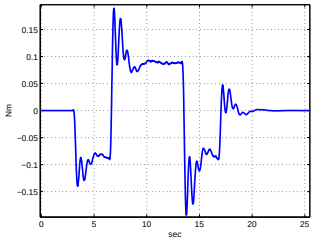

(b) Operator torque

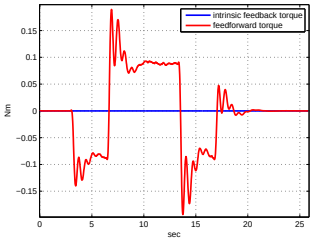

(c) Operator FFW-FB torques

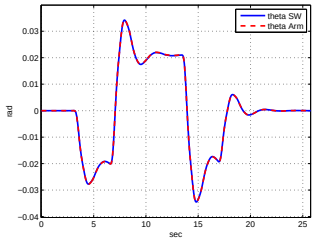

(d) Arm angle

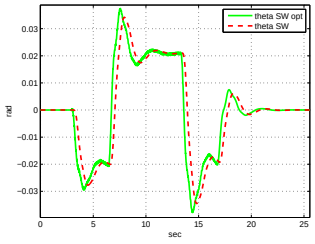

(e) SW angle

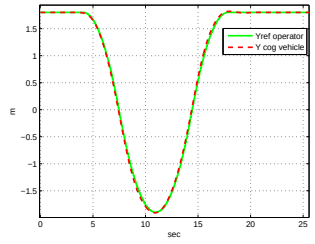

(f) Reference following

FIGURE 3.16: Manual control (PT) in lane change

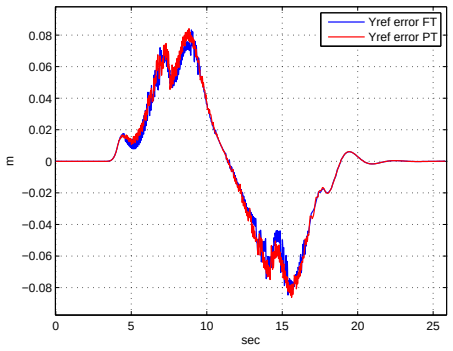

FIGURE 3.17: Manual control comparison FT-PT in lane change

In this second test, a noise signal on the steering wheel has been generated to simulate a lateral wind disturbance on the car. The employed road profiles is a large turn. In figures 3.18 and 3.19 are shown plots for FT and PT respectively.

The total torques are displayed in figures 3.18a-3.19a. Notice the presence of

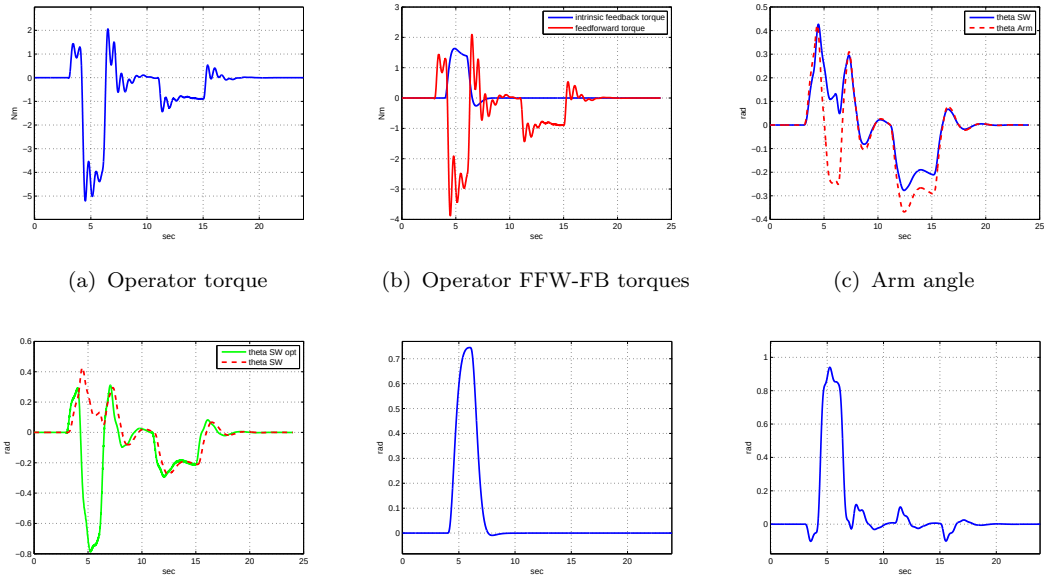

(a) Operator torque (b) Operator FFW-FB torques (c) Arm angle

(d) SW angle (e) Error arm angle (f) Error SW angle

FIGURE 3.18: Manual control (FT) in lane change with disturbance

a feedback torque in this case due to the disturbance and the higher feedback in PT (figures 3.18b-3.19b). In figures 3.18c-3.19c-3.18d-3.19d are displayed optimal steering wheel angles, actual angles and arm angles. The slip between arm angle and steering wheel angle, as well as the error between optimal and current wheel angle are lower in PT (figures 3.18c-3.19c-3.18d-3.19d). It can be observed from figure 3.20a that the reference following error for PT is lower. The comparisons for FT and PT of steering wheel errors and torques are displayed respectively in figures 3.20b-3.20c. It can be concluded that when a torque disturbance on the steering wheel is present it is convenient to adopt a position task in order to reject the noise and optimize road following performance.

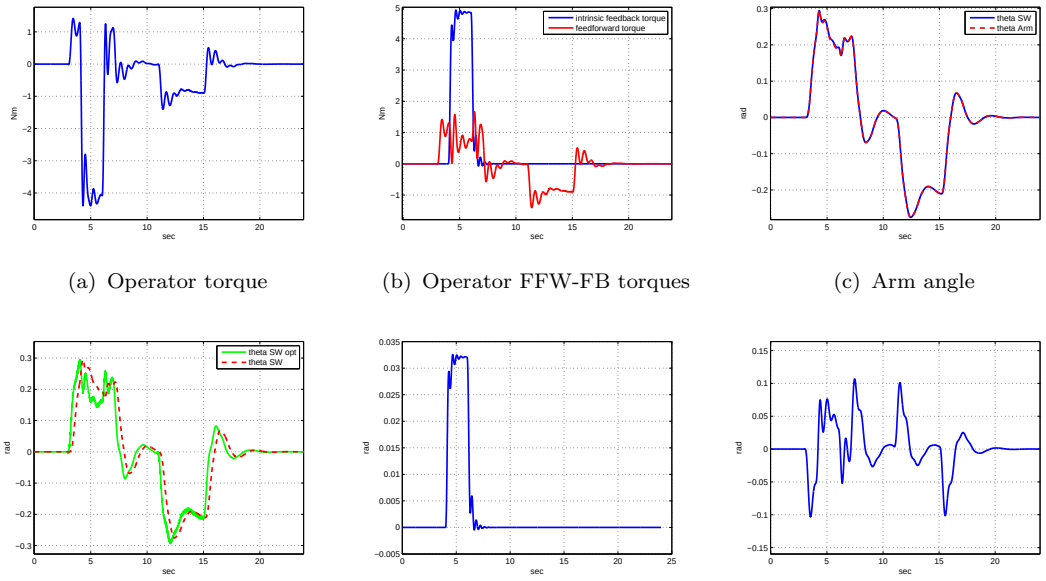

(a) Operator torque (b) Operator FFW-FB torques (c) Arm angle

(d) SW angle (e) Error arm angle (f) Error SW angle

FIGURE 3.19: Manual control (PT) in lane change with disturbance

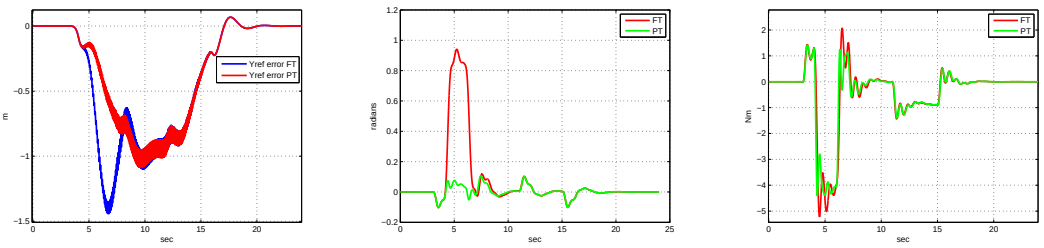

(a) Reference following errors (b) SW angle errors (c) Operator torques

FIGURE 3.20: Manual control comparison FT-PT in lane change with disturbance

3.2.2 Manual control-DHA-IHA

After the manual control behaviour has been tested, manual control is compared to shared control with DHA and IHA in this section. An obstacle avoidance road profile is employed. First the behaviour of DHA and IHA is analysed separately with different NMS settings. The internal model of the controller is set as explained in section 3.1.6. Finally a comparison will be made between manual control and shared control.

First the DHA controller is tested in a shared control scheme. In figures 3.21-3.22 are shown plots for shared control with DHA in FT a PT for the operator NMS respectively. First notice that in FT there is no intrinsic feedback, where the operator decides to give way to the force feedback from the controller, while in PT there is resistance to it (figures 3.21a-3.22a). The optimal and actual steering wheel angles are displayed in figures 3.21b-3.22b. Operator and controller torques

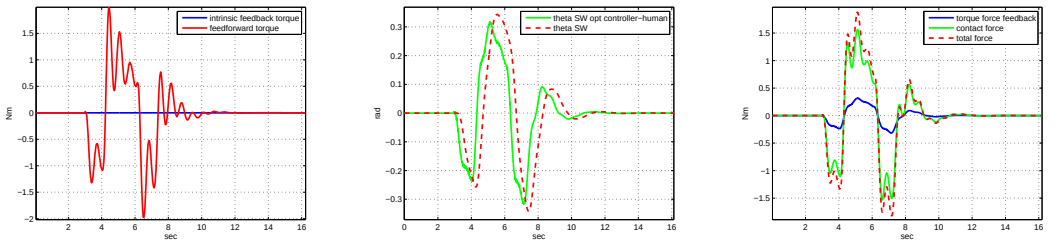

(a) Operator FFW-FB torques (b) SW angle (c) Operator and controller torques

FIGURE 3.21: DHA shared control (FT) in obstacle avoidance

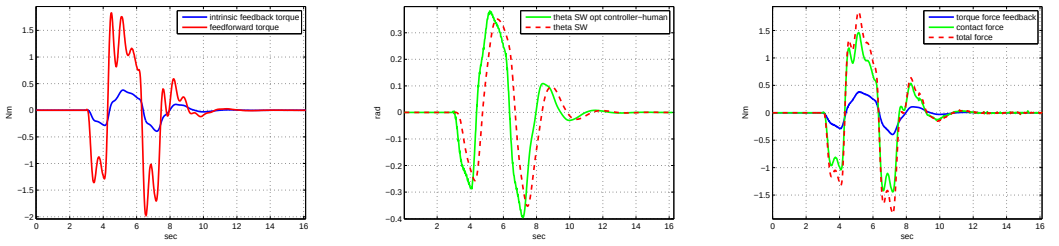

(a) Operator FFW-FB torques (b) SW angle (c) Operator and controller torques

FIGURE 3.22: DHA shared control (PT) in obstacle avoidance

are shown in figures 3.21c-3.22c, notice the lower controller power compared to the operator one. The total torque, which determines the steering action and consequently the vehicle behaviour, is obtained by adding up operator torque and controller torque. If we compare the Y-reference errors for FT and PT (figure

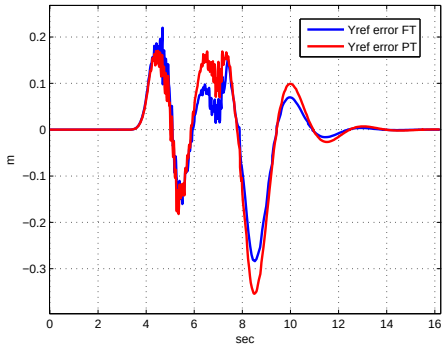

FIGURE 3.23: DHA shared control comparison FT-PT in obstacle avoidance

3.23) it can be seen that for a FT the error is slightly lower than PT, this meaning that it is convenient for the operator with DHA shared control to adopt a FT by giving way to the controller torques instead of resisting to it with some muscle co-contraction. The Y-reference following is shown for FT in figure 3.24.
Secondly, the IHA controller behaviour is analysed in a shared control scheme. In figures 3.25 and 3.26 results are shown for IHA in FT and PT of the operator NMS respectively. Notice from figures 3.25a-3.26a that some intrinsic feedback is

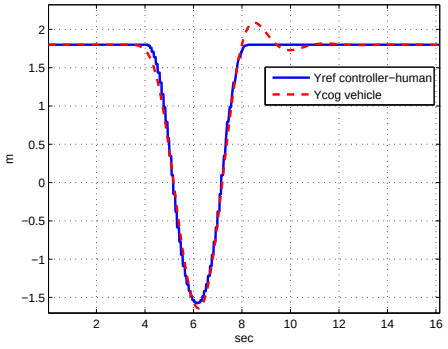

FIGURE 3.24: DHA shared control (FT) in obstacle avoidance

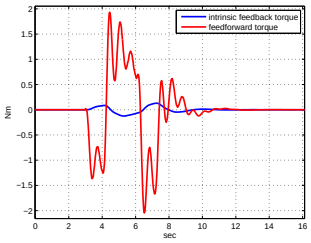

(a) Operator FFW-FB torques

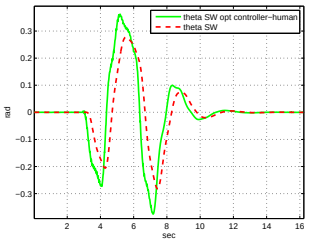

(b) SW angle

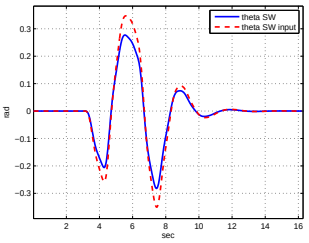

(c) Input angle

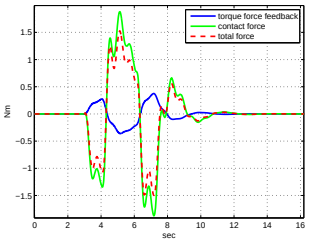

(d) Operator and controller torques

FIGURE 3.25: IHA shared control (FT) in obstacle avoidance

always present because the operator is interpreting the controller aiding in a form of disturbance that must be rejected. Intrinsic feedback is higher for a PT. Optimal and actual steering wheel angles are shown in figures 3.25b-3.26b. However, it is more interesting to compare the actual steering wheel angle and the angle that goes in input to the vehicle after the correction realized with the IHA approach (figures 3.25c-3.26c). Notice that the actual steering wheel angle is lower than the input angle. This is the fundamental principle of the IHA approach: the operator has to resist to the controller torque by keeping the steering wheel closer to the central position, therefore the steering wheel angle that is produced is lower than in manual control or with DHA. The current steering wheel angle is then amplified by the final correction before going in input to the vehicle. Operator and controller torques are displayed in figures 3.25d-3.26d. Notice here with IHA that the controller torque is always opposite in sign to the operator torque, in contrast with the behaviour of DHA (figures 3.21c-reffig:res3f) where they have

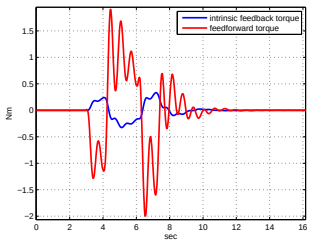

(a) Operator FFW-FB torques

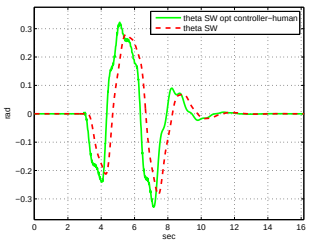

(b) SW angle

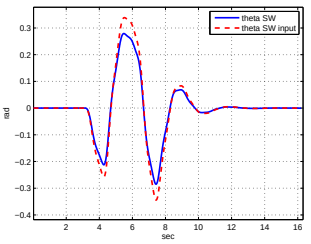

(c) Input angle

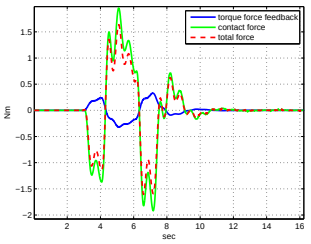

(d) Operator and controller torques

FIGURE 3.26: IHA shared control (PT) in obstacle avoidance

the same sign. It can be observed from figure 3.27 that the Y-reference error is

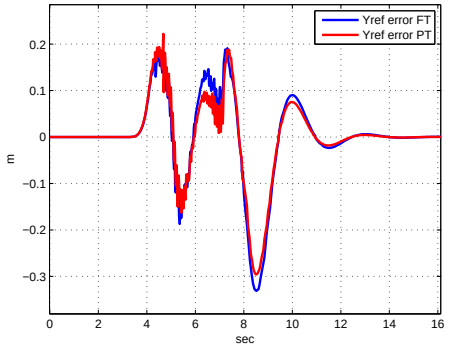

FIGURE 3.27: IHA shared control comparison FT-PT in obstacle avoidance

lower for a PT. It is convenient for the operator to adopt a PT and resist with more co-contraction to the controller torque in order to actually follow the aiding. In figure 3.28 it is shown the Y-reference trajectory for a PT.
A final comparison can be made between results with manual control, DHA (FT) and IHA (PT) to emphasize the characteristics of these approaches and how they affect performance and workload. In figure 3.29a it is shown the comparison of the Y-reference errors in the three cases. It can be noticed that performance for DHA and IHA is similar and slightly better than with manual control. In figure 3.29b the operator torque signals are compared. With DHA the required workload from the operator is the lowest among the three cases. The controller is indeed directly helping the operator with the torque signal on the steering wheel and so part of the workload is produced by the DHA controller. With manual control the workload stays in between DHA and IHA. With IHA the human torque is slightly

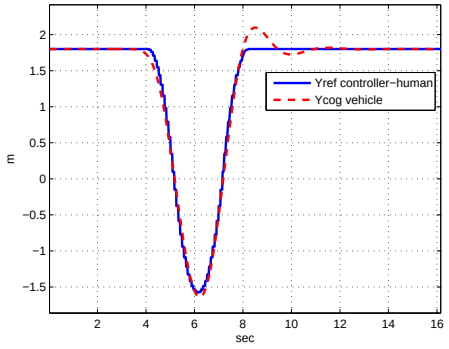

FIGURE 3.28: IHA shared control (PT) in obstacle avoidance

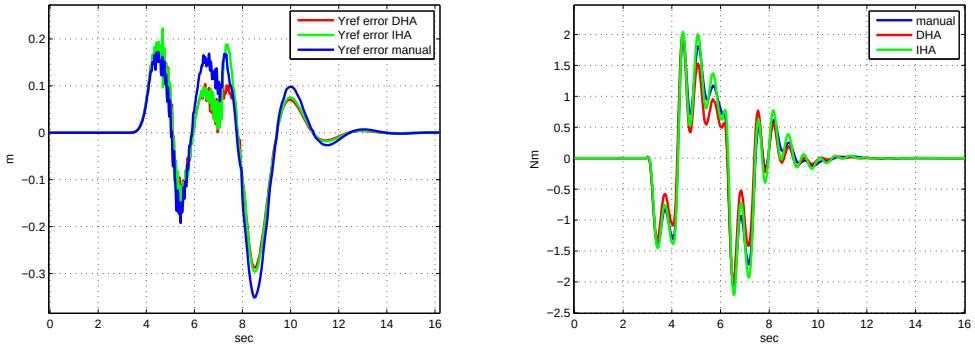

(a) Reference following errors

(b) Operator torques

FIGURE 3.29: Comparison manual control-DHA-IHA in obstacle avoidance

higher than with manual control: the operator has to resist to the controller signal to actually follow the aiding and this requires more power than manual driving.

3.2.3 Manual control-DHA-IHA with operator low visibility

In this section the shared control schemes are tested for the lane change profile with low visibility for the operator. The operator should exploit the force feedback from the shared controller that in this situation is more accurate than his own visual feedback.

First the DHA controller is employed with FT and PT settings for the human NMS. Results are displayed in figures 3.30-3.31.
In figures 3.30a-3.31a are shown optimal and actual steering wheel angles for FT and PT respectively. It can be observed that in a PT the actual steering wheel angle is closer to the optimal one of the operator. In figures 3.30b-3.31b operator and controller torques are displayed. It is interesting to look at the comparison plots of Y-reference following and operator torque of figure 3.32. With a FT the controller reference is better followed (lower error) than with PT in this case. This

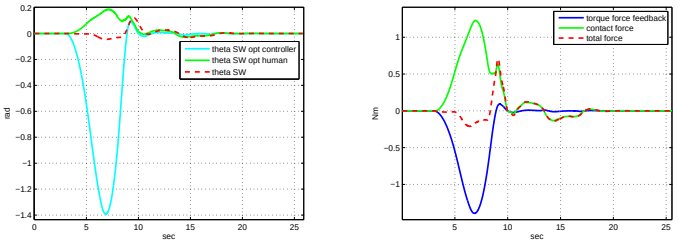

(a) SW angle (b) Operator and controller torques

FIGURE 3.30: DHA shared control (FT) in lane change with low visibility

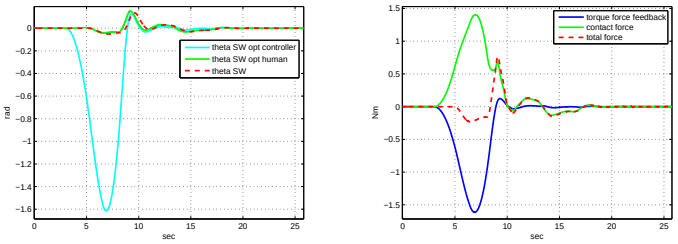

(a) SW angle (b) Operator and controller torques

FIGURE 3.31: DHA shared control (PT) in lane change with low visibility

means that in a situations of low visibility it is convenient to adopt a FT with DHA by giving way to the controller forces in order to follow the aiding. What happens is that the operator has a delay in detecting the obstacle. The controller torque feedback is helpful since it allows the operator to feel the obstacle in advance to seeing it. The controller can guarantee in this situation a safer maneuver, provided that the driver follows the aiding. Furthermore, as it can be seen from figure 3.32b with a FT the required workload from the operator is lower and this also yields better performance in this situation.
The IHA controller has also been tested in the same condition of operator low visual feedback. In figures 3.33a-3.34a are shown optimal and actual steering wheel angles for FT and PT respectively. Again in a PT the actual steering wheel angle is closer to the optimal one of the operator. In figures 3.33b-3.34b are displayed the input angles to the vehicle. In figures 3.33c-3.34c operator and controller torques are plotted. Regarding performance, it can be observed from figure 3.35a that with PT the operator is more able to follow the controller aiding according to the IHA functioning. Moreover, the operator torque is also slightly lower with a PT as it can be observed from figure 3.35b. It is possible to compare in a final plot 3.36 the controller reference following for manual control, DHA (FT) and IHA (PT) shared control. Performance with both DHA and IHA is higher than for manual control. The force feedback from both the shared controllers allow the operator to compensate for his own bad visual feedback. Whereas, in manual control the operator follows his own reference and the whole visual delay is maintained.

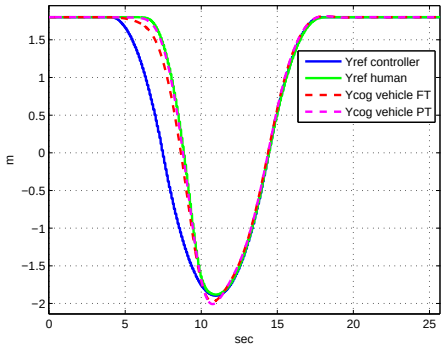

(a) Reference following

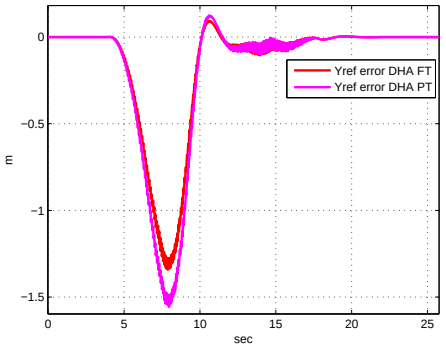

(b) Error to controller reference

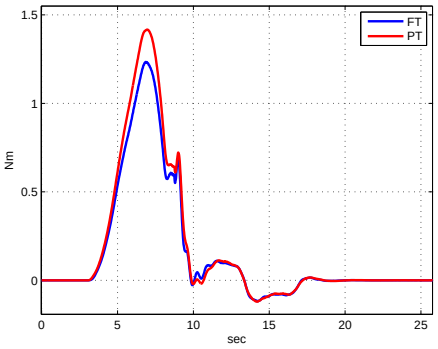

(c) Operator torques

FIGURE 3.32: DHA shared control comparison FT-PT in lane change with low visibility

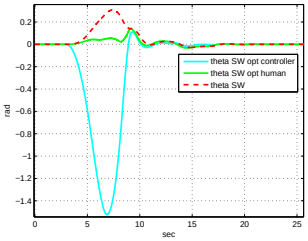

(a) SW angle

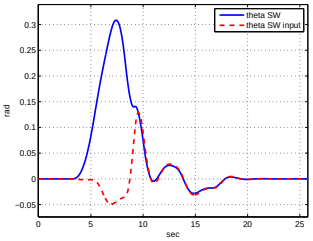

(b) Input angle

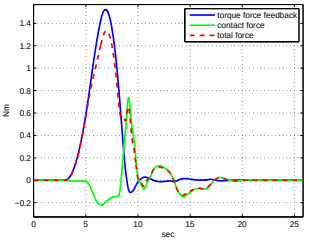

(c) Human and controller torques

FIGURE 3.33: IHA shared control (FT) in lane change with low visibility

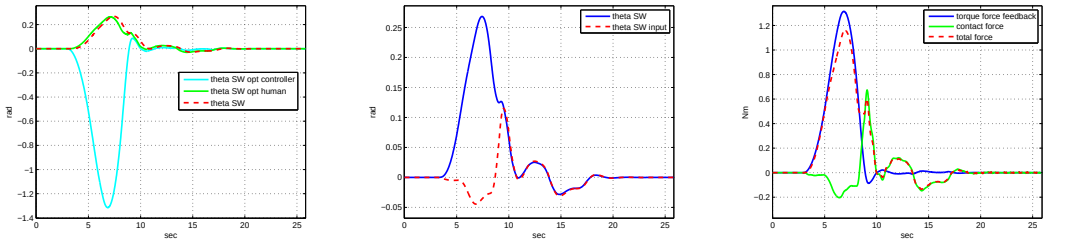

(a) SW angle (b) Input angle (c) Operator and controller torques

FIGURE 3.34: IHA shared control (PT) in lane change with low visibility

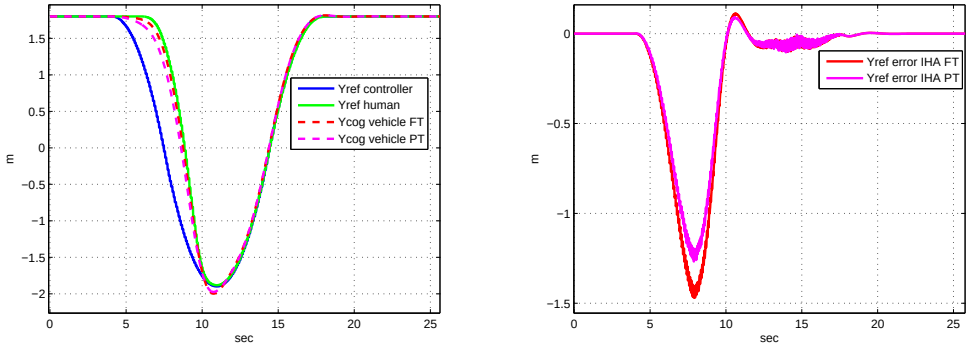

(a) Reference following (b) Error to controller reference

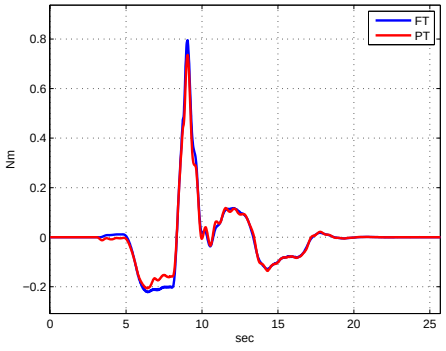

(c) Operator torques

FIGURE 3.35: IHA shared control comparison FT-PT in lane change with low visibility

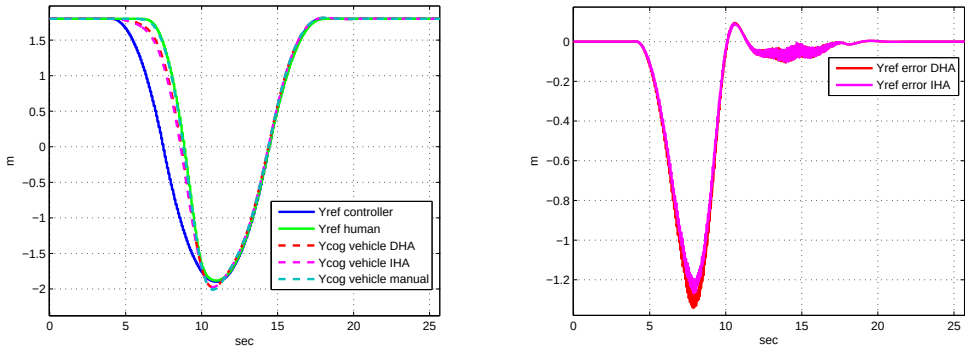

(a) Reference following (b) Error to controller reference

FIGURE 3.36: Comparison manual control-DHA-IHA in lane change with low visibility

3.2.4 DHA-IHA with controller error

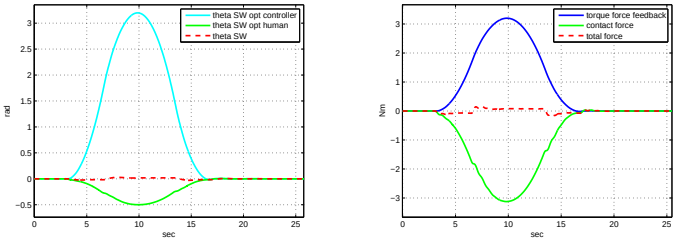

(a) SW angle (b) Operator and controller torques

FIGURE 3.37: DHA shared control (FT) in lane change with controller error

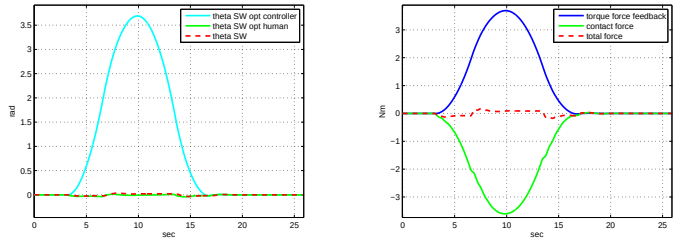

(a) SW angle (b) Operator and controller torques

FIGURE 3.38: DHA shared control (PT) in lane change with controller error

In this final section the lane change profile with controller error is tested with DHA and IHA shared control schemes. This time the situation is opposite to that of lane change with operator low visibility. The controller does not detect the obstacle. Therefore, the operator should resist to the force feedback in order to reject the error and ensure a successful evasive maneuver.
First the DHA controller is tested with FT and PT settings for the operator NMS. In figures 3.37a-3.38a are displayed optimal and actual steering wheel angles. In a

PT the actual steering wheel angle is closer to the operator optimal one. In figures 3.37b-3.38b operator and controller torques are displayed. Regarding performance

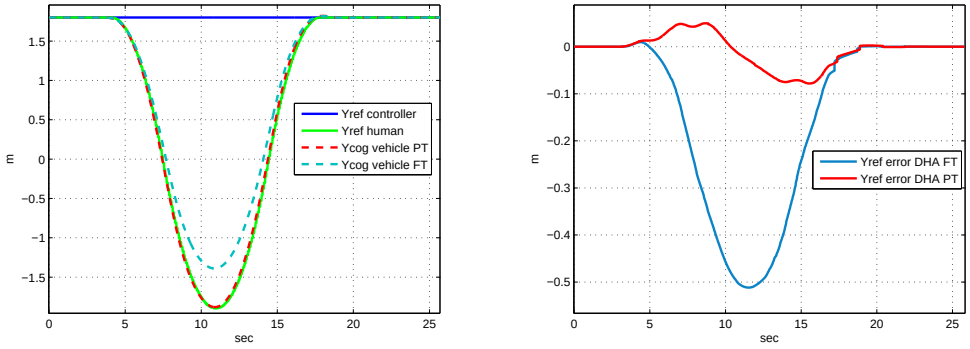

(a) Reference following

(b) Error to operator reference

FIGURE 3.39: DHA shared control comparison FT-PT in lane change with controller error

of figure 3.39, with PT the vehicle is better following the operator reference by rejecting the error in the controller reference. Therefore, in this situation it is convenient to resist to the faulty feedback from the DHA shared controller.

If we look at the torque comparison plot of figure 3.40 it can be realized that with

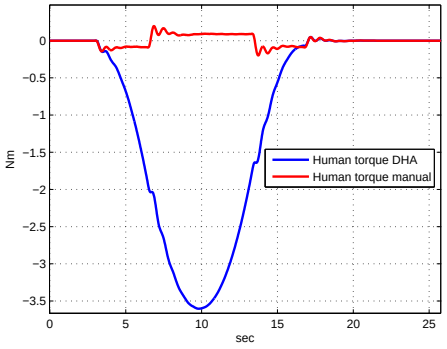

FIGURE 3.40: Comparison manual control-DHA in lane change with controller error

DHA in case of error the torque input from the operator to reject the error is much higher to the torque in case of DHA controller in normal conditions and with the same lane change road profile. This is a critical point for the DHA working in this condition: a high force required from the operator to reject the controller faulty feedback.

Secondly, the IHA controller is tested. In figures 3.41a-3.42a are displayed optimal and actual steering wheel angles and in figures 3.41b-3.42b the input steering angle to the vehicle. In figures 3.41c-3.42c are plotted operator and controller torques.

It can be noticed from figure 3.43 that with FT performance is higher: the vehicle trajectory is closer to the operator reference. What happens is the exact opposite of the situation with a DHA error. In order to reject the wrong aiding, with IHA

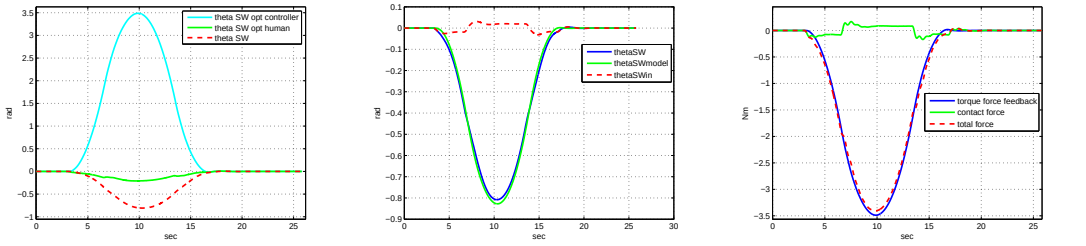

(a) SW angle (b) Input angle (c) Operator and controller torques

FIGURE 3.41: IHA shared control (FT) in lane change with controller error

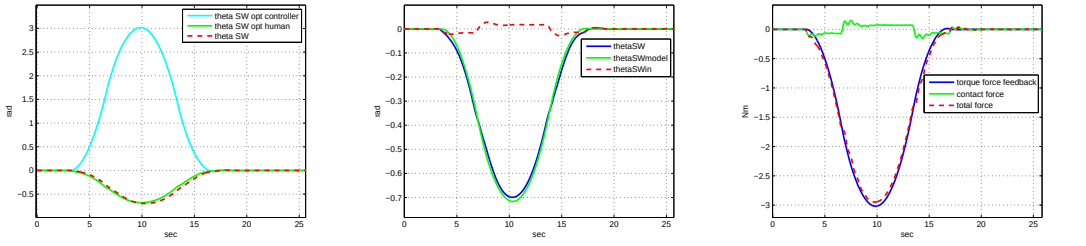

(a) SW angle (b) Input angle (c) Operator and controller torques

FIGURE 3.42: IHA shared control (PT) in lane change with controller error

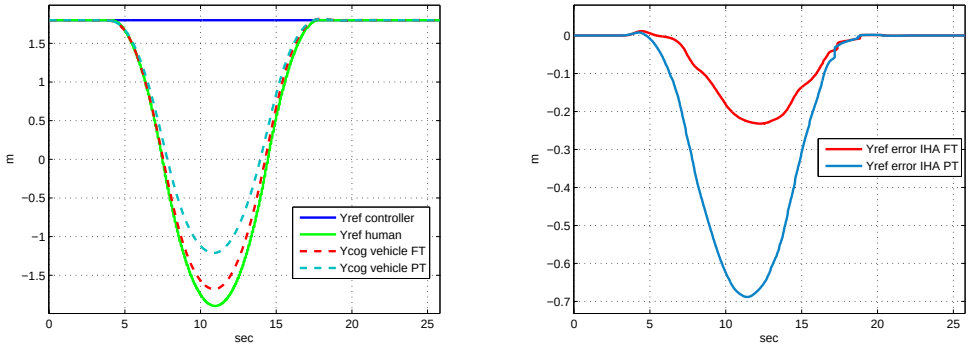

(a) Reference following (b) Error to operator reference

FIGURE 3.43: IHA shared control comparison FT-PT in lane change with controller error

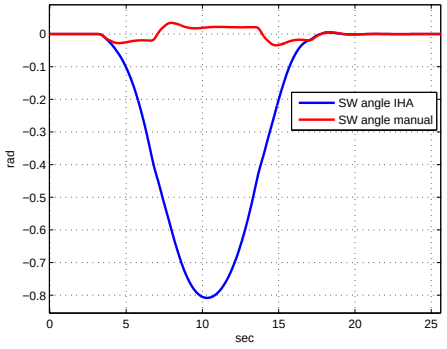

FIGURE 3.44: Comparison manual control-IHA in lane change with controller error

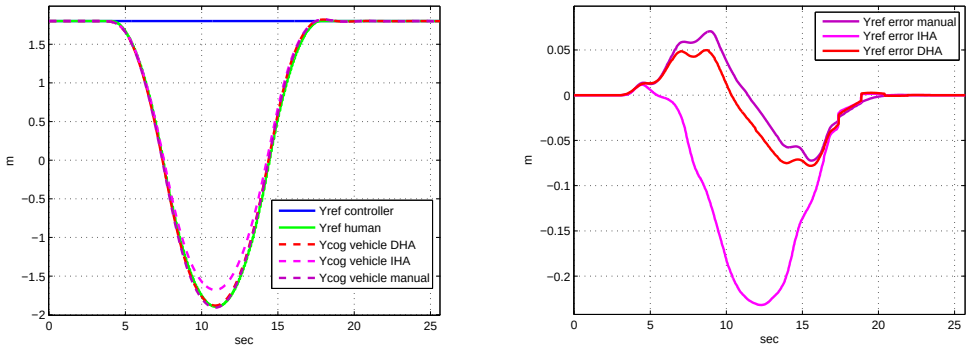

(a) Reference following

(b) Error to operator reference

FIGURE 3.45: Comparison manual control-DHA-IHA in lane change with controller error

a FT must be adopted. The more slack the grip is, the less control energy will come from the shared controller into the system dynamics. With DHA it has been observed a critical behaviour in terms of operator torque required. With the IHA the operator input in case of error is similar to the one in case of normal conditions. However, a critical behaviour can be observed in the actual steering wheel angle. In this case the steering wheel angle is much higher than the one in normal conditions (figure 3.44) and this is the critical point for IHA in case of error.
Finally in figure 3.45 reference following performances are compared to manual control. The worst performance is obtained with IHA (FT), while performance with DHA (PT) and manual control are close to each other. It can be argued that with IHA, even if the operator muscular co-contraction is low, a certain amount of the total control energy from the controller still enters the system dynamics. Therefore, a faulty IHA controller will influence the evasive maneuver more than a faulty DHA. Whereas with DHA it is sufficient to maintain resist to the force feedback in case of error and almost the whole control energy from the controller will be rejected.

3.3 Recommendations and Conclusions

Before going through the next chapter a clarification must be done on the model employed. In section 2.1.2 the Human operator model was introduced along with the description of the intrinsic feedback mechanism. The intrinsic feedback and grip parameters have been identified in previous experiments [8] where the driver was blindfolded and had to give way to or contrast torque disturbances presented on the SW. The model employed in this analysis contains an intrinsic feedback mechanism which was set between the current arm state and an arm state predicted from an Internal interaction model, also including an Internal model of controller possibly. The new model is very promising in the study of the human behaviour with a shared controller but has not been validated yet. Therefore, the results cannot be considered numerically reliable. In particular, it can be argued that a change in the muscular co-contraction activity from FT to PT should yield a higher difference in the results than that obtained in the situations investigated (normal functioning of DHA and IHA, operator low visibility, error in the controller reference).
However, the modeling study allowed us to understand the behaviour of these shared control systems with more insight. Different driving conditions were investigated with a particular focus on the operator approach in dealing with the shared controller, that is deciding to give way to the force feedback or resist to it. The outcome of this study is the starting point for setting up a Human-Factor experiment.

Chapter 4

Design of an experiment on HSC for curve negotiation

4.1 Experimental hypotheses

The modeling study, where two haptic control strategies were tested in different driving conditions, allowed us to get a better insight of the functioning of these systems in relation to the operator behaviour.
From the results of the modelled systems, some hypotheses can be stated for a Human-Factor experiment. However, notice that in the Simulink models employed the operator is modelled with a static behaviour (Force task or Position task) with no transitory effects due to human adaptation to the system. Therefore, the experimental hypotheses are based both on the modeling study and on other foreseen effects that cannot be obtained from the current model.
In the experimental hypotheses three main properties are used to compare DHA, IHA and Manual Control, that are:

- Performance
- Control activity
- Control effort

These are general concepts that can be used to describe both the vehicle and the operator behaviour in a curve negotiation task. *Performance* can be defined in a general way as how well the vehicle is following the desired trajectory. On the other side, *Control activity* refers to the mental effort from the operator to control the vehicle, while *Control effort* can be defined as the driver physical effort during the maneuvers. In the first section of chapter 5, statistical metrics will be introduced as measurements of these general properties for this specific experiment.

4.1.1 Normal visibility

From previous studies [3], the benefits of a Direct Controller have been proven in a condition where the operator is driving with normal road visibility. The positive outcome was a reduced control activity and slightly higher performance with respect to Manual Control of the vehicle. However, a higher control effort had been found with DHA, result which was pointed out to be controversial and yet not fully understood.
In section 3.2.2, DHA and IHA have been tested with a computer simulation in a full visibility condition where the operator agrees with the shared controller on the reference trajectory to follow. The optimal NMS setting found for the operator model is a FT for DHA, that is giving way to feedback forces, and PT for IHA that is resisting the forces from the controller. With a shared controller, reference trajectory following (performance) seems to be slightly improved with respect to Manual Control (figure 3.29a). Regarding the level of operator torque required (control effort), the least effort is produced with DHA while the largest one is with IHA (figure 3.29b).
Having introduced a different approach in shared control, that is the Indirect Controller, firstly we want to compare it to the Direct Controller and Manual Control in a normal condition with full visibility to show if same benefits as the ones obtained with DHA in [3] can be also obtained with IHA.
The first hypothesis is:

A)*In a normal visibility condition, with the DHA support better performance than Manual control and lower control activity/effort can be achieved. With the IHA support, better performance and lower control activity than Manual control are expected, but higher control effort.*

4.1.2 Low visibility

In section 3.2.3 a situation of low visibility of the operator has been tested in computer simulation. This has been modelled as a delay of the reference trajectory of the operator with respect to the shared controller trajectory, in case of a lane change maneuver. Again the optimal NMS setting for the operator was found to be FT for DHA and PT for IHA. This means that with DHA the operator has to employ the force feedback, which is in advance to the operator visual feedback due to the low visibility, and give way to it. The same goes for IHA except that the operator has to contrast the force feedback in order to actually follow the aiding. The results found tell us that performance is improved with a shared controller (figure 3.36). Moreover, it can be expected that control activity/effort is reduced with a shared controller with respect to Manual Control. In fact, when visual feedback is low and there is no haptic feedback available, sudden steering maneuvers are likely to occur in response to curves and also straight roads not seen well. The second hypothesis is:

B) *In a condition of low visibility, the operator can achieve better performance and lower control activity/effort with a shared controller than with Manual control.*

4.1.3 Controller error

A situation of controller error has been tested in section 3.2.4 with a computer simulation. The controller is not detecting an obstacle on the right lane so its reference is a straight trajectory, while the operator decides to switch to the left lane to avoid the obstacle.
With DHA the operator NMS setting for the controller error rejection is a PT, that is contrasting the faulty aiding. In this case the operator torque required to change lane and contrast the controller is much higher than in Manual control for the same lane change task, as observed in figure 3.40. On the other side, with IHA the best NMS setting for error rejection is a FT that is giving way to the faulty feedback. However, the drawback is a steering wheel angle much higher than the one in Manual control for the same lane change task, as we can see in figure 3.44. From figure 3.45 it can be observed that performance in the lane change maneuver degrades with a shared controller.
However, with the current model it is not possible to predict all the possible reactions of the operator to a controller error. For example, the vehicle trajectory can be badly influenced by the critical condition found with DHA and IHA and get too close to the obstacle. It is therefore interesting to investigate a controller error in simulated car driving to show if the operator is able to change lane by contrasting the faulty support.
The third hypothesis is:

C) *An evasive maneuver can be endangered by a faulty support providing a wrong reference trajectory, due to a critical condition in force or SW angle that will arise with DHA and IHA respectively.*

4.1.4 Adaptation and After-effects

The current model cannot be employed to make previsions on how the operator will adapt to the haptic support system. In particular, some after effects are likely to be observed if the driver is used to drive with the support system and at some point the support is switched off.
Drivers used to DHA generally tend to put less effort on the SW to maneuver the vehicle since part of the total required effort is directly provided by the controller. Therefore, a possible negative after-effect with DHA could be degraded performance due to a lack of control effort. However, DHA guarantees mechanical coupling between SW and the vehicle wheels that is the same dynamic system to control as with Manual control.
With IHA the required effort from the operator to maneuver the vehicle is the same as with Manual control, since the haptic support is not directly controlling

the vehicle. This is though achieved by decoupling the SW from the vehicle wheels. Drivers used to be assisted by IHA can therefore lose perception of the system to control after the controller is switched off. In particular, they could tend to an incorrect usage of the SW system. This would lead to worse performance.
More in general, with both the systems negative after-effects on performance, control activity/effort are likely to be observed for drivers confused with the controller switching-off and during the adaptation process to Manual control.
The described effects are likely to have a bad impact on the lane keeping in particular during the first curves after the controller switching-off, when the human adaptation process is more intense. It is therefore interesting to investigate after-effects in drivers used to a haptic support system after the system is switched off. The forth hypothesis is:

D) *When full Manual control is regained after being used to an haptic support system, performance and/or control activity/effort can be negatively affected with respect to drivers used to Manual control. Moreover, the controller switching off can endanger the lane keeping.*

4.2 Experiment design

In this section the design of a Human-Factor Experiment with haptic shared control for curve negotiation in a driving simulator is presented. This experiment is designed in order to verify the hypotheses figured out from the modeling study.
The simulation apparatus is introduced with the haptic controllers implementation and tuning, followed by the experiment structure and settings.

4.2.1 Driving Simulator Apparatus

The experiment was performed in the fixed-base driving simulator inside the Human-Machine Interaction (HMI) Laboratory in the Aerospace Engineering Faculty at Delft University of Technology.
The driving simulator program runs on a distributed network of computers which communicate via ethernet at 100 Hz update frequency. The real-time communication is implemented by the DUECA interface, that stands for Delft University Environment for Communication and Activation. DUECA organizes the program into modules, which are entities producing or reading data, and channels which are communication buses between modules. Modules are installed and run in different computers. Each computer, which is a node of the network, is dedicated to some specific activity for the driving simulator:

- Node 1: running the program and logging data
- (Node 2: not used)

- Node 3: road and scene visualization
- Node 4: interface to the control loading computer
- Node 5: dashboard display visualization
- Node 6: vehicle dynamics and shared controller

Node 1 is the main computer used to set-up and run the simulation program and gather data from the experiment.
Node 3 is the interface to four Sanyo PLC-XU33 beamers placed on the ceiling of the simulation room that visualize the scene at a rendering frequency of 50 Hz on the front wall and the lateral walls. The projectors configuration yields a 180° horizontal and 40° vertical field of view. The scene (figure 4.1) consists of a two-lane road and to improve speed perception, reflector poles lined the shoulder of the road and trees were placed randomly along the road.

Node 4 is the interface to the control loading computer of the steering wheel

FIGURE 4.1: Driving scene

(CLC) running locally at 2500 Hz. The CLC has the function of setting the virtual passive behaviour of the steering wheel as a mass-spring-damper system. The CLC computer has also the function to actuate the steering wheel in order to provide the force feedback computed by the haptic controller. The electrical actuator is a MOOG-FCS S-motor. The steering wheel is also provided with a torque sensor which measures the torque applied by the human operator. This torque is measured from the relative torsion of the steering wheel bar on the side of the operator with respect to the side controlled by the CLC.
The electrically adjustable seat and the steering wheel, from a Nissan Luxury Car, are shown in figure 4.2.

Node 5 is the interface for the dashboard display which contains a counter for the vehicle speed and driving distance.
A non-linear dynamic model of the vehicle is implemented in Node 6 (Module *CarDynamics*), where it is also installed the Module *IDSS* which contains the shared controller logic.

FIGURE 4.2: Seat and Steering Wheel

4.2.2 Driving Simulator: C++ Programming

The existing simulation software is written in C++. The DHA controller had already been implemented in the *IDSS* module, but new functionalities were added for the IHA controller implementation:

- Creation of the *ComputedWheelAngle* channel
- New features in Module *CarDynamics* in Node 6
- New features in Module *IDSS* in Node 6

It is advisable to review the scheme in figure 2.10-2.11 to have clear the IHA controller structure and understand the following implementation.
First the new channel *ComputedWheelAngle* was created to implement the mechanical decoupling functionality of the IHA controller. In this channel a signal can be written that is the steering wheel angle computed by the IHA controller.
In the standard usage of the steering wheel, the module *CarDynamics* reads from a channel called *MeasuredWheelAngle*. This channel contains the current angle measured from the steering wheel device. This normal configuration is used with Manual Control and also with DHA. On the other side, with IHA a decoupling between steering wheel and vehicle wheels must be implemented. The module *CarDynamics* has been therefore set in such a way that it is either possible to maintain mechanical coupling by reading the angle from channel *MeasuredWheelAngle* (with Manual Control and DHA) or to decouple the SW from the simulated vehicle wheels by reading from channel *ComputedWheelAngle* (with IHA). The read angle is then scaled with the gear ratio to become the angle of the wheels of the simulated vehicle.
The following changes were made to the module *IDSS* that contains the control logic of the shared controllers. The *IDSS* module uses the functionalities of a

class called *PotentialField* where the haptic control laws are implemented. In the *PotentialField* class the DHA control method had already been designed. Before introducing the IHA controller implementation, the DHA control logic will be explained.
The DHA method takes in input the body state of the vehicle and its global state by reading from channel *VehicleState*. From this, it calculates within a pre-set look-ahead-time the future lateral error and heading error of the vehicle from the reference trajectory. The current reference trajectory is also computed from the global vehicle state. Two different proportional gains are applied to the future errors and then the results are added up to produce the optimal steering wheel angle (4.1), that is written to a channel called *OptimalWheelAngle*.

$$\theta_{SW,opt} = P\, e_{lateral,future} + D\, e_{heading,future} \tag{4.1}$$

Another gain is finally applied on the optimal angle to calculate the force feedback (4.2), written in the *ForceFeedback* channel.

$$T_{FB} = G\, \theta_{SW,opt} \tag{4.2}$$

This implementation resembles the structure of shared controller of figure 2.7, with a Visual block that takes in input the vehicle state and computes an optimal steering wheel angle, and a Haptic block that converts the optimal steering wheel angle into a force feedback, in this case a simple proportional law.
The implemented IHA method is an exact reproduction of the DHA in the computation of the optimal wheel angle. The only difference is the haptic proportional gain, that has been set negative in order to produce the force feedback on the steering wheel that makes it turn in the opposite direction of the next curve.
The last step to implement the IHA controller was to create a discrete model of the current steering wheel, to which the feedback force of the controller is fed in input in order to calculate the computed wheel angle, from the subtraction of the SW model angle from the measured angle from the actual steering wheel (figure 2.11). First a state-space continuous model of the SW was calculated as a mass-spring-damper system, that has to match the virtual mass-spring-damper system controlled by the CLC. In the continuous model, the state is $(x_1, x_2) = (\theta_{SW}, \dot{\theta}_{SW})$ where θ_{SW} is the model steering wheel angle and $\dot{\theta}_{SW}$ is the model steering wheel velocity. The state-space continuous model equations are (4.3)-(4.4), where the SW parameters are I_{SW}, K_{SW} and B_{SW} and the system input is the force feedback from the controller T_{FB}.

$$\dot{x_1} = x_2 \tag{4.3}$$

$$\dot{x_2} = -(K_{SW}/I_{SW})\, x_1 - (B_{SW}/I_{SW})\, x_2 + T_{FB} \tag{4.4}$$

The continuous model has been written in a MATLAB script and converted with a Zero-Order-Hold procedure (sampling time = 0.01 sec, inverse of the update frequency of 100 Hz) into the discrete model of the steering wheel. The model parameters I_{SW}, K_{SW} and B_{SW} were set to match the real steering wheel device. The state-space discrete model of the steering wheel is implemented by the new *SteeringWheelModel* method in the *IDSS* module. This method reads from channel *ForceFeedback* and *MeasuredWheelAngle*. It computes the steering wheel model

angle and finally subtracts this from the measured wheel angle. The obtained signal is written in the *ComputedWheelAngle* channel.
Once the IHA controller was implemented, the DHA and IHA were tuned to prepare the system for the experiment. The tuning phase was divided into four steps:

- Visual block for DHA and IHA
- Haptic block for DHA
- Haptic block for IHA
- Steering wheel

4.2.3 Visual subsystem tuning

The parameters of (4.1), which are the proportional gains on future lateral error and heading error had already been tuned for former experiments [9] and this setting was found acceptable. Regarding the look-ahead time at which the future vehicle state is predicted, the pre-existing setting was changed in order to give the driver a sufficient preview of the curves from the haptic feedback, whether it is from the DHA controller or from the IHA. The employed parameters for the Visual block are:

- Look-ahead-time TLH = 1.25 s
- Gain on the future lateral error $P = 0.08\, deg/m = 1.396 \times 10^{-4}\, rad/m$
- Gain on the future heading error $D = 0.9\, deg/rad = 0.01571$

Notice that the gain P is small if compared to D. This way it is given more weight to maintaining the right orientation of the vehicle than keeping the vehicle exactly in the center of the right lane. The driver has more freedom to be slightly off the reference trajectory as long as he keeps the vehicle in the right driving direction. These settings were adopted for the Visual block of both the DHA and the IHA controller.

4.2.4 DHA haptic subsystem tuning

The proportional gain G of the Haptic block (4.2) was tuned separately for DHA and IHA.
In the tuning of the force gain for the DHA Haptic block, a compromise has to be reached. In fact, the higher G_{DHA} is, the stronger the force feedback is and therefore, with the current Visual block setting, the controller is more capable of guiding the vehicle by itself without the human intervention. However, according

to the shared controller philosophy [3] the feedback intensity should be limited. This way the driver is able to potentially override the controller decision in case of malfunctioning. In addition to the safeness issue, a too high feedback force can be perceived as annoying by a driver who decides to cut curves slightly differently from the controller preference. Cutting curves sharply does not directly harm the driving safeness and subjects can have different way of doing it, more or less aggressively [10]. A certain freedom in cutting curves must be therefore kept in consideration when tuning the DHA controller.

$$G_{DHA} = 2.0\ DU/rad = 28.8166\ Nm/rad = 0.5029\ Nm/deg \tag{4.5}$$

In (4.5) DU stands for Dueca-Units which the standard measure unit for torque in the Driving Simulator program. The conversion between DU and Nm is as in (4.6).

$$x_{Nm} = 14.3714\, x_{DU} + 0.0738 \tag{4.6}$$

The chosen setting (4.5) in the configuration XML file gives an acceptable compromise between performance of the DHA shared controller when used as an automatic system and driving comfort when cooperating with the system, as well as possibility of contrasting it in case of non-desired functioning. With the current setting, since the controller power is limited, in sharp turns the driver has to put an additional steering input on the steering wheel in order to keep the lane. Whereas in large turn the DHA controller is able to guide the vehicle almost by itself with this tuning.

4.2.5 IHA haptic subsystem tuning

Regarding the force gain for the IHA controller, a compromise has to be found also in this case.
With (2.9) we demonstrated that the steering wheel is used with the IHA controller as a force interface rather than a position interface, which is its conventional manual usage and with DHA. Therefore in theory the force gain does not directly influence the amount of force that the driver must put on the steering wheel to perform a specific maneuver. If we choose a high force gain, it will be easier for the driver to guide the vehicle by keeping the steering wheel to the central position and simply contrasting the force feedback. If we wanted to implement the IHA as an automatic controller the best performance would be then achieved with such a force gain that is sufficient for the pilot to turn himself into a 'pilot made of concrete' and simply keep the steering wheel to the center all the time. This is of course in contrast with the shared control philosophy, where the driver has to employ the controller as an additional feedback channel. On the other side if the force gain is too low, the risk is to have a haptic feedback that cannot be perceived by the driver. This way the shared controller authority would be too low and the feedback not helpful at all. The first requirement is therefore to have a sufficient perception of the force feedback, such that the driver has to contrast the IHA force but still it is required to add some steering action especially when curves are sharp. Another important requirement comes along in the IHA tuning.

In apparent contradiction with what explained earlier, the IHA controller does not make the steering wheel a pure force sensor. In fact, the force input from the human operator is bound to the force feedback from the IHA. In order to clarify this, let us introduce a situation where the operator decides to contrast the controller action. During the normal functioning of the IHA, if the operator agrees with the controller he has to contrast the force feedback, as in (4.7).

$$T_{hum}\, T_{IHA} < 0, \tag{4.7}$$

where T_{hum} is the operator torque on the SW and T_{IHA} is the IHA controller torque feedback. If the operator does not agree with the controller action we have (4.8) instead.

$$T_{hum}\, T_{IHA} > 0 \tag{4.8}$$

For example in the situation presented in section 3.2.4, the faulty controller is not detecting an obstacle on the right lane of a straight road and its reference trajectory lies in the center of the right lane. However, an aware driver decides to avoid the obstacle by switching to the left lane, therefore a situation of contrast will arise. The driver applies on the steering wheel a torque $T_{hum} < 0$ (anticlockwise) to steer towards the left lane. Since this is not considered the right maneuver by the IHA controller, this will provide a force feedback $T_{IHA} < 0$ as well, to inform the operator that he has to contrast this force to bring back the car to the right lane. The two force signals are basically adding up in this situation, which is the opposite of the normal functioning.

In figure 4.3 are shown some plots which were manually drawn to show the expected behaviour of how the input from the human operator can be influenced by the IHA force feedback.

The lane change maneuver is initiated by the human operator at the time instant $t = 0$ for the sake of simplicity. In the time interval $[0, t_d]$ the human input T_{hum} is increasing (figure 4.3a). Now with a delay of t_d seconds the IHA reacts to the operator torque and since the maneuver is perceived as wrong, an increasing torque F_{IHA} is provided on top of the operator one (figure 4.3b).

The increasing T_{IHA} entails however that T_{hum} is decreasing. In fact, T_{hum} is measured by the torque sensor from the relative torsion of the SW bar. Therefore, T_{hum} drops down in presence of a signal T_{IHA} of the same sign until an instant t_f where $T_{hum} = 0$ that coincides with the steering wheel hard boundary. In fact no T_{hum} can be exerted beyond this point. Regarding the steering wheel angle θ_{SW}, it is growing up to its boundary (figure 4.3c). On the other side, the vehicle lateral error e_{lat} from the center of the right lane grows up with $\ddot{e}_{lat} > 0$ until t_d (inflection point) and then it switches to concave down $\ddot{e}_{lat} < 0$ to t_f, after which it is saturated to its maximum since $T_{hum} = 0$. This error is shown in figure 4.3d. This means that the operator is able to disagree with the controller up to a certain point, that coincides with a $\theta_{SW} = \theta_{SW,max}$ which is the steering wheel hard boundary. However, the relation between the vehicle lateral error and the steering wheel angle is not static. This means that having $\theta_{SW} = \theta_{SW,max}$ does not imply $e_{lat} = e_{lat,max}$. In fact the maximum lateral error from the center of the right lane achievable depends on the profile of the T_{hum} signal, that in turn depends on the T_{IHA} as explained above.

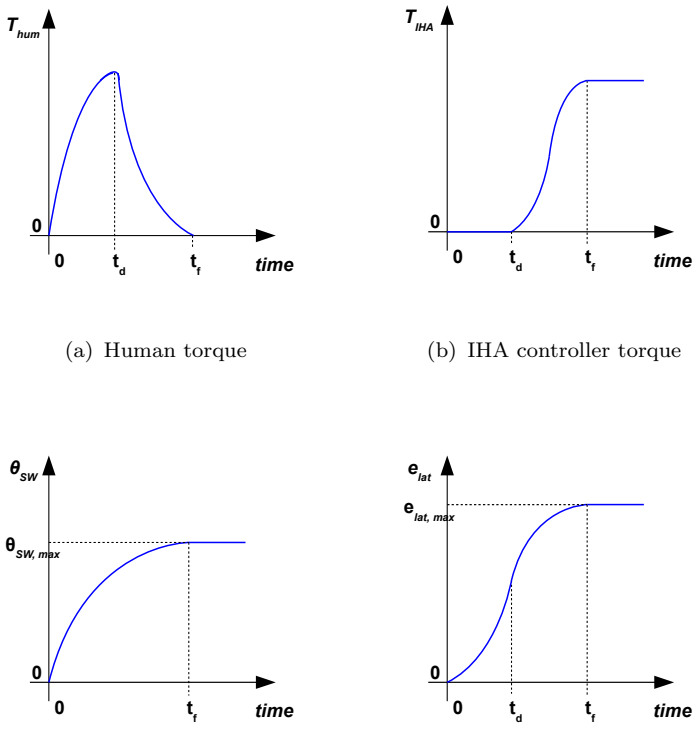

(a) Human torque

(b) IHA controller torque

(c) SW angle

(d) Error from center of right lane

FIGURE 4.3: IHA in lane change with controller error (sketches)

In order to make this clear, let us consider a case where the operator holds the steering wheel, with the vehicle following the controller reference, then at some points he gives a small $T_{hum} < 0$ as a perturbation on it such that $e_{lat} \neq 0$. The feedback force will be $T_{IHA} < 0$. Now imagine in a ideal case that the operator, instead of contrasting the controller force, decides to follow it by turning the steering wheel in perfect synchrony with the IHA controller by cancelling out his own arms inertia. At the end of this maneuver the steering wheel reaches its boundary, provided that the IHA force is higher than the steering wheel self-alignement force (we will come back to this later), and still the e_{lat} would be unaltered from the initial value that yielded the force feedback. This is because the T_{hum} actually measured consists only of the initial perturbation and then $T_{hum} = 0$.
Of course the human arm inertia and any tiny asynchrony of the operator maneuver will cause some T_{hum} to be measured and then some effect on the vehicle position. However, this was only to prove that ideally it would be possible to reach $\theta_{SW} = \theta_{SW,max}$ and $e_{lat} \approx 0$, that is no static relation between θ_{SW} and e_{lat} with the IHA controller. The final displacement $e_{lat,max}$ at the end of the maneuver depends only on the measured force profile T_{hum}.
This thorough discussion on how the steering wheel usage changes with the IHA controller was mainly presented in order to introduce the second requirement that must me met. The force gain G_{IHA} is directly related to the maximum lateral distance reachable from the controller reference, that is $e_{lat,max}$.

Again some plots were manually drawn and here are reported to show how the

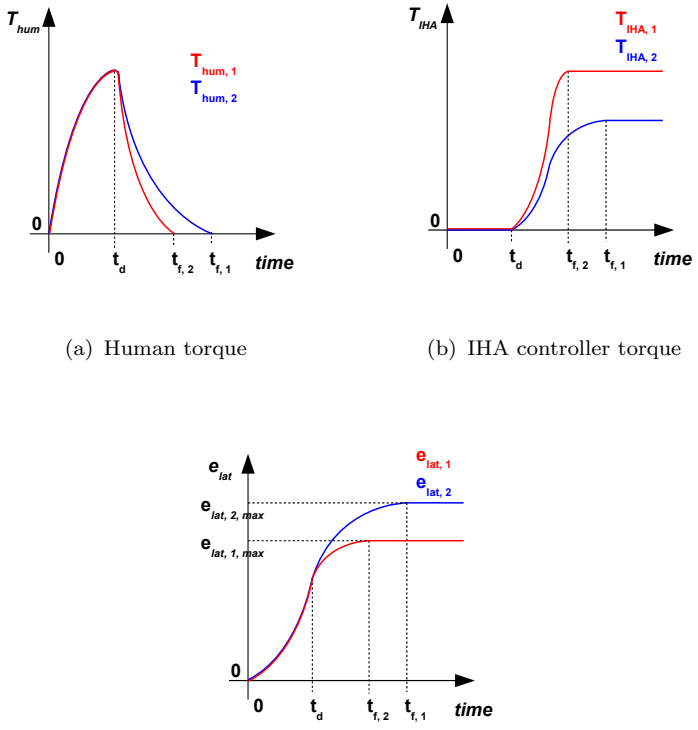

(a) Human torque

(b) IHA controller torque

(c) Error from center of right lane

FIGURE 4.4: Influence of the IHA force gain on the maximum deviation from the controller reference (sketches)

force feedback gain with IHA is related to the second requirement. In figure 4.4 we have two force feedback gains G_1, G_2, $G_1 > G_2$. From 0 to t_d, delay for the controller action, the signals $T_{hum,1}$ and $T_{hum,2}$ have the same profile and also e_{lat}. After t_d, since G_1 is higher than G_2, $T_{IHA,1}$ goes up steeper than $T_{IHA,2}$, so $t_{f,2} < t_{f,1}$ and also $e_{lat,1,max} < e_{lat,2,max}$. This means that the higher the gain on the force feedback, the lower the maximum deviation from the IHA reference reachable in case of contrast between operator and controller.
To summarize, the IHA controller must be tuned in order to have a sufficient perception of the feedback forces, but still the force gain must be limited to be able to possibly contrast a faulty controller. The chosen setting done in the configuration XML file is (4.9), which guarantees a satisfying intensity of the feedback as well as the possibility to move the vehicle to the center of the left lane in case of a faulty controller, that is reaching a $e_{lat,max} \approx 3.6\,m$ to the left of the controller reference.

$$G_{IHA} = 3.5\ DU/rad = 50.3737\ Nm/rad = 0.8792\ Nm/deg \tag{4.9}$$

Having turned the steering wheel into a force interface limits the control over the vehicle when the IHA controller provides a force feedback. This resembles what found with the DHA controller in case the haptic aiding is faulty, but in that case

the contrast lies at a force level. It is sufficient to contrast the force feedback and the driver will impose his authority. With the IHA, the contrast lies instead at a position level, that is in the steering wheel usage, although the relation with the deviation from the controller reference is not static as explained earlier.

4.2.6 SW tuning

After the implementation of the IHA controller some additional settings had to be changed.
A driver guiding the vehicle with the IHA controller can perceive the steering wheel more slack than with manual control or DHA, although the linear parameters I_{SW}, B_{SW}, K_{SW} are not changed. The realigning behaviour of the steering wheel has not changed but what happens is that the force of the IHA controller overtakes the self-alignment force and the steering wheel is more loose in the operator hands whenever the steering wheel angle is different than zero. This can be explained with (4.10), where the IHA controller force T_{IHA} is higher in absolute value than the self-alignment force of the steering wheel T_{align}.

$$\mid -K_{SW}\,\theta_{SW} - B_{SW}\,\dot{\theta}_{SW} - I_{SW}\,\ddot{\theta}_{SW} \mid = \mid T_{align} \mid < \mid T_{IHA} \mid \tag{4.10}$$

This behaviour is not symmetric: let us assume that the steering wheel is at a certain anticlockwise angle different from zero. This means that there is a certain contrast between operator and shared controller goals. The IHA force tends to amplify this angle, so it is a anticlockwise torque perceived by the operator as a tendency of the wheel to turn even more anticlockwise. However, since the right maneuver for the controller would be to bring back the steering wheel to the center, if the operator tries to turn it clockwise, he will perceive a force from the controller to contrast. Therefore the SW is perceived more loose in one direction and tighter in the other direction.
The steering wheel linear parameters B_{SW}, K_{SW} had to be adjusted in order to smooth an annoying sensation experienced while holding the steering wheel in the central position.
Let us assume that the operator is holding the steering wheel in the central position while the vehicle is following the reference road. Now in the ideal situation, the future errors $e_{lat,future}$, $e_{head,future}$ are zero so the IHA controller should not provide any feedback force on the SW. In the real situation there will be anyways some small errors detected and so a small IHA force. On top of this force we can consider the self-aligning torque of the steering plus the human arms inertia as a total alignment torque $T_{align,tot}$ opposite to the feedback force T_{IHA}. In this situation where the deviation is small, it happens that the aligning torque is higher than the feedback force (4.11).

$$\mid -K_{SW}\,\theta_{SW} - B_{SW}\,\dot{\theta}_{SW} - (I_{SW} + I_{arm})\,\ddot{\theta}_{SW} \mid = \mid T_{align} \mid > \mid T_{IHA} \mid \tag{4.11}$$

If we consider future oscillations of the errors around zero, this gives a $T_{IHA} = \pm\epsilon$ repeatedly acting on the steering wheel. This feedback force from the IHA is

perceived by the operator as a 'bumpy' SW around the central position. By increasing the steering wheel parameters, $T_{align,tot}$ will be sufficiently higher than T_{IHA} to stabilize the steering wheel around the center and the 'bumpy' sensation will be gone.
The steering wheel parameters in the initialization file *dueca.mod* were therefore set for the whole experiment to:

- Moment of inertia $I_{SW} = 0.3\ Nms^2/rad$
- Stiffness $K_{SW} = 4.2\ Nms/rad$
- Damping $B_{SW} = 0.9\ Nm/rad$

The same parameters were adopted for the three systems compared in the experiment.

4.2.7 Experiment structure

In this experiment we want to compare three different systems in a curve negotiation task: Manual Control, Shared control with DHA, Shared control with IHA. These systems are going to be compared under the different driving conditions examined in the experimental hypotheses. In order to make this comparison, three separate groups of subjects are required with each group working with a specific system:

- Group A: Manual Control
- Group B: Shared Control with DHA
- Group C: Shared Control with IHA

Let us describe how the subjects were recruited and organized. In total 27 subjects were tested, with 9 subjects per group. All the subjects were students or personnel from Delft University of Technology and they voluntarily agreed to participate to the experiment without any form of compensation. Before participating to the experiment, they were asked to fill in an online form where some information about their driving experience were gathered. Here is the entry form:

- Name
- Age
- Sex
- Do you have any physical disabilities that could interfere with your performance? (for example, muscle weakness in the arms, seeing problems, etc.)

- Do you have a regular driving licence?
- How long have you been driving for? (number of years)
- How many kilometers per year do you drive in average?
- How do you judge your driving style? (choose between cautios, normal and aggressive)

26 of the tested subjects were male and only one was female. They are aged between 20 and 32. The answers from the questionnaire were used to divide subjects into three groups with a similar variability within group in terms of age, driving license years, kilometers per year and driving style. The most significant differences between tested subjects were age and number of kilometers per year (between 1000 and 25000), while driving license years were found proportional to age and driving style was in most cases normal. The following average age and kilometers per year were ensured with the chosen division:

- Group A: Age 25.2 years, 8100 km/year
- Group B: Age 25.2 years, 9100 km/year
- Group C: Age 25.3 years, 8700 km/year

Before starting to drive, specific experiment instructions were given to subjects from each group. All the subjects were instructed to keep the car in the center of the right lane, unless some particular condition requires to switch to the left lane. They were asked to adjust the seat in a comfortable and proper position and to hold the steering wheel in the 10-to-2 standard position, disregarding the use of the pedals. Moreover, the functioning of the specific shared controller was explained to subjects from groups B and C. They were also asked to be absolutely concentrated on the road and try not to over-rely in the haptic support.

A preliminary 5-minute training session preceded the actual experiment. This training was used to allow subjects to take confidence with the driving simulator environment, the control interface (SW) and especially the support system they are going to work with.

The experiment was structured in order to gather data that can be used to verify the stated experimental hypotheses. In figure 4.5 the whole structure of the experiment is illustrated for each group. Before the experiment there is the 5-minute training session, where subjects can learn how to drive the simulated vehicle with the shared controller, DHA for group B and IHA for group C, or simply learn how to manually drive the vehicle (group A).

After the training, the actual experiment begins. The total duration is about 16 minutes with no breaks between one part and the next one.

In the first part, which we will call from now on *Normal Visibility*, subjects are driving in full visibility condition for 5 minutes. Figure 4.6 is a snapshot from the first part of the experiment. Data from this part are collected and will be analysed to verify hypothesis A.

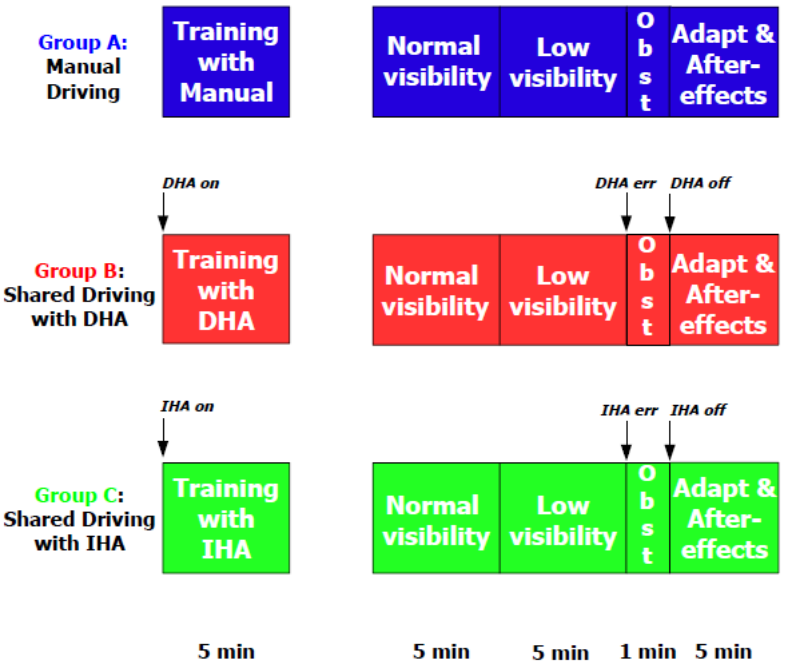

FIGURE 4.5: Structure of the experiment

FIGURE 4.6: Normal visibility scene

In the second part of the experiment *Low visibility* a foggy condition visualization is activated. Figure 4.7 is a snapshot from the second part of the experiment. Data collected in this session will be used to verify hypothesis *B*.

FIGURE 4.7: Low visibility scene

After the foggy condition, visualization is set back to normal and in the next straight road an obstacle is put on the right lane, as in figure 4.8. Notice that

the obstacle occupies the whole right lane if we consider the traffic cones in the middle of the road. . This obstacle is not detected by the controller, for which

FIGURE 4.8: Obstacle on the right lane

the desired reference trajectory lies in the center of the right lane. Therefore here it is possible to collect data in a condition of faulty support system in order to test hypothesis *C*. We will call this part of the experiment *Obstacle avoidance with Controller Error*.
Finally, after the error the controller is switched off and in the final 5-minute part the driver has to manually drive the vehicle. From this part called *Adaptation and After-Effects* data are collected to verify hypothesis *D*.

4.2.8 Other settings

Some additional settings in the driving simulator were required to set-up the experiment.
First the channel *GasPedalPosition* was set with a constant value (12.058° of deflection) in the configuration XML file so that the vehicle velocity was fixed at 20 m/s and the actual gas pedal was no longer used to control the vehicle longitudinal velocity.
In order to make the force feedback safe and prevent any harm to the driver's arms, an additional maximum threshold was put on the computed force feedback. This saturation is implemented in both the DHA and IHA methods of *PotentialField*, right before the computed force feedback is written in the *ForceFeedback* channel. The saturation was manually tuned to 20 Nm that is a level of steering force that can be reached by any normal driver with some physical effort.
A final setting was implemented in the DHA and IHA methods of the *PotentialField* class in order to make it possible to switch off the controller feedback at some desired point. Before writing the computed force feedback to the specific channel, the methods read from *NearestRoadPoint* channel that contains the closest road point of the vehicle to the reference trajectory. This signal is monotonically increasing as the car goes along the track. This way the force feedback can be set to zero after the read road point exceeds a certain threshold.
A single continuous road layout was created for this experiment, constituted by the four parts described. Given the vehicle longitudinal velocity set constant to 20 m/sec, each 5-minute part corresponds to 6 Km of road. The total length of the

track is therefore about 18 Km. The track was designed by combining together several pieces of road:

- Straight pieces
- Pieces with constant radius of curvature, from 100 m to 600 m
- Pieces with multi-sine curvature

A pre-existent MATLAB script was employed to create this road layout and the scenario. Inside the script are defined the pieces of road, an option to add random trees around the road and the reflector poles on the road shoulders. A triggering event was set in order to activate a static layer to be put on top of the scene to simulate the foggy condition in the second part of the experiment. An obstacle object was also placed in the third part of the track. The script automatically generates the mesh file containing the whole scenario.
The experiment (figure 4.5) was run under the described conditions and with the performed tuning of the haptic shared controllers and the additional settings.

Chapter 5

Testing HSC for curve negotiation in a driving simulator

5.1 Data analysis

In chapter 4 the designed experiment on haptic shared control for curve negotiation has been introduced. Experimental data were gathered from the experiment and a statistical analysis based on them is carried out, in order to investigate the behaviour of the shared control systems in different driving conditions.
In this section the data analysis procedure is presented. First the signals measured in the experiment are described along with some preliminary corrections carried out on them. A set of statistical metrics were calculated on these data separately for each group and each part of the experiment. An ANOVA an post-hoc tests were performed to detect significant differences between groups.

5.1.1 Measured data and preliminary corrections

The Driving Simulator gathered data from each subject who participated to the experiment (figure 4.5). Each driving session is saved as a MAT-file for MATLAB. The following signals were chosen for a statistical analysis:

- Lateral reference error e_{lat}
- Time-to-lane crossing TLC
- Measured steering wheel angle θ_{SW}
- Measured torque from the operator T_{hum}

Notice that all these signals are automatically logged and saved from the simulation program.

The lateral error of the vehicle is calculated between the position of the vehicle and the nearest road point of the center of the right lane, which was set as the shared controller reference for the whole duration of the experiment.
The TLC with respect to the right lane of the road is not geometrically calculated but approximated as in (5.1) which is proven to be reliable when the vehicle is staying within the lane boundaries [11].

$$TLC \approx y/(\dot{y} + \ddot{y}) \tag{5.1}$$

In (5.1) the TLC is approximated by using the vehicle lateral position y, its lateral velocity $\dot{y}$ and acceleration $\ddot{y}$.
The angle from the steering wheel θ_{SW} is measured along with the torque T_{hum} applied from the human operator.
A first correction was performed on the TLC: the original logged data had peaks going to $\pm\infty$ due to the approximation used. A maximum absolute threshold for TLC was chosen equal to 30 sec, by looking at the longest straight road followed by the curve with the largest radius of curvature in the track, considering this as the best case scenario for TLC. This way TLC is limited as in (5.2).

$$TLC \in [-30, 30]\, sec \tag{5.2}$$

In addition, all the data were checked for errors, such as NaN values, unexpected peaks and values outside normal boundaries. This check was performed for each signal both visually and numerically. A boundary for each signal was reasonably chosen as in (5.3)-(5.4)-(5.5).

$$T_{hum} \in [-20, 20]\, Nm \tag{5.3}$$

$$\theta_{SW} \in [-200, 200]\, deg \tag{5.4}$$

$$e_{lat} \in [-10, 10]\, m \tag{5.5}$$

Values outside those boundaries were replaced with a linear interpolation between the immediately preceding and following normal values.
Apart from the correction performed on TLC, the gathered data were almost totally free from errors, except for e_{lat} on which unexpected peaks were found only two times.

5.1.2 Statistical metrics

In section 4.1 some hypotheses from the modeling study and the experiment to verify them were introduced. The general concepts of *Performance*, *Control activity* and *Control effort* are yet to be defined with specific statistical metrics. Those metrics were calculated for each subject and according to the structure of the experiment in figure 4.5 separately for the following sections:

- Normal visibility (NVB)

- Low visibility (LVB)
- Obstacle avoidance with Controller Error (OAE)
- Adaptation (ADP)
- After-effects (AEF)

This division matches the structure of the experiment except for *Adaptation and After-Effects* which was divided into two parts, that is the first curves after the controller switching-off and the rest of the final part. This is because transient effects were observed mainly in those first curves during which the operator adapts to manual control after being used with a shared controller.
Here the statistical metrics will be introduced. They will also also characterized for each condition and possibly with further divisions of each condition into straight pieces of roads and curves. This further split can be necessary for certain metrics which are influenced by the curvature of the road.
Performance can be referred to as how well the vehicle is following the correct reference, that is keeping the right lane, if there are no obstacles on the road. It was previously mentioned that drivers can have different driving styles, more or less aggressive, in the way they decide to cut curves [10]. In general a good *Performance* is guaranteed when the vehicle is staying on the right lane, as long as there are no obstacles on the street. Remember that the drivers were instructed to do so, therefore the TLC can be a good signal to be manipulated in order to measure *Performance*. Since the track used for the experiment contains many pieces of straight roads, the TLC tends to be biased to the threshold chosen for it (5.2) as it was observed from a visual check on the signals. In order to get rid of the bias, the TLC signal was sorted in descending order. Since the TLC signal contains many oscillations between positive and negative values (it happens every time the future crossing jumps from the left to the right boundary and vice-versa), it is taken the absolute value of TLC. Finally the average is computed over the first 10% of the sorted absolute signal. We will call this metric $min_{10\%}|TLC|$, which stands for *Minimum 10% of absolute TLC*.
This metric can be used for sections *NVB-LVB* and *AEF* without any problems. In section *OAE* it cannot be used since the approximation used to calculate TLC is not valid for lane changes and neither in section *ADP* where the transient effects of the controller switching-off caused some oscillations of the vehicle trajectory outside the right lane. It is advisable to calculate $min_{10\%}|TLC|$ separately for straight roads and curves, since for straight roads it will be still close to its threshold while in curves it can drop down to values closer to zero.
If we want to measure the oscillations of the vehicle trajectory the *Standard Deviation of the Lateral Reference Error* can be taken into account $std(e_{lat})$. However, since the road is composed of many different curves and straight roads, this metric is reliable only if the Std operator is calculated for small segments of the signal. It will be used as a metric of *Performance* for section *ADP* in place of $min_{10\%}|TLC|$ which is not reliable in this case. It can also be calculated for all the straight segments for sections *NVB-LVB-AEF*, since in this case the oscillations of the vehicle are around a trajectory that is more or less straight.

During the experiments it was observed that subjects tend to keep the vehicle at a certain distance from the center of the right lane mainly along straight roads. The *Mean of the Absolute Lateral Reference Error*, $mean|e_{lat}|$, indicates the bias of the vehicle position with respect to the center of the right lane. However, it cannot be used to measure *Performance* but rather *Preference* and it can be interesting to look at it in section *NVB*, only for straight roads, when visibility is normal to see how it can be influenced by a shared controller.
Control activity is a synonym for mental effort from the operator in controlling the vehicle in the different conditions presented in the experiment. In previous studies [3] *Standard Deviation of the Steering Wheel Angle* and *Steering Wheel Reversal Rate* were employed as measurements of low-frequency and high-frequency *Control activity* respectively. This is however when the SW is used as a position control interface, which directly commands the vehicle wheels angle. In the current experimental conditions, the normal use of the steering wheel stands only for Manual control and DHA, but not for IHA. In the IHA scheme, the steering wheel is decoupled from the wheels. This implies that the operator is not controlling the vehicle directly through the steering angle. Actually with IHA the operator is guiding merely through his own force that is contrasting the controller force. Since *Control activity* is the level of mental effort to perform the required task, we can choose to look at the variability of the measured torque from the operator as an index of *Control activity*.
A first way to measure the variability of the operator torque is to define a *Reversal Rate of the Measured Torque*, TRR, that is the number of direction changes (oscillations) per second of the measured torque signals which go beyond a certain threshold of variation. Whenever the signal oscillates from a descending profile to ascending and the amplitude of this oscillation is higher than the chosen threshold, the counter of direction changes is incremented. The total number of changes are then divided over the amount of time and this way TRR is calculated. The threshold was chosen after a visual check on the torque signal profile and some tests, considering that if it is too low the measurement noise would be counted as direction change, while if it is too high some significant oscillations would be neglected. Now the point is how to define *significant* oscillations on this signal. Since from the experiments it was observed that subjects from group A driving in section *LVB* had more troubles in following the right lane and there were many oscillations on the vehicle trajectory than in section *NVB*, the measured torque signals from those conditions were analysed in order to choose a threshold on the TRR appropriate for discriminating those conditions. After this analysis the threshold was set to 2 Nm in absolute value.
The TRR can be calculated separately for straight roads and curves to see where *Control activity* is higher. It is a metric that is not influenced by the curvature of the road and it is valid for all the conditions of the experiment.
Another metric of *Control activity* can be computed from the measured torque from the operator, that is *Standard Deviation of Measured Torque*, $std(T_{hum})$. However this metric is influenced by the curvature of the road as $std(e_{lat})$ so it can be used only for small segments of road or separately for the straight pieces of road. It will be adopted for the straight roads of sections *NVB-LVB-AEF* and for section *ADP*.

TRR can be considered as a measure of high-frequency *Control activity* since it indicates how noisy is the measured torque signal, while $std(T_{hum})$ can be used for measuring slow variability of the measured torque that is low-frequency activity.
Regarding the metrics used for *Control activity* in previous experiments [3], they can still be used to compare groups A and B, to see if results obtained in those studies are also found with this experiment. *Steering Wheel Reversal Rate*, SRR, can be calculated separately for straight roads and curves, while *Standard Deviation of Steering Wheel Angle*, $std(\theta_{SW})$, can be used only for straight roads. These metrics will be computed only in section *NVB*.
Finally a statistical metric must be chosen for *Control effort* which is the physical demand from the operator to guide the vehicle in the presented experimental conditions. The *Root mean square of Measured Torque* can be employed in this case as it measures the magnitude of the torque signal. $rms(T_{hum})$ will be calculated separately for straight roads and curves for all the sections of the experiment.
With hypothesis C we stated that the controller error can put the evasive maneuver in danger. A way to measure this criticality is to calculate the *Minimum Distance of the Vehicle Trajectory from the Obstacle*, $min(d_{obst})$. The distance calculated is precisely between the line created by the road pylons to delimit the obstacle area and the vehicle center of mass. If we consider that normal commercial cars have a width $w_{car} = (1.5 \div 1.8)m$, we can assume that there is an obstacle hitting when $min(d_{obst}) < w_{car}/2$.
Tables 5.1-5.2 contain the chosen statistical metrics in the different conditions of the experiment. In these tables S indicates only the straight pieces of road of a certain part of the track, while C indicates only the curves.

Table 5.1: Statistical metrics for the experiment

Condition	**Road**	**Performance**	**Control activity**	**Control effort**
NVB	S	$min_{10\%}\|TLC\|$, $std(e_{lat})$	TRR, $std(T_{hum})$	$rms(T_{hum})$
	C	$min_{10\%}\|TLC\|$	TRR	$rms(T_{hum})$
LVB	S	$min_{10\%}\|TLC\|$, $std(e_{lat})$	TRR, $std(T_{hum})$	$rms(T_{hum})$
	C	$min_{10\%}\|TLC\|$	TRR	$rms(T_{hum})$
OAE	S	$min(d_{obst})$	TRR, $std(T_{hum})$	$rms(T_{hum})$
ADP	C	$std(e_{lat})$	TRR, $std(T_{hum})$	$rms(T_{hum})$
AEF	S	$min_{10\%}\|TLC\|$, $std(e_{lat})$	TRR, $std(T_{hum})$	$rms(T_{hum})$
	C	$min_{10\%}\|TLC\|$	TRR	$rms(T_{hum})$

Table 5.2: Other metrics for the experiment

Condition	**Road**	**Preference**	**SW use**
NVB	S	$mean\|e_{lat}\|$	SRR, $std(\theta_{SW})$
	C	-	SRR

5.1.3 ANOVA and comparison tests

The statistical metrics were calculated for each subject in each condition presented in table 5.1. Then three groups were created: Group A (Manual Control), Group B (Shared Control with DHA), Group C (Shared Control with IHA).
The following statistical analysis was performed using MATLAB. See [12] for the theory of statistics, ANOVA and multi-comparison test on which the analysis is based.
An ANOVA (Analysis of Variance) is carried out between the three groups per each condition to find out if there are statistically significant differences between groups. For example, the first ANOVA is executed on the $min_{10\%}|TLC|$ values in the straight roads of *NVB*. We have three groups, each with 9 values of $min_{10\%}|TLC|$. We are looking for significant differences between groups, that is between the means of different groups. This difference must be significant with respect to the data variability within each group.
Notice that the ANOVA can be executed provided that data have a normal distribution. A preliminary check on normal distribution plots confirmed that data are distributed in such a way that resembles a normal distribution.
Before running the ANOVA, 95% confidence intervals are calculated and a plot is drawn where groups means and confidence intervals are shown. From this plot, a visual test can be executed to see if means are different and whether confidence intervals are overlapping each other. If they are not, significant differences are very likely to be found.
The ANOVA is therefore carried out ($\alpha = 0.05$) and this produces two values, F and p. When p is lower than α it can be stated there are differences somewhere between groups. However, this only tells if there is a difference but we don not know yet between which groups.
Therefore, a multi-comparison analysis follows ANOVA. The post-hoc Bonferroni test has been chosen as multi-comparison test. A multiple t-test would produce an α value of about 0.0975, that is close to a 10% chance of I-Type error, that is detecting a significant difference when actually there is not one. A Bonferroni test instead protects the statistical analysis from I-Type error although it is quite conservative. From the multiple-comparison test we can finally see where the significant differences are.
In the next section the results from the statistical analysis on the experimental data are finally presented and discussed.

5.2 Experiment results

In this section the results of the proposed statistical analysis (tables 5.1-5.2) in for the experiment of figure 4.5 are presented. Each of the following paragraphs contains results for each condition of the experiment along with a discussion.
In each plot there are three bars corresponding to the mean and the 95% confidence interval of a precise statistical metrics for the three groups:

- Group A: Manual Control
- Group B: Shared Control with DHA
- Group C: Shared Control with IHA

The results of each ANOVA are presented in terms of F value and p value. The multi-comparison tests tells us where the significant differences are, and differences between means of the analysed statistical metrics are reported.
In some condition plots of the signal from which the metrics are calculated will be also shown in order to clarify and stress the results found from the statistical analysis.

5.2.1 Normal visibility

Here the results of the statistical analysis in Normal visibility condition are reported and discussed.
In figure 5.1 are shown the comparison plots for $min_{10\%}|TLC|$ for straight roads

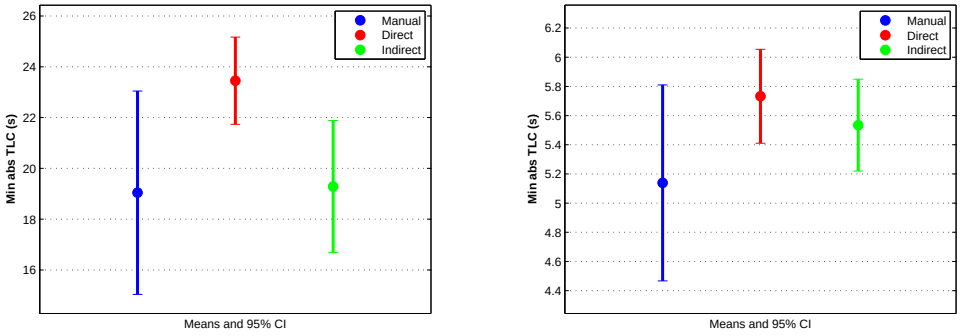

(a) straight roads (b) curves

FIGURE 5.1: NVB - Minimum 10% of absolute TLC

and curves. It can be noticed that the mean values are higher for straight roads (around 20 sec) than in curves (5-6 sec) as it was expected. $min_{10\%}|TLC|$ is not significantly different with a shared controller, neither in straight roads nor in curves.
$std(e_{lat})$ for straight roads is shown in figure 5.2. It is significantly different for DHA (0.20 m difference) and IHA (0.22 m difference) from Manual control, with $F = 32.3, p = 2 \times 10^{-7}$.
In terms of TLC there have not been real improvements with a shared controller. This result denies what found in a previous research [3], where DHA had been found to be enhancing TLC. It can be argued that manual driving was as easy as driving with DHA in the Normal visibility condition since curves were not very demanding. However, it was found an improvement in the oscillations of lateral error with DHA and IHA, this meaning that the shared controller helps to stabilize

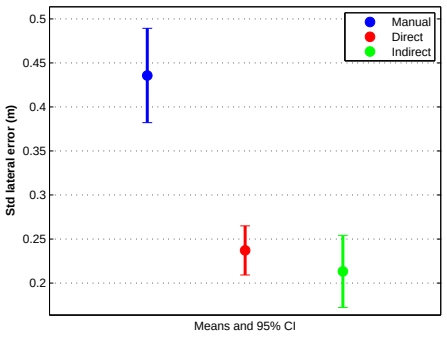

FIGURE 5.2: NVB - Std of lateral reference error - straight roads

the trajectory and it is able to cancel out the natural torque noise introduced by the driver on the steering wheel. Notice that this noise is so small that it does not affect TLC.

Before presenting results for control activity and effort, plots of the torque T_{hum}

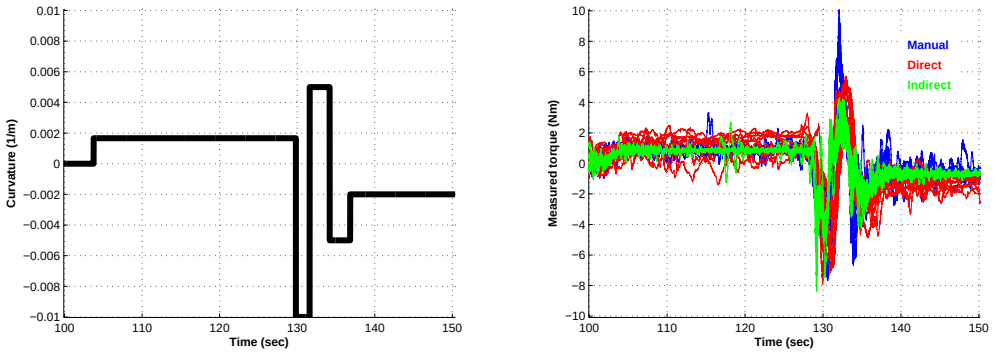

(a) Road curvature

(b) Measured torque

FIGURE 5.3: NVB - Measured torque signals

measured from the test subjects of the three groups are presented. These plots come along with the plot of the road curvature at the same time interval, in order to compare the operator effort to the specific maneuver. It is useful to look at differences between signals to try to anticipate what could come out from the statistical metrics.

In figure 5.3 these signals are displayed for a chosen interval of time during the Normal visibility condition. From this plot it can be observed that in large curves signals with Manual and IHA are quite close to each other (only some more oscillations with Manual) while with DHA there is more variability between subjects and in most cases the signal has a higher average. In the sequence of short curves, the signals with DHA and IHA are closer and peaks with Manual are higher. Therefore, it seems that with DHA there was more average physical effort but not mental, while with Manual a higher mental effort can be expected.

In figure 5.4 are reported the comparison plots for TRR in straight roads and curves. No significant differences were found in them. $std(T_{hum})$ is shown in figure

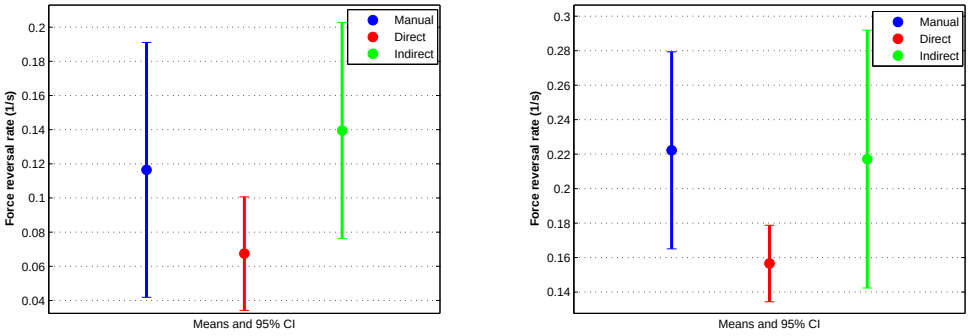

(a) straight roads (b) curves

FIGURE 5.4: NVB - Torque Reversal Rate

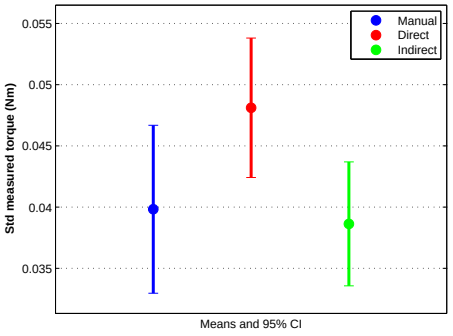

FIGURE 5.5: NVB - Std of measured torque - straight roads

5.5 for straight roads. No significant differences were found.
Again in contrast with what found in [3], no improvements were found in the mental effort from the operator with DHA with respect to Manual control. This was also for IHA. This part of the experiment was probably too easy to be manually performed so that no benefit came out with the help of a shared controller.

$rms(T_{hum})$ is shown for straight roads and curves in figure 5.6. Notice that the mean effort in all the three conditions is higher in curves than in straight road. In straight roads there are no significant differences, while in curves DHA was found different from Manual (0.62 Nm difference) and IHA (0.77 Nm difference), with $F = 60.27, p = 4 \times 10^{-10}$.
This controversial result confirms what found in [3] for the DHA controller.
From the results found it seems that there was some fight between the operator and DHA controller mainly in curves. This fight is probably due to a slightly different control goal. In this task, in spite of the instructions given to subjects to keep the car in the center of the right lane, still there can be some differences between subjects on where they think the center of the lane is. Since the haptic feedback was voluntarily not chosen too strong to force drivers to stay exactly on the reference chosen by the controller, subjects were more or less free to slightly deviate from the controller path and to cut curves differently.
Therefore, it can be argued that there was a small contrast between operator and

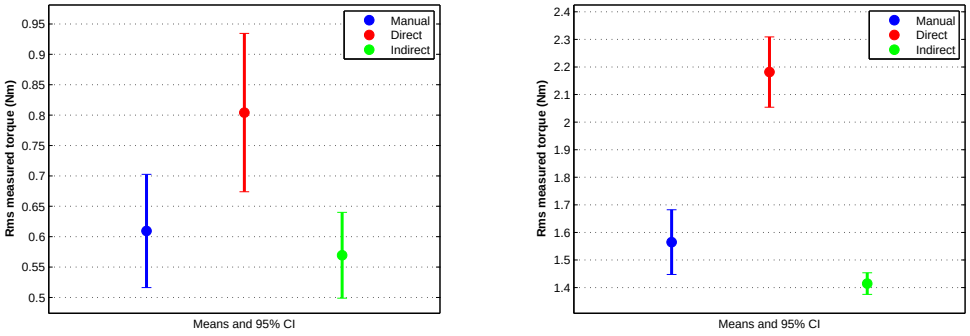

(a) straight roads (b) curves

FIGURE 5.6: NVB - Rms of measured torque

shared controller, which produced a higher physical effort with DHA. Also with IHA there was a similar contrast but, according to the IHA functioning, this is not translated into a higher effort but a misuse of the steering wheel, as it has been found in section 3.2.4 and it will be clear soon from results.

In figure 5.7 is shown the additional metrics $mean|e_{lat}|$ for straight roads which

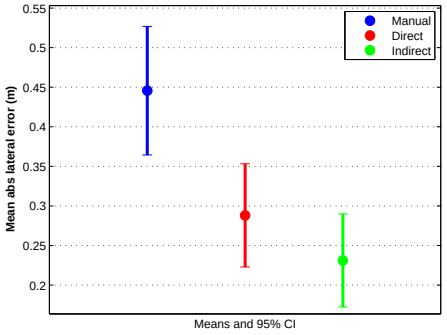

FIGURE 5.7: NVB - Mean of lateral reference error - straight roads

has been chosen as an index of Preference, that is where the operator decides to keep the vehicle in the right lane. There is a significant difference both for DHA (0.29 m difference) and IHA (0.34 m difference) from Manual, with $F = 60.27, p = 4 \times 10^{-10}$.

This means that in straight roads there can be a difference from the detected center of the lane to follow and with the haptic support subjects are more compliant to follow the controller reference, while with Manual control subjects prefer to stay on a biased reference trajectory. However, even with a shared controller, there is still a certain distance of 0.2-0.3 m from the exact center of the lane. This confirms the higher control effort found with DHA which is the result of a situation of contrast between operator and this haptic support system.

In figure 5.8 are shown steering wheel angles executed by subjects in a specific interval of time. The road curvature during these maneuvers is also reported. It can be observed that SW angles are similar for DHA and Manual (only some higher

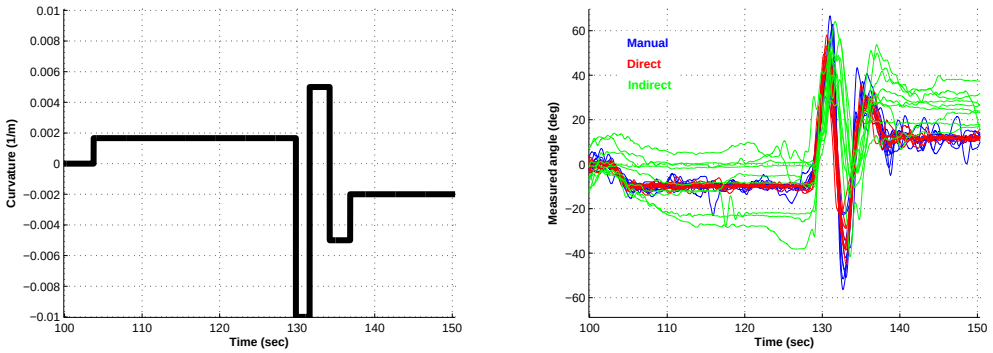

(a) Road curvature (b) Steering angle

FIGURE 5.8: NVB - Steering angle signals

peaks with Manual) but quite different from IHA. With IHA there is a bias for all the subjects that can be different between them. Oscillations around the bias are however quite small. From this it can be anticipated that the metrics representing fast variability of the steering wheel angle will not be significantly different, but something will come out about the steering wheel usage with IHA.

SRR is reported in figure 5.9 for straight roads and curves. It was not found sig-

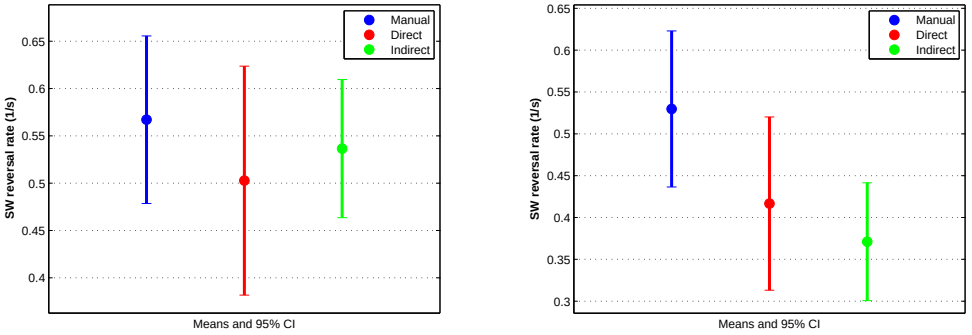

(a) straight roads (b) curves

FIGURE 5.9: NVB - Steering Reversal Rate

nificantly different. $std(\theta_{SW})$ in figure 5.10 is higher with IHA (12°-13° difference from Manual and DHA), but there are no differences between DHA and Manual. The value from ANOVA are $F = 87.09, p = 1 \times 10^{-11}$. If we choose these last two metrics as Control activity measurements, no benefits were found with DHA, in contrast again with results from previous studies [3].

Here it comes the slight contrast in the control goal between shared controller and IHA. In case of DHA we said it entails a higher effort, while with IHA it causes a misuse of the steering wheel. The steering wheel will have higher angles whenever the operator decides to disagree with the support system, according to what found in 2.3.4.

In brief, in Normal visibility condition new results were found with respect to previous studies. The haptic controllers were argued to reduce control activity and

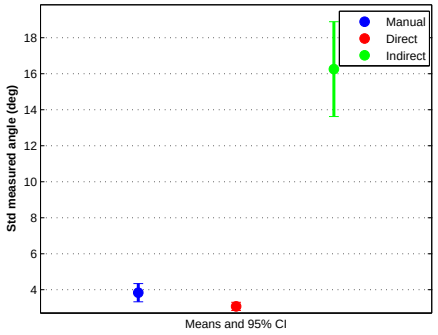

FIGURE 5.10: NVB - Std of steering angle - straight roads

effort and produce slight benefits in performance. However, since the task was probably easy, no benefits came out in terms of performance or control activity. Moreover, a slight contrast between operator and controller in deciding the reference trajectory produced a higher control effort with DHA and a misuse of the steering wheel with IHA.

5.2.2 Low visibility

In this paragraph the results of the statistical analysis in Low visibility condition. In figure 5.11 are shown comparison plots for $min_{10\%}|TLC|$ in straight roads and

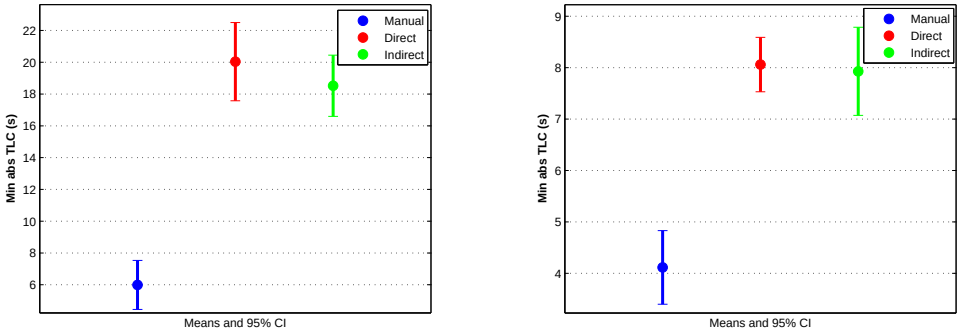

(a) straight roads (b) curves

FIGURE 5.11: LVB - Minimum 10% of absolute TLC

curves separately. In straight road there are significant differences between DHA and Manual (14.05 s difference) and also between IHA and Manual (12.53 s), with $F = 56.46, p = 8 \times 10^{-10}$. Notice that, while the mean values are around 20 s for DHA and IHA, there is a dramatic drop to 6 s for the Manual control group. Also in curves there are similar differences, although they are less pronounced (3.94 s between DHA and Manual and 3.81 s between IHA and Manual), with the parameters $F = 37.9, p = 4 \times 10^{-8}$.

Regarding $std(e_{lat})$ in straight roads of figure 5.12, there are again signifi-

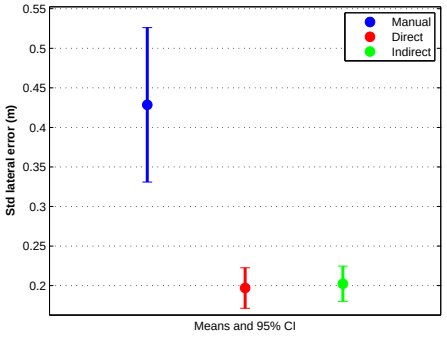

FIGURE 5.12: LVB - Std of lateral reference error - straight roads

cant differences between Manual control and DHA (0.23 m difference) and between Manual and IHA (0.22 m difference). The values from the analysis are $F = 18.83, p = 1 \times 10^{-5}$.
In the Low visibility condition improvements in performance have been therefore extensively found both with DHA and IHA, in terms of $min_{10\%}|TLC|$, where differences are very large in straight roads, and $std(e_{lat})$. Haptic feedback helped the operator to better perform the task in this critical condition.

In figure 5.13 are reported the signals of measured torque from subjects in the

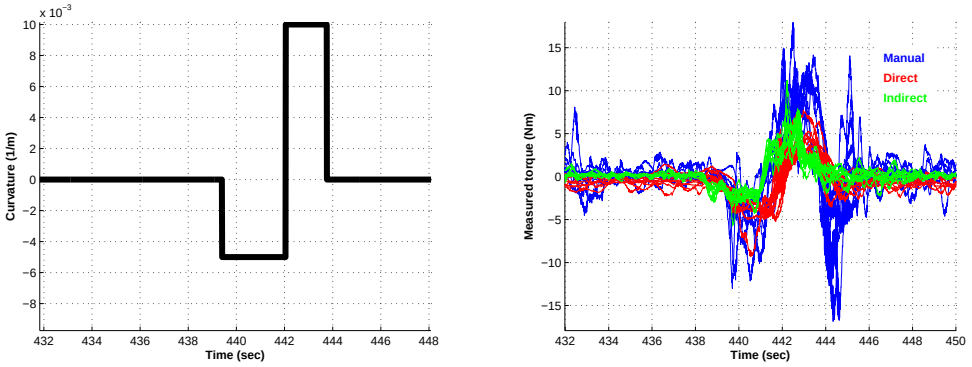

(a) Road curvature

(b) Measured torque

FIGURE 5.13: LVB - Measured torque signals

three groups for a short interval of time, along with the road curvature profile in the same interval. It is clear that more oscillations and higher peaks occur with Manual control, since it is harder to guide the vehicle when visual feedback is limited.

TRR comparison plots are displayed in figure 5.14 for straight roads and curves. In contrast with what found in Normal visibility condition, TRR is now lower with a shared controller than Manual, both in straight roads (around 0.4 1/s differences with DHA and IHA, $F = 27.42, p = 1 \times 10^{-7}$) and even higher in curves (around 0.6 1/s differences, $F = 50.05, p = 3 \times 10^{-9}$).
$std(T_{hum})$ in figure 5.15 is also lower with a shared controller than Manual in straight roads (0.04 Nm difference with DHA and 0.06 Nm difference with IHA),

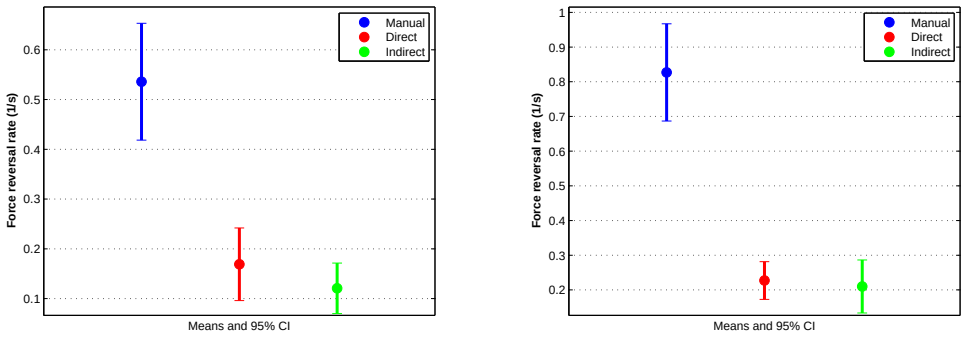

(a) straight roads (b) curves

FIGURE 5.14: LVB - Torque Reversal Rate

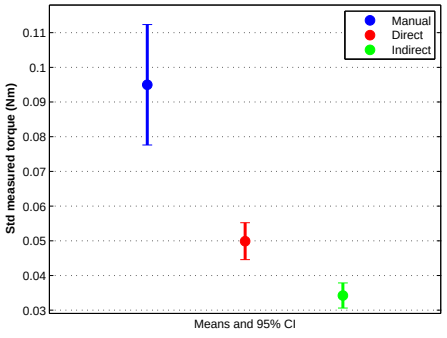

FIGURE 5.15: LVB - Std of measured torque - straight roads

with $F = 33.49, p = 1 \times 10^{-7}$.
$rms(T_{hum})$ in figure 5.16 is lower with a shared controller, the lowest with IHA both in straight roads (0.4 Nm difference DHA-Manual and 0.9 Nm difference IHA-Manual, $F = 27.49, p = 6 \times 10^{-7}$) and curves (0.5 difference DHA-Manual and 1 Nm difference IHA-Manual, $F = 49.47, p = 3 \times 10^{-9}$). The differences are also significant between DHA and IHA.

In Low visibility condition there have been noticeable improvements in Control activity and effort both with DHA and IHA with respect to subjects driving without a shared controller.
In this condition, since the operator visual feedback is limited, it is easier for subjects to totally agree with the haptic feedback when it is provided. The slight contrasts observed in Normal visibility condition, due to subjects' preferences, are now disappeared. This produced higher Performance and lower Control activity and effort for subjects guided by the haptic support.

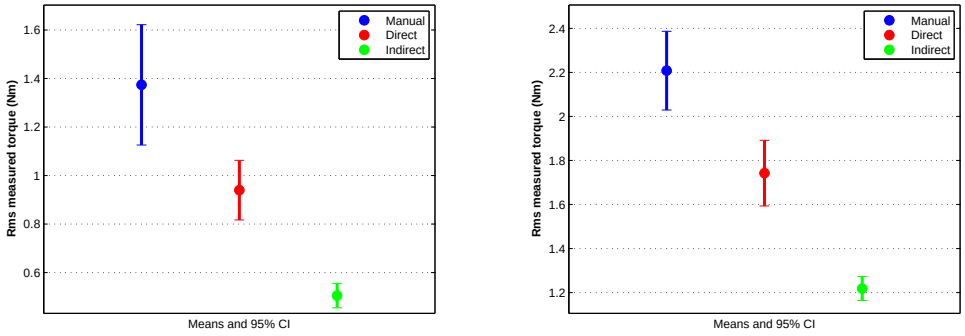

(a) straight roads (b) curves

FIGURE 5.16: LVB - Rms of measured torque

5.2.3 Obstacle avoidance with Controller error

In this paragraph the results from the obstacle avoidance maneuver with a faulty shared controller are presented.

Before introducing the statistical analysis results, it is interesting to show plots

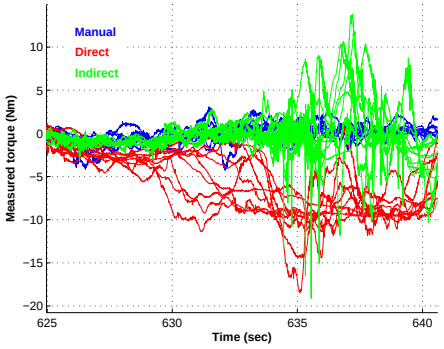

FIGURE 5.17: OAE - Torque signals

of the measured torque signals and steering angle signals. Measured torque signals are in figure 5.17. With DHA, they are biased around -10 Nm when the driver decides to switch to the left lane and stay there to avoid the obstacle. Notice also that the fight in force with the controller starts from the beginning of the maneuver. With Manual control, the operator torque to perform such a task is much smaller since there is no faulty support going against the operator. With IHA there is no bias around -10 Nm but higher oscillations occur for many subjects.

Regarding the steering angle signals in figure 5.18, with Manual control and DHA the signals for the obstacle avoidance maneuver are quite similar. There are only some higher oscillations with DHA. When the vehicle is on the left lane the SW angle is close to zero. With IHA the signals get higher than 180° when the vehicle is staying on the left lane, close to the SW hard boundary.

From these plots the critical conditions previously described when there is a faulty DHA controller and IHA controller (section 3.2.4) are clearly displayed. The DHA

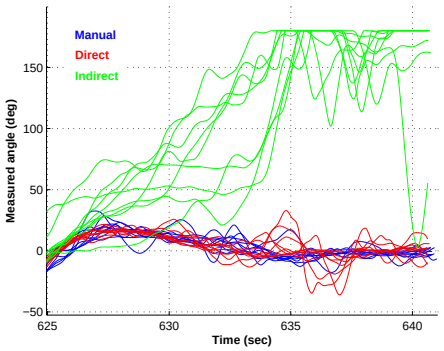

FIGURE 5.18: OAE - Steering angle signals

faulty controller requires a higher torque from the operator to contrast the controller force feedback, while in order to contrast the IHA faulty controller the operator has to steer in the same direction of the force feedback and this yields a large steering angle. Moreover, with IHA it has been shown that there are oscillations in the torque signals during the maneuver, probably caused by the driver being confused with the faulty behaviour of the system. With DHA there are lower oscillations, therefore the driver has more clear in his mind what to do to avoid the obstacle by going against the faulty support system.

In figure 5.19 are shown plots of the vehicle trajectories during the evasive maneuver with the minimum distance points for each driver. The red line indicates the road pylons delimiting the obstacle on the right lane. It can be noticed that all the maneuvers begin with a good advance with respect to the obstacle since it was placed on a straight road and the preview was large. The minimum distance is in fact reached laterally, while the vehicle is staying on the left lane, and not in the obstacle approaching. Trajectories of different subjects with Manual control are quite similar while with a shared controller there is more variability between subjects.

The critical conditions in case of a controller error can affect performance, which is measured here as the minimum distance from the obstacle $min(d_{obst})$ during the evasive maneuver. In figure 5.20 is shown a comparison plot for $min(d_{obst})$. There are no significant differences between DHA and Manual control, while with IHA the minimum distance is significantly lower than with Manual (0.98 m difference) and DHA (0.70 m difference), with $F = 14.2, p = 8 \times 10^{-5}$. Notice that with DHA and Manual the mean of the minimum distance is between 1.8 and 2.2 m, while with IHA it drops to 1.2 m, which is still higher than half of a normal commercial car width $w_{car}/2$. Therefore, in spite with IHA the safety distance from the obstacle drops down, still the drivers were in average able to avoid the obstacle.

TRR is presented in the comparison plot of figure 5.21. Differences between Manual and IHA (0.58 1/s) and between DHA and IHA (0.42 1/s) are significant, with $F = 21.04, p = 5 \times 10^{-6}$. High-frequency control activity was higher with IHA, confirming that the subjects were confused with the system faulty behaviour. $std(T_{hum})$ is shown in figure 5.22. Significant differences are between Manual and DHA (0.12 Nm difference) and between Manual and IHA (0.14 Nm difference), with $F = 19.39, p = 1 \times 10^{-7}$. There was more low-variability of the torque signals

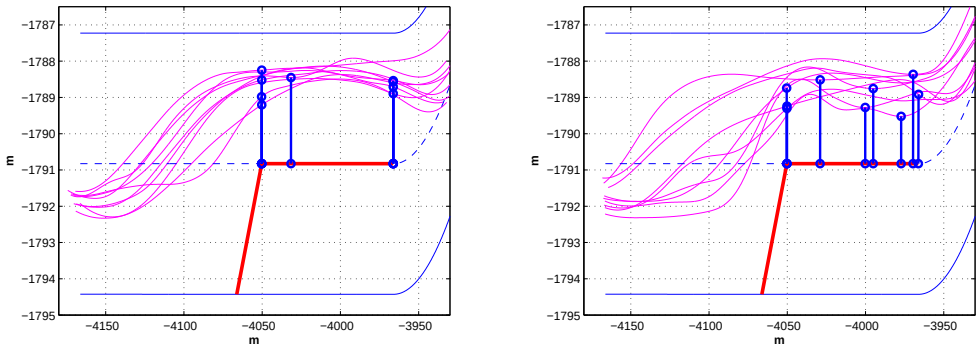

(a) Manual

(b) DHA

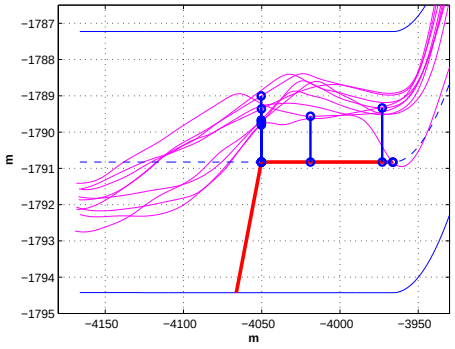

(c) IHA

FIGURE 5.19: OAE - Obstacle avoidance trajectories

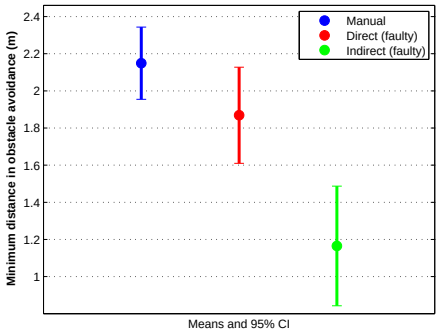

FIGURE 5.20: OAE - Minimum distance from obstacle

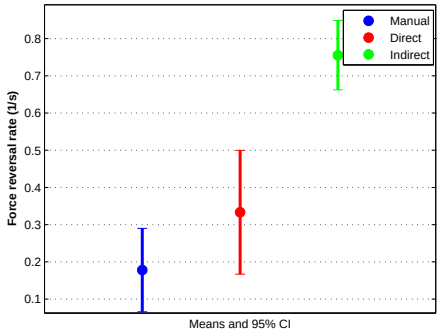

FIGURE 5.21: OAE - Torque Reversal Rate

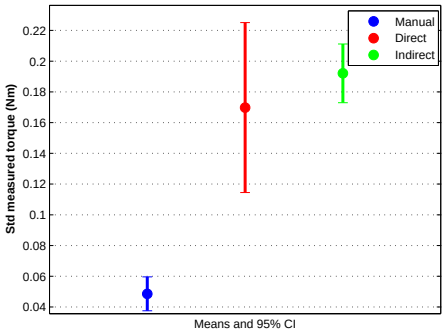

FIGURE 5.22: OAE - Std of measured torque

also with DHA, confirming what observed in figure 5.17.

In figure 5.23 is displayed the $rms(T_{hum})$ comparison. Significant differences are

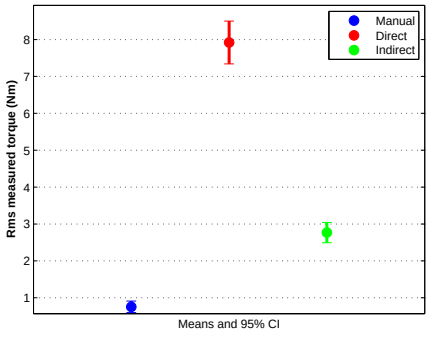

FIGURE 5.23: OAE - Rms of measured torque

between all groups: Manual-DHA (7.16 Nm), Manual-IHA (2.01 Nm) and DHA-IHA (5.15 Nm), with $F = 360.72, p \approx 0$. It is evident that the highest control effort is with DHA, confirming that the contrast with this system requires a higher physical effort. However, the effort with IHA is also higher than with Manual, although lower than with DHA.

From the analysis in the evasive maneuver with controller error, the critical conditions in force with DHA and steering angle with IHA have been clearly shown.

These condition caused a damage to Performance with IHA, in terms of minimum distance from the obstacle that is also safety. The highest physical effort was found with DHA, confirming the fight in force with the faulty support system. However, control activity was found higher than with Manual not only with DHA but also with IHA, in particular in high-frequencies due to the drivers confusion when fighting with this system.

5.2.4 Adaptation

Here the results from the statistical analysis in the *Adaptation* part are presented. Remember that this is made of only the first curves of the final manual driving part, where transient effects were observed during the experiments. In these first curves drivers adapt to the manual control after the controller has been switched off.

In figure 5.24 the vehicle lateral error with respect to the center of the right

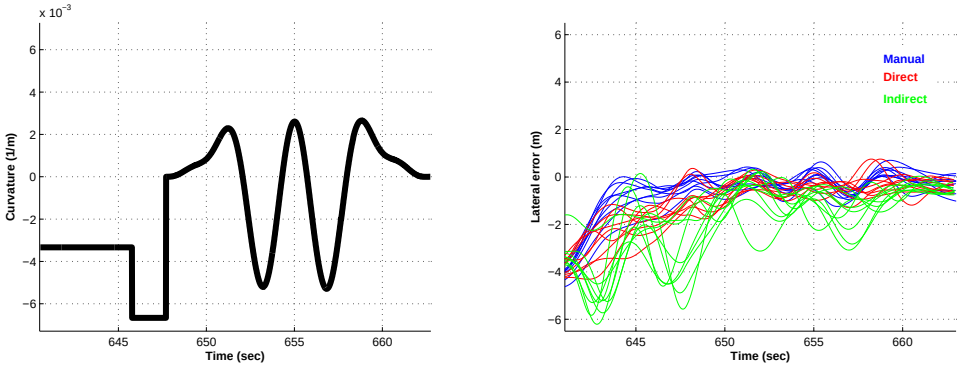

(a) Road curvature

(b) Lateral reference error

FIGURE 5.24: ADP - Lateral reference error signals

lane is shown along with the curvature of the road in these curves. A bias to negative values in the first curve and high oscillations also in the following curves are present on the Lateral Error with IHA, while with DHA the negative bias is quite small and less oscillations occur. It seems that adaptation to Manual control from subjects who learned how to use IHA is much more troubled than for subjects used to DHA. Notice that in order to keep the vehicle on the road it must be $-5.4\,m \leq e_{lat} \leq 1.8\,m$, where the error is negative if the vehicle is to the left of the center of the right lane and positive if it is to the right. Some subjects with IHA were not able to keep the vehicle on the road and crossed the road left boundary. Remember that the controller switching-off comes right after the evasive maneuver, during which subjects with IHA were keeping the SW to the left with a large steering. After the error the driver had to bring the steering wheel back to the center and drive manually. The adaptation process is more intense for subjects used to IHA than for those driving with DHA. In fact, in the latter case the steering wheel usage does not change after the controller is disabled but only the force feedback vanishes.

The $std(e_{lat})$ comparison plot is in figure 5.25. As expected, it is significantly

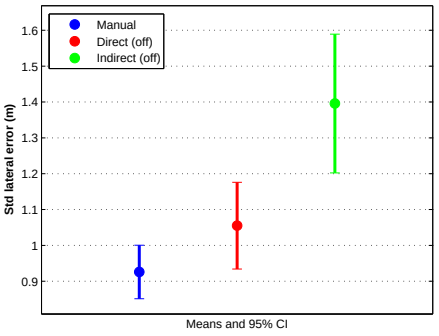

FIGURE 5.25: ADP - Std lateral reference error

higher with IHA than Manual (0.47 m difference) and DHA (0.34 m difference), with $F = 11.78, p = 0.0003$. There are no significant differences between DHA and Manual.
Drivers used to guide with the IHA support performed the worst in the first curves after the controller switching-off, while drivers used to DHA did not have particular troubles to adapt to manual driving.

The measured torque signals are displayed in figure 5.26. It can be observed that

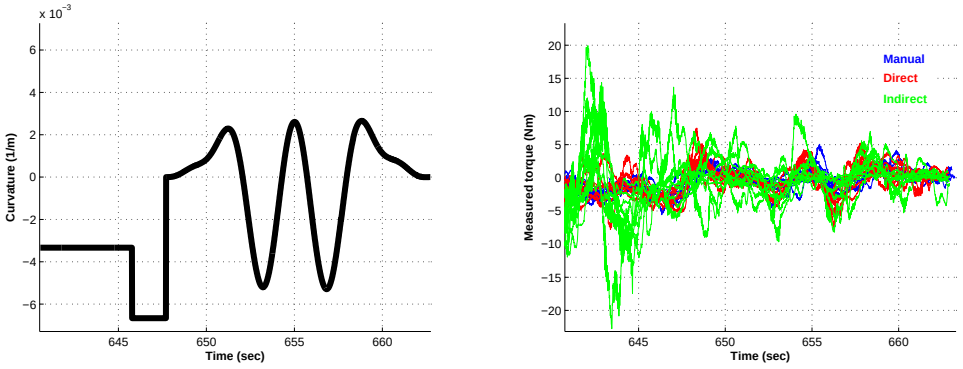

(a) Road curvature (b) Measured torque

FIGURE 5.26: ADP - Measured torque signals

there are higher oscillations and peaks with IHA.

In figure 5.27 it is shown TRR. The only significant difference is between Manual and IHA (0.31 1/s difference), with $F = 5.29, p = 0.01$. $std(T_{hum})$ is shown in figure 5.28. IHA is significantly different from Manual (0.13 Nm difference) and from DHA (0.1 Nm difference), with $F = 14.96, p = 6 \times 10^{-5}$.
Therefore, both high-frequency and low-frequency control activity was higher for subjects used to IHA, confirming the more intense adaptation process. It seems instead that subjects used to DHA did not have higher mental effort during the adaptation to manual driving.

In figure 5.29 it is displayed $rms(T_{hum})$. It is higher with IHA with respect to Manual (1.88 Nm difference) and DHA (1.48 Nm difference), with $F = 14.79, p =$

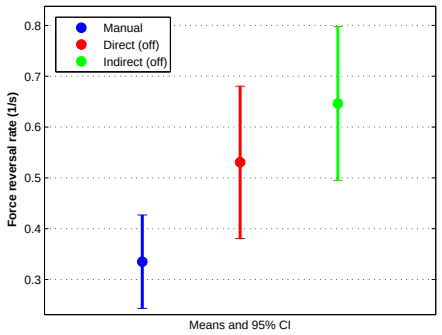

FIGURE 5.27: ADP - Torque Reversal Rate

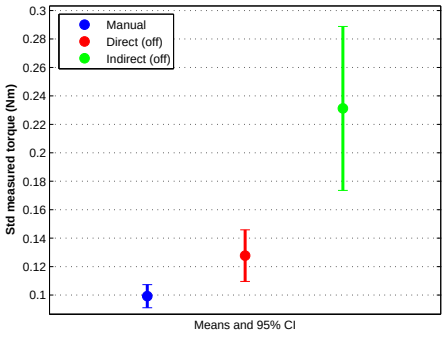

FIGURE 5.28: ADP - Std of measured torque

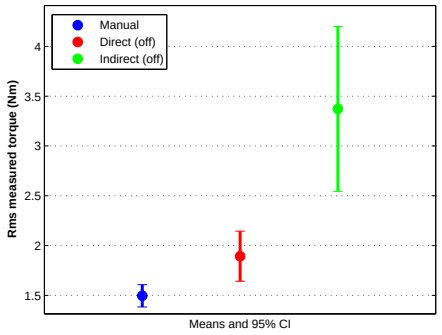

FIGURE 5.29: ADP - Rms of measured torque

6×10^{-5}. No differences were found between DHA and Manual.
Also control effort was higher for subjects used to IHA but not for the ones who had been driving with DHA.
From the analysis in this part of the experiment, it emerges that the adaptation process was the most intense for subjects used to the support from IHA. They can have troubles in keeping the car in the right lane since the use of the steering wheel is totally changed by the IHA switching-off and therefore they have to adapt to a system that has a different dynamics to control. On the other side, the use of the steering wheel is the same for DHA and therefore in this case they only have to adapt to the absence of the force feedback. The required effort for the adaptation process was also higher only for IHA subjects.

5.2.5 After-effects

Finally, results from the final part after the first curves are analysed in this paragraph. The adaptation process to manual driving is now expected to be completed and only after-effects can remain.
In figure 5.30 the $min_{10\%}|TLC|$ comparison plots are shown separately for straight

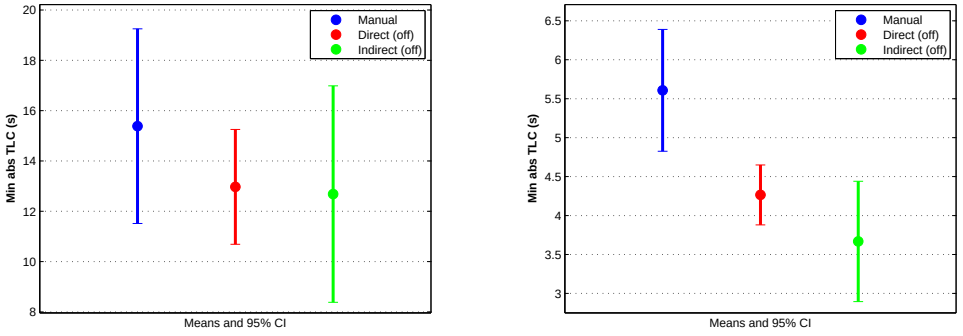

(a) straight roads (b) curves

FIGURE 5.30: AEF - Minimum 10% of absolute TLC

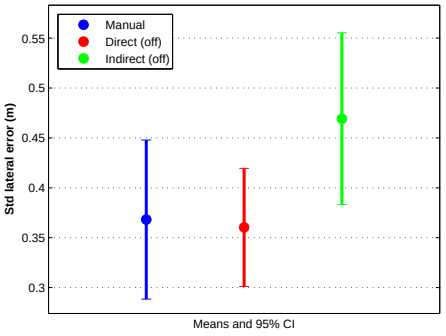

FIGURE 5.31: AEF - Std of lateral reference error

roads and curves in this final part of the experiment. The only significant differences are in curves, between Manual and DHA (1.34 s) and between Manual and IHA (1.94 s), with $F = 8.38, p = 0.0017$. $std(e_{lat})$ for straight roads in figure 5.31 is not different for the three systems.
It seems that with a shared controller, there have been some residual after-effects that cause a slight drop in performance.
TRR for straight roads and curves is presented in figure 5.32 and $std(T_{hum})$ in

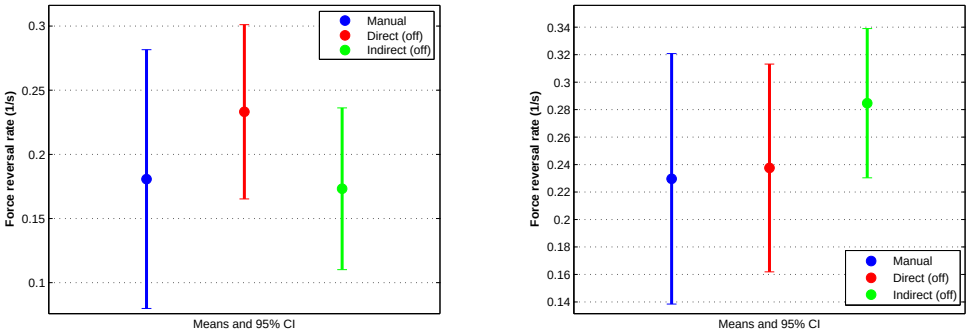

(a) straight roads (b) curves

FIGURE 5.32: AEF - Torque Reversal Rate

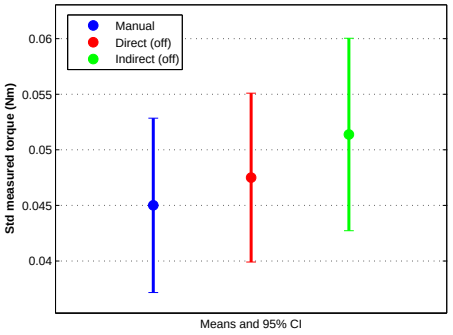

FIGURE 5.33: AEF - Std of measured torque

figure 5.33. There were no significant differences in any case.
No after-effects on control activity were found with the two shared controllers.
$rms(T_{hum})$ is shown separately for straight roads and curves in figure 5.34. There are no significant differences.
Neither control effort was found different between the systems.
Only a slightly negative after-effect was found in performance for subject used to both DHA and IHA. Control activity and effort were not influenced. Therefore, in general almost no after-effects were encountered and it can be stated that the adaptation process was almost completed in the first curves after the controller switching-off.

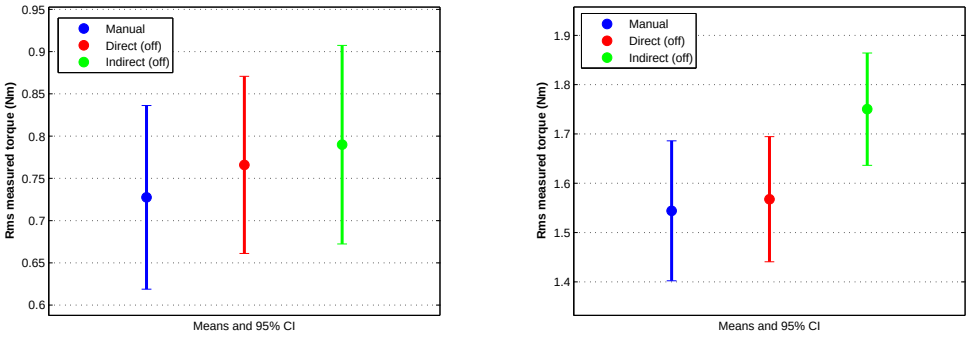

(a) straight roads (b) curves

FIGURE 5.34: AEF - Rms of measured torque

5.3 Discussion

The results from the experiment were presented in the previous sections, separately for the different driving conditions (figure 4.5). In this section the results of the experiment are discussed with reference to each of the experimental hypotheses of section 4.1.

5.3.1 Normal visibility

Hypothesis A in section 4.1.1 stated that:

A)*In a normal visibility condition, with the DHA support better performance than Manual control and lower control activity/effort can be achieved. With the IHA support, better performance and less control activity than Manual control are expected, but higher control effort.*

The results from the *NVB* condition of section 5.2.1 are used to verify this first hypothesis.
In terms of Performance, no particular benefits were found with a shared controller, neither with DHA nor with IHA, with respect to Manual control. The only difference with a shared controller was that the vehicle trajectory in straight roads had less oscillations, thanks to the force feedback that cancels out the torque noise from the human operator.
Control activity, that is mental effort from the operator, was not found different with a shared controller either.
Finally, it came out a higher Control effort only with the DHA shared controller with respect to both Manual control and IHA.
From the additional analysis performed on the Steering Wheel usage, a strong bias in the SW angles was found with IHA with respect to Manual control and DHA.

The first hypothesis is proved in the Performance part only, but denied with respect to Control activity and effort. It can be argued that Manual driving in this condition was a simple task since curves were not demanding, therefore no particular benefits on Performance or Mental effort can be obtained from cooperating with a shared controller. Moreover, the results on Control effort with DHA and SW usage with IHA are expected to come from a slight contrast of control goals between shared controller and operator. While for the shared controller the reference trajectory lies in the exact center of the right lane, the human operator can have a bias in the detection of the center of the right lane in straight roads, while in curves he can decide to cut them differently. The higher Control effort with DHA and the biased usage of the SW with IHA are argued to be caused by this contrast. However, this contrast did not affect Performance.

5.3.2 Low visibility

In Hypothesis B of section 4.1.2 it was stated that:

B) *In a condition of low visibility, the operator can achieve better performance and lower control activity/effort with a shared controller than with Manual control.*

The results from the *LVB* condition of section 5.2.2 are used to verify this hypothesis.
Both Performance, Control activity and Control effort were found highly improved with the DHA and IHA shared controllers with respect to Manual control. This second hypothesis is totally confirmed from the results of the experiment. Driving with the visual feedback lowered by fog on the street can be a lot safer with a shared controller which provides an additional force feedback signal to the operator.

5.3.3 Controller error

Hypothesis C (section 4.1.3) was:

C) *An evasive maneuver can be endangered by a faulty support providing a wrong reference trajectory, due to a critical condition in force or SW angle that will arise with DHA and IHA respectively.*

The results from the *OAE* condition of section 5.2.3 are used to verify this third hypothesis.
With DHA it was found a critically higher control effort in this maneuver, while with IHA the SW usage was strongly biased. However, only the critical condition

with IHA endangered the evasive maneuver, while with DHA there were no differences with respect to Manual control. Moreover, a higher Control activity was found with IHA with respect to Manual control and DHA.
The hypothesis is confirmed for the IHA controller but denied for the DHA controller. The faulty IHA controller can be harmful in an evasive maneuver with an obstacle not detected, since a higher steering action is required from the operator in order to contrast the controller action and this odd maneuver can also confuse the operator. Whereas it is easier to contrast a faulty DHA shared controller by simply applying a force against it. Therefore, it is likely that DHA is less damaging than IHA in case of a controller error as the one investigated on the reference trajectory detected from the sensor system.

5.3.4 Adaptation and After-effects

Hypothesis D in section 4.1.4 stated that:

D) *When full Manual control is regained after being used to an haptic support system, performance and/or control activity/effort can be negatively affected with respect to drivers used to Manual control. Moreover, the controller switching off can endanger the lane keeping.*

The results from the *ADP-AEF* conditions of sections 5.2.4-5.2.5 respectively are used to verify this third hypothesis.
In this final part the human operator had to adapt from driving with a shared controller to Manual driving. In the first curves after the controller switching-off, strong adaptive effects were found with the IHA controller. Performance deteriorated with IHA and also Control activity and effort were higher with respect to DHA and Manual control. No differences were found instead between DHA and Manual. However, in the rest of this final part after the first curves, no after-effects were found on Control activity and effort neither with IHA this time, while Peformance was only slightly degraded with both DHA and IHA.
With respect to Hypothesis D, the results with IHA confirmed that this controller can cause some negative after-effects mainly in the first curves after it has been switched-off, while DHA does not practically cause any damage. Since the IHA controller totally changes the usage of the SW from a position control device to force control, the adaptation process to Manual control is intense, implying higher effort from the operator, and it can also harm the driving safety. The operator has to adapt to a system with a different dynamics to control than the one he has learned. On the other side, the DHA controller does not change the usage of the SW and the dynamics of the system, but only provides an additional force. After the DHA is switched off, the operator has only to adapt to the absence of the force feedback but the system to control is unaltered.
However, the human adaptation process to the absence of the IHA support is very quick and after the first curves the after-effects practically disappear and the curve negotiation task is performed the same as for subjects used to a DHA

shared controller and almost as good as for subjects not used to any haptic support system.

Chapter 6

Conclusions

6.1 Conclusions on this work

This project was based on the analysis of two different haptic shared control systems for curve negotiation and experiments on them in a driving simulator.
In the preliminary survey, two main control strategies for haptic shared guidance were found in literature, which have been called Direct haptic aiding (DHA) and Indirect haptic aiding (IHA) respectively. The baseline idea of this project was to implement the IHA controller for the first time for a curve negotiation task and test it in an experiment.
The first step was to create models of shared control with the IHA controller to simulate how this system can be used for curve negotiation support. A scheme from previous studies was used which included a model of the human behaviour in curve negotiation and the DHA controller.
First, the IHA controller was implemented in this scheme, with a structure which is a replica of the DHA controller but with a negative gain on the force feedback. A model of the control interface was also added to the IHA structure and a mechanical decoupling block was created. This way the IHA controller does not affect directly the dynamics of the vehicle and provides its aiding by merely shifting the steering wheel neutral point. Secondly, the original model of human operator was modified in the intrinsic feedback block, which is the part modeling the human NMS reacting to external signals. This feedback mechanism was extended with an internal model of the dynamic interaction between human NMS and steering wheel and with an internal model of shared controller. These new features allowed us to simulate situation where the operator decides to give way to the force feedback or to resist to it.
The model of shared control guidance with DHA and IHA allowed us to investigate different situations in car driving (normal visibility, low visibility, controller error) and make previsions on the behaviour of the human operator with these systems. The modeling study turned out to be very insightful, in particular in figuring out what happens when the operator decides to disagree for some reason with the two shared controllers.

From the results of the modeling study, a Human-Factor experiment was designed and carried out. The experiment was performed in the driving simulator inside the Human-Machine Interaction Laboratory in the Aerospace Engineering Faculty at Delft University of Technology. The DHA controller had already been implemented and tested in previous experiments, therefore the setting-up procedure required only to add the features in the software to implement the IHA controller. After building the IHA support, the two shared controllers were separately tuned and an experiment was set-up, structured into four parts (normal visibility, low visibility, controller error, after-effects) in order to verify the previsions figured in the modeling study. The results of the experiment were conveyed into a statistical analysis and interesting results came out of it.
In the low visibility condition, both the DHA controller and the IHA controller were found beneficial in terms of performance, mental effort and physical effort with respect to manual control. Driving with fog on the street was obviously a hard task and therefore the shared controller could provide a force feedback compensating for the lack of the operator visual feedback and ensuring a safe driving. However, in normal visibility conditions no benefits were found with the two systems. A slightly higher effort from the operator was found with the DHA controller, while by analysing the use of the steering wheel it was found that subjects driving with the IHA controller tended to steer more than necessary. This result proved that when the task is easy, a contrast between shared controller and operator can arise due to a slight difference in their control goal, which in this case was the drivers deciding to cut curves differently from the controller.
In the situation of controller error, where an obstacle not detected from the shared controller was put on the right lane of a straight road, the critical conditions found out in the modeling study were confirmed. A higher effort was found to contrast the faulty DHA controller, while large steering actions were found with IHA. In terms of avoiding the obstacle, compared to the maneuvers of manual drivers, the DHA did not harm the maneuver. Whereas the shared control with IHA produced vehicle trajectories closer to the obstacle which can be a problem of safety.
Finally, in the last part of the experiment where the controllers had been switched-off after the error, some after-effects were found in particular with the IHA controller. In the first curves the vehicle trajectories had high oscillations and the operator effort was also higher since the operator had to adapt to a system with a different dynamics to control. Instead with DHA no significant after-effects were found, this confirming that it is easier for subjects to switch from DHA to manual driving than from IHA. However, the after-effects with IHA vanished after the first curves and no residual effects were found in the rest of the final part. The drivers were able to rapidly adapt to manual control in a short time.
In conclusion this project, starting with a a modeling study of two shared controller strategies for curve negotiation support, was founded on an experimental campaign where different driving conditions were tested with the DHA controller and for the first time with the IHA controller. Insightful results were produced on human behaviour and his ability to cooperate with a shared controller.

6.2 Future works

The knowledge acquired with this experimental study puts the foundation for two possible developments, the first on human behaviour modeling and the second on improving the IHA controller.
The model of muscular co-contraction was modified with new features which allowed us to test different behavioural settings of the operator with the shared control systems. However, the parameters used were taken from a previous study where they had been identified in a passive driving task without any visual feedback. From the results of the modeling study, it seems that these parameters should be tuned in a different way for the new model. In fact, the differences in results between a Force task and a Position task from the operator with the two systems are supposed to be stronger than those obtained from the model. Although the results obtained allowed us to make previsions and formulate some general hypotheses, they are not numerically reliable. Therefore, a first possible development would be to enhance the model of human operator by identifying the human NMS parameters.
The IHA controller was in general well-accepted and beneficial for the most part of the experiment. However, this approach can have some drawbacks: when it is faulty the operator is likely to find himself in troubles with a system which has an odd dynamics to control. The main issue is the usage of the steering wheel which is changed by the IHA controller into a force interface, while at the same time the whole steering capability is unaltered. We argue that the misuse of the steering wheel in case of controller errors is the main cause of confusion in the driver's internal representation of the system to control. Therefore, the second possible development would be an enhancement of the IHA controller internal structure in order to overcome this weak point highlighted from the results of the experiment.

Bibliography

[1] P. Griffiths and R.B. Gillespie. Shared control between human and machine: Haptic display of automation during manual control of vehicle heading. *Proceedings of the 12th International Symposium on Haptic Interfaces for Virtual Environment and Teleoperator Systems*, pages 358–366, 2004.

[2] David A. Abbink, Mark Mulder, and Erwin R. Boer. Haptic shared control: smoothly shifting control authority? *Cognition, Technology and Work*, (14): 19–28, 2011.

[3] Mark Mulder, David A. Abbink, and Erwin R. Boer. The effect of haptic guidance on curve negotiation behavior of young, experienced drivers. *The IEEE International Conference on Systems, Man, and Cybernetics*, 2008.

[4] Samantha M. C. Alaimo, Lorenzo Pollini, Jean Pierre Bresciani, and Heinrich H. Bülthoff. A comparison of direct and indirect haptic aiding for remotely piloted vehicles. *19th IEEE International Symposium on Robot and Human Interactive Communication*, 2010.

[5] Samantha M. C. Alaimo, Lorenzo Pollini, Jean Pierre Bresciani, and Heinrich H. Bülthoff. Evaluation of direct and indirect haptic aiding in an obstacle avoidance task for tele-operated systems. *18th World Congress of the International Federation of Automatic Control*, 2011.

[6] D. Cleij. *Design of Haptic Shared Control. Analysing Driver-Controller Interaction to Improve Haptic Shared Control Systems.* Master of Science Thesis, Delft University of Technology, 2011.

[7] Egbert Bakker, Nyborg Lars, and Pacejka Hans B. Tyre modelling for use in vehicle dynamics studies. *Society of Automotive Engineers*, 1987.

[8] Abbink D.A. and Mulder M. Neuromuscular analysis as a guideline in designing shared control. *Advances in Haptics*, (27):499–516, 2010.

[9] Kakin K. Tsoi, Mark Mulder, and David A. Abbink. Balancing safety and support: Changing lanes with a haptic lane-keeping support system. *The IEEE International Conference on Systems, Man, and Cybernetics*, 2010.

[10] Yi Lu Murphey, Robert Milton, and Leonidas Kiliaris. Driver's style classification using jerk analysis. *Computational Intelligence in Vehicles and Vehicular Systems*, pages 23–28, 2009.

[11] W. van Winsum, K.A. Brookhuis, and D. de Waard. A comparison of different ways to approximate time-to-line crossing (tlc) during car driving. *Accident Analysis and Prevention*, (32):47–56, 2000.

[12] Andy Field. *Discovering Statistics using SPSS*. SAGE Publications Ltd, 2009.